Univerzita Karlova v Praze / Charles University in Prague
Přírodovědecká fakulta / Faculty of Science

Studijní program: Molekulární a buněčná biologie, genetika a virologie
Study programme: Molecular and Cell Biology, Genetics and Virology

Mgr. Antonín Brož

Adheze, růst a diferenciace osteoblastů a kmenových stromálních buněk na povrchu biokompatibilních nanomateriálů

Adhesion, growth and differentiation of osteoblasts and mesenchymal stromal cells on biocompatible nanomaterial surfaces

Dizertační práce / Doctoral thesis

Vedoucí závěrečné práce / Supervisor: doc. RNDr. Marie Hubálek Kalbáčová, Ph.D.

Praha / Prague, 2017

Prohlášení:

Prohlašuji, že jsem závěrečnou práci zpracoval samostatně a že jsem uvedl všechny použité informační zdroje a literaturu. Tato práce ani její podstatná část nebyla předložena k získání jiného nebo stejného akademického titulu.

Statement of authorship:

I declare that I prepared the dissertation independently and that I stated all the information sources and literature. This work or a substantial portion thereof has not been submitted to obtain another academic degree or equivalent.

V Praze/In Prague, 25.04.2017

Podpis/Signature

I would like to express my sincere gratitude to all the colleagues and collaborators from Institute of Metabolic Disorders of Charles University and General University Hospital in Prague, Institute of Physics, Jaroslav Heyrovský Institute of Physical Chemistry and Institute of Physiology of Czech Academy of Sciences that either participated on the work presented in this thesis or shared their professional knowledge, expertise and high spirits.

I especially thank my thesis supervisor doc. Marie Hubálek Kalbáčová Ph.D. for her patient and persistent care and doc. Lucie Bačáková CSc. for her scholarly advice.

Abstract

The thesis is based on articles describing the fundamental research of carbon based nanomaterials and their surface modifications for their possible utilization in biomedicine. The aim of this thesis was to describe the way how human osteoblasts (SAOS-2 cell line) and primary human mesenchymal stem cells (hMSC) adhere, grow and behave on surfaces made of several carbon allotropes – nanocrystalline diamond (NCD), single walled carbon nanotube (SWCNTs) films and graphene. The utilization of carbon as the basic material promised good biocompatibility and possibility of useful surface modifications. The NCD had modified surface nanotopography (nanoroughness and nanostructuring prepared by dry ion etching). All the materials had modified surface atomic termination with oxygen and hydrogen which changes the surface electrical conductivity, energy and wettability. It was hypothesized that the surface termination can also influence the cell adhesion and growth on these surfaces. It turned out that all the studied materials were suitable as substrates for cultivation of mentioned cell types with certain modifications. Various nanoroughnesses of NCD surface had different effect on the cell adhesion and cell metabolic activity. Nanostructuring of the NCD influenced the formation of focal adhesions. The surface terminations of NCD and the other studied nanomaterials in cooperation with the fetal bovine serum proteins influence the rate of cell adhesion. Supposed future utilization of the studied materials in biomedicine can be fabrication of bone prosthetics coatings and construction of wide variety of bio-electronic devices.

Table of Contents

1 Introduction

The first attempts to replace damaged, diseased or missing part of a human body are known from the antiquity. This human effort did not reach any significant progress up until the 20th century. However, throughout the recent decades this endeavor developed into important branch of bio-medicine. In the recent decades, the words biomaterial and biocompatibility entered the human vocabulary as the artificial prostheses started to be implanted inside human body and living eukaryotic cells were studied in *in vitro* cultures. Many definitions of biomaterials and biocompatibility were presented in scientific publications approaching this complicated issue from various aspects – physical, chemical and biological properties, composition and utilization. The definition has changed in time with the developing field. To give an idea, here are some of the attempts of the biomaterial definition:

"A biomaterial is a non-viable material used in a medical device, intended to interact with biological systems."

(Williams, 1987)

„Biomaterial is a material intended to interface with biological system to evaluate, treat, augment or replace any tissue, organ, or function of the body. "

(Williams, 1999)

"A biomaterial is a non-drug substance suitable for inclusion in living system which augments or replaces the function of bodily tissue or organ."

(Geckeler and Nishide, 2009; Jayaswal et al., 2010)

These deffinitions often accentuate some but not all the possible biomaterial properties and utilizations. Perhaps the best way to define the word biomaterial and closely related biocompatibility would be a simplistic approach that leaves enough space for all the various uses and properties of biomaterials today. The basic defining feature of any biomaterial distinguishing it from any other non-biomaterial is the mere possibility of coexistence in close contact with a living cell, tissue or within a

living organism without harming or damaging it in any significant way. The utilization of biomaterials is not only in regenerative medicine. Various kinds of biomaterials are used for production of consumables for biomedical sciences, in construction of biosensors (Du et al., 2016) or for production of drugs for targeted disease therapies (Akhtar et al., 2012; Raffa et al., 2011; Yuan et al., 2011) and fluorescence markers for molecular biology (Fucikova et al., 2014). The biomaterials considered for use in regenerative medicine are sometimes loosely classified in three generations (Hench, 2002). The first generation includes materials that are only "bio-inert". These materials are easy to obtain, non-toxic and non-inflammatory without any intended physiological effect. The first generation of biomaterials acts as a structural support of surrounding tissues. The second generation of biomaterials includes "bioactive" or "biodegradable" materials - e.g. fixed heparin coatings were used for prevention of blood clothing on various types of materials (Wendel and Ziemer, 1999) to enhance their function in circulatory system. The biodegradable materials are, as the name suggests, meant to resorb and disappear in the organism and are supposed to be replaced by an original bodily tissue. This ability is not always needed if the implant is meant to act as a permanent replacement. The third generation of biomaterials can carry both features of second generation and is often defined by utilization of knowledge of molecular interaction between the living cells and the biomaterial to give the cells a specific signal that would drive them towards the tissue regeneration or differentiation (Dingal and Discher, 2014).

The sources of bio-materials are numerous. The word "*non-viable*" in the first mentioned definition above given by prof. Williams does not mean that the source of a certain biomaterial cannot be a living organism. A big source of biomaterials is obviously the living nature itself. In fact, any structural compound that composes bodies of living organisms (cellulose, nacre and components of extracellular matrix of different connective tissues in animals) can be considered a biomaterial. However, biomedicine scientists and material engineers are trying to fabricate artificial biomaterials to have the process of production and the material properties fully under control. The composition of a biomaterial is obviously another very important issue. We can distinguish materials that are completely alien to living systems like alloys used in different types of bone and joint implants - typically titanium based alloys (Kulkarni et al., 2014), organic materials that attempt to mimic some properties that are common in living systems (e.g. polycaprolactone, polylactic acid, polyglycolide

acid acrylamides) (Peña et al., 2016) and materials which are nature-identical (e.g. collagen, hyaluronan) (Jha et al., 2011; Matthews et al., 2002). The biomaterials are prepared as composites combining mechanical or biochemical features of several components to achieve a wanted effect (Arash et al., 2014; Olivas-Armendariz et al., 2013). However, some biomaterials can be based only on one chemical compound – often polymer (Van Vlierberghe et al., 2011) or on one element like the materials studied in this thesis.

This work is comprised of studies investigating the biocompatibility of non-degradable carbon based materials – nanocrystalline diamond (NCD), graphene and carbon nanotubes (CNT). These materials are able to withstand the corrosive conditions of a living environment or a body. However, these materials can also influence the cell behavior and are able to guide the cells in different ways by their surface topography and chemistry. The supposed utilization of these materials would be as coatings for bone or dental prostheses or basic material for construction of biosensors.

2 Current State of Knowledge

2.1 Nanomaterials in Biomedicine

The unit prefix "nano" is dedicated for a billionth of a basic unit. The unit nanometer is obviously used in the size range 1 - 999 nm, however commonly used definitions shift the "nanoscale" size between 0.1 nm and 100 nm. The sizes above 100 nm and below 1 μm are often denoted as "submicron" (Khang et al., 2008). Nanomaterials in general are materials carrying a "size feature" (particle diameter, fiber diameter, surface topography) in the above described nanoscale. The size of subcellular components including surface membrane proteins (e.g. receptors, ion channels) through which the cells communicate with the environment is in the nanoscale range. Therefore, the nanotechnology and nanomaterials can be used for construction of devices with possibility to influence and control cellular processes and behavior on the size level of biomolecules. Another feature of all nanomaterials in general is high relative surface area. This can be used to enhance either the interaction of cells and tissues with the biomaterial or to incorporate high amounts of biologically active chemical compounds to the nanomaterial.

Nanomaterials can be classified by the number of spatial dimensions that are in the nanoscale range: 1) nanoparticles (all 3 dimensions in nanoscale), 2) nanofibers (2 dimensions in nanoscale) and 3) nanoplates (1 dimension in nanoscale). Materials with surface nanotopography or surface nanostructures and materials with nanopores can be considered as another separate group of nanomaterials.

The nanoparticles are studied as possible agents for targeted (often cancer) therapies as carriers of drugs or even treatment effectors (Akhtar et al., 2012; Li et al., 2010; Markovic et al., 2011). Semiconductor nanoparticles called quantum dots (Reed et al., 1988) are used for fluorescence imaging (Faklaris et al., 2009; Kairdolf et al., 2013). The size of the quantum dots is close to the size of organic macromolecules (few nanometers). Together with the semiconductor material properties this creates conditions under which a physical phenomenon called quantum confinement can be observed where the wave function of electrons is of comparable size to the size of the nanoparticle. This limits the number of quantum states that the particle can populate. Under such conditions the particles can exhibit fluorescence. The fluorescence wavelength (color) is tunable by the size of the nanoparticle. The methods used for nanoparticle production include for example grinding or milling (Salah et al., 2011), electrochemical etching (Fucikova et al., 2014) and combustion or detonation under special conditions (Krüger et al., 2005)

The nanofibers are used in tissue engineering for fabrication of mashes and scaffolds that are meant for replacement of soft tissues like skin (Sundaramurthi et al., 2014) or nervous tissue (Xie et al., 2010) and also connective tissue like bone (Shih et al., 2006; Sisson et al., 2010). However, the nanofibers are also studied for other applications. Recently a composite nanomaterial - polycaprolactone nanofibers with zeolite nanoparticles was used as a filter for blood dialysis (Namekawa et al., 2014). Biocompatible nanofibers are prepared from organic polymers like polylactic acid or already mentioned polycaprolactone (Ai et al., 2013; Sundaramurthi et al., 2014) or even nature identical materials like collagen (Matthews et al., 2002; Shih et al., 2006). For production of such materials newly developed methods like electrostatic spinning are used (Zhang et al., 2005). This spinning method allows to control the properties of the material like the diameter of the fibers and size of the pores between the fibers and orientation of the fibers (Neves et al., 2007). Such

properties influence the permeability for various molecules and specific surface area of the material.

The nanotopographical modifications of implants are mostly relevant regarding the solid bone implants. As was already said above, the nanotopographical modifications increase the specific surface of the implant in this case also possibly improving the integration of the implant in the tissue. It is also known that certain nanotopography is innate to the bone tissue extracellular matrix (ECM) (Kane and Ma, 2013). Nanostructured surfaces can be made by various physical and chemical methods including grinding and polishing (Huang et al., 2004), physical or chemical vapor deposition methods (Ariano et al., 2009; Khang et al., 2008, 2008; Nebel et al., 2006; Potocky et al., 2006), plasma spraying (Liu et al., 2005), and etching (Schliephake and Scharnweber, 2008). The surface of the bone implants can be also modified by various types of ceramic materials like zirconia, bioglass or calcium phosphate based materials like hydroxyapatite. This group of materials is a direct competitor of diamond-like materials in the biomaterial field. (Jayaswal et al., 2010; Samavedi et al., 2013; Webster et al., 2000).

2.2 Carbon Based Nanomaterials

Carbon is relatively abundant and the most chemically potent element in the universe. This fact is reflected in the existence of separate science fields of organic chemistry and biochemistry. It is the basic element of the only example of life we know. These principle facts predestine the carbon to be a suitable element for construction of biomaterials.

Elementary carbon exists in several forms - “allotropes” (Figure 1). Some of the allotropes occur naturally (diamond, graphite) and some were prepared only artificially (carbon nanotubes). The carbon allotropes can be classified by their crystallinity and predominant hybridization of the valence orbitals in the material. Carbon often forms highly ordered allotropes like diamond, graphite, carbon nanotubes and fullerenes, however carbon can be also found in less ordered or amorphous state - pyrolytic carbon, glassy carbon, diamond-like carbon (DLC). The sp3 materials (diamond, lonsdaleit, diamond-like carbon) are amongst the hardest materials known to human. The sp2 materials (graphene, carbon nanotubes) have also some extraordinary physical properties like high electric conductivity and tensile

strength. Some carbon allotropes are by definition also nanomaterials (carbon nanotubes, graphene, fullerenes) and some can be prepared in a form of nanomaterial (nanocrystalline diamond). The articles contained in this thesis describe the investigation of *in vitro* biocompatibility of three of the carbon allotropes – nanocrystalline diamond (NCD), single-walled carbon nanotubes (SWCNTs) and graphene.

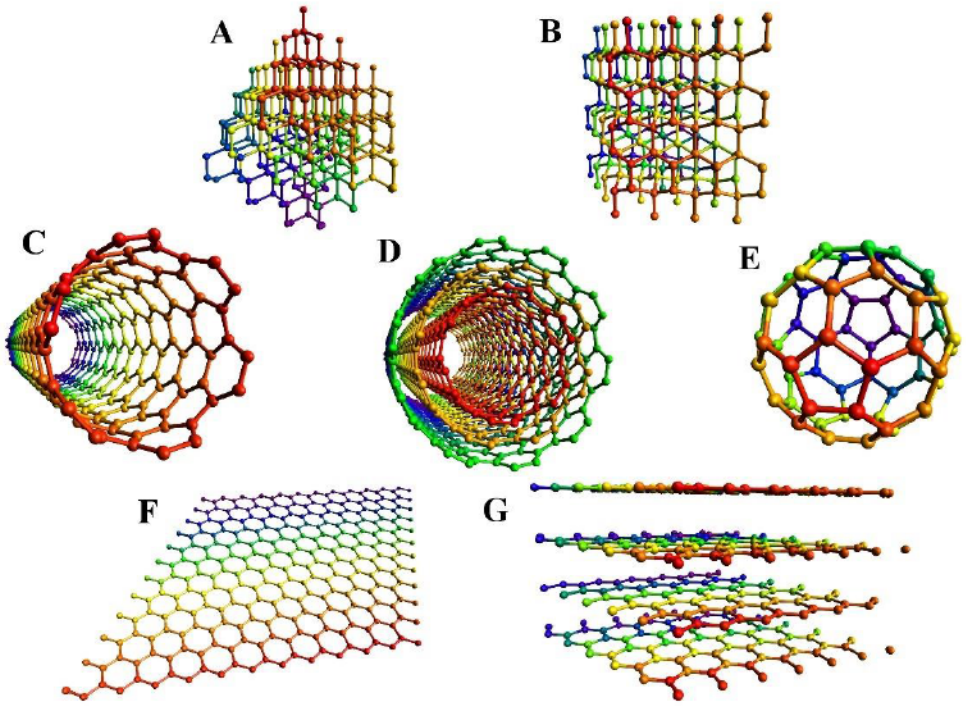

Figure 1: Examples of crystalline structure of several ordered carbon allotropes: A – diamond, B – lonsdaleite, C – single-walled carbon nanotube (SWCNT), D – multi-walled carbon nanotube (MWCNT), E – Fullerene C60, F – graphene, G – graphite.

2.2.1 Nanocrystalline Diamond

The diamond is a cubic crystal of sp3 bonded carbon atoms. It is one of the most resilient materials known to human both physically and chemically. The synthetic diamonds can be prepared by several methods including high pressure high temperature (HPHT) method (Abbaschian et al., 2005), detonation of TNT in low oxygen atmosphere (Ozawa et al., 2007) and ultrasound cavitation (Khachatryan et al., 2008). For covering of a large area of a substrate with a diamond layer the chemical vapor deposition (CVD) is probably the best choice. There are several types of CVD methods including hot filament HF CVD (Amaral et al., 2008a) and

microwave plasma assisted (MP CVD) (Kromka et al., 2009; Potocky et al., 2006). The nanocrystalline diamond is, as the name suggests, formed from nanosized diamond monocrystals with some sp2 phase at the crystal boundaries (Popov et al., 2007; Rubio-Retama et al., 2006). The MP CVD production process consumes cheap and available material – methane as a source of the carbon and hydrogen (Potocky et al., 2006). The fabrication process of NCD films enables a good control of crucial surface property – nanoroughness through polishing of underlying substrate or deposition time of the NCD. The size of the crystals is closely related to the amount of sp2 phase present between the diamond crystals in the material structure and basically governs the physical properties of the material from its electrical conductivity to Young's modulus (Williams, 2011). The possibilities of modification of the NCD include implantation of foreign atoms (Kromka et al., 2010), surface plasma treatment in various atmospheres and dry ion etching (Yoshikawa et al., 2006; Zhang et al., 2013). From the viewpoint of tissue engineering the topography and surface functionalization are the most important parameters. The size of the diamond grains and the topography influences the surface area where the interaction with the living matter occurs and the functionalization governs the molecular interactions on the diamond surface. The NCD used for our studies had crystal size ranging from 50 - 150 nm, i.e. in the nano- and low submicro-crystalline region. The intrinsic roughness measured as root mean square (RMS) of the profile height deviations from the mean line, recorded within the evaluation area of the diamond layer was in nano-region around 20 nm.

The studies presented within this thesis were preceded by publications pioneering the NCD biocompatibility studies (Kalbacova, Kalbac et al. 2007, Kalbacova, Michalikova et al. 2008). These studies ascertained a high biocompatibility of MP CVD produced NCD layer on Si substrate and pioneered the investigation of the influence of nanotopography and surface atomic termination on different cell types using SAOS-2 cell line and human mesenchymal stem cells (hMSC).

2.2.2 Graphene

Graphene is a rarity amongst nanomaterials. It is a single atom thick hexagonal lattice sheet of sp2 bonded carbon atoms. This nanomaterial, although

closely related to other carbon allotropes based on hexagonal lattice like fullerenes and carbon nanotubes (CNTs), is unique because of the integrity of its "macrosized" sheets with by definition nanosized thickness and also its electrical properties. Graphene is the principal component of naturally occurring graphite which is layered graphene bonded by van der Waals forces. This carbon allotrope attracted a lot of attention in recent years since Andre Geim and Konstantin Novoselov were awarded the Nobel Prize in Physics in 2010 for its preparation by exfoliation method (Novoselov et al., 2004). Since then other methods of preparation of this material were developed. Amongst them also the preparation by CVD on copper foil (Li et al., 2009) used for fabrication of large sheets of graphene for this work. The method is based on already known preparation of single-walled carbon nanotubes by CVD (Kong et al., 1998). Graphene is truly extraordinary nanomaterial considering its physical properties. It is one of the strongest if not the strongest material ever tested considering it is only one atom thick. Its tensile strength is 130 GPa (Lee et al., 2008), spring constant is ranging from 1 to 5 N/m (Frank et al., 2007) and Young's modulus is possibly exceeding 2TPa (Lee et al., 2012). The 2D character of graphene has tremendous advantages when considering the construction of biosensor. It has extremely fast electron motility and very low electric resistance which are hardly achievable with other materials (Geim and Novoselov, 2007; Novoselov et al., 2005). These characteristics were already utilized in construction of electric devices (Xia et al., 2009) and composite materials (Li et al., 2014; Ramanathan et al., 2008). The mechanical and electrical properties of graphene combined allow the construction of high quality low noise and mechanically and chemically stable biosensors (Feng et al., 2011, 2013; Shao et al., 2010). Before our first publication on graphene, there were no studies investigating the biocompatibility of large graphene sheets.

2.2.3 Single-Walled Carbon Nanotubes

The single-walled carbon nanotube (SWCNT) is artificially prepared carbon allotrope closely related to graphene or fullerenes. It can be described as a single graphene sheet rolled into a tube. The SWCNTs are one of several carbon nanotube materials studied in biomedicine alongside the multi-walled (Olivas-Armendariz et al., 2013) and double-walled carbon nanotubes (Ma and Wen, 2008). SWCNT are produced by arc discharge (Bethune et al., 1993), laser ablation (Thess et al., 1996),

CVD method (Kong et al., 1998) and gas phase catalysis (Nikolaev et al., 1999). The SWCNT used for preparation of the films studied in this thesis are were prepared by CVD process called High Pressure carbon monoxide (HiPCO) method (Bronikowski et al., 2001; Nikolaev et al., 1999). This method is suitable for preparation of high purity SWCNTs. Their unique physical properties range from extreme tensile strength and chemical durability to possibility of modification of their electrical conductivity. Depending on the chirality the SWCNT can achieve metallic conductivity or semiconductive state (Wildöer et al., 1998).

2.3 Biocompatibility of studied nanomaterials

Any candidate biomaterial must be tested for its potential harmfulness to human or eukaryotic tissues. However, biomaterials are often studied also for their antibacterial or bacteriostatic properties because this ability is wanted in the implantology or for disease treatment. Toxicity to eukaryotic cells and antibacterial effect are closely related topics. Considering toxicity and antibacterial activity of nanomaterials it must be distinguished between activity of free nanoparticles (diamond nanoparticles, graphene flakes, free CNT) and bulk materials like NCD or graphene layers and CNT surfaces. The toxicity of insoluble nanoparticles in general can be based on mechanical damage, accumulation and production of reactive oxygen species (ROS) (Li et al., 2008). Sharp NPs like graphene or CNT can cause mechanical damage (literally cutting and penetrating membranes) of cell organelles (Hu et al., 2010; Singh, 2016) disrupting osmotic and ion homeostasis. The surface chemistry of nanoparticles can influence the penetrability and toxicity of the NPs (Akhavan and Ghaderi, 2010; Movia et al., 2011). The surface termination influences production of radicals and ROS that in turn can damage all kinds of key organic molecules inside cells (Hsieh et al., 2014).

The biocompatibility of CVD grown diamond like carbon is studied using various cell types since it was prepared. Using human granulocytes *in vitro* and implantation in rats, Tang et al. already in 1995 proved that the CVD diamond has at least similar biocompatibility as the titanium and stainless steel used for implants at that time (Tang et al., 1995). Study of Bajaj et al. compared the adhesion of human carcinoma HeLa, rat adrenal pheochromocytoma PC12 and murine osteogenic MC 3T3 cell lines on platinum, silicon and thin MP CVD ultrananocrystalline diamond

(UNCD) (Bajaj et al., 2007). The study indicates that the UNCD substrate is the most suitable from the studied materials for the cell adhesion and spreading. Further studies on human osteoblast cell line MG63 confirmed biocompatibility of the HF CVD deposited NCD using human gingival fibroblast and human bone marrow osteoblasts (Amaral et al., 2008a, 2008b)

The biocompatibility of graphene was at least prior to our studies unknown. It could be estimated from the studies of related materials like carbon nanotubes or fullerenes. However, these materials have intrinsically a nanoparticulate character and are certainly not fully analogous to large graphene sheets in their dimensions. Also, the recent studies of graphene biocompatibility are often focused on graphene nanoflakes. A comprehensive review of graphene nanoparticle and composite cytotoxicity *in vivo* and *in vitro* was given by Pinto in 2013 (Pinto et al., 2013). Various effects were observed on different cell types depending on the concentration and chemical modifications of the graphene. Another way to estimate the graphene biocompatibility were the studies made on graphite. Agarwal et al. compared the biocompatibility of SWCNT film and reduced graphite oxide surface using PC12 neuroblasts. The results indicated higher biocompatibility of reduced graphite oxide and higher differentiation potential of this material (Agarwal et al., 2010). Liu et al. studied small graphene oxide flakes as possible substrate for construction of biosensors using ARPE-19 human retina epithelium cells. The results also promised good biocompatibility of the graphene oxide fixed on platinum substrate.

The biocompatibility of SWCNTs is often considered controversial. And again, parameters including the surface modification or functionalization, dimensions and purity determine the harmfulness of this material (Mao et al., 2013). The toxicity of SWCNT was studied from various aspects *in vivo* and *in vitro* often in free dispersed state; however, our SWCNT study was conducted on SWCNT film fixed on glass substrate.

Wang et al. studied the exposure of PC12 rat cells to long (20 μm) and short (2 μm) SWCNTs (Wang et al., 2011). The toxic effect was observed through production of reactive oxygen species, malondialdehyde, content of antioxidant glutathione in the cells. The toxicity was dependent on the dose and time of exposure. Comparison of PC12 cell adhesion on graphene oxide and SWCNT sheets in already mentioned study of Agarwal resulted in better adhesion on graphene oxide (Agarwal et al., 2010).

Important aspect of the SWCNT toxicity is also their purity. Production processes use various catalysts and SWCNT purification processes may be imperfect. The study of Kalbáčová et al. indicates that the high quality SWCNTs can be less toxic than carbon fibers (Kalbacova et al., 2006). Another work of Kalbáčová et al. showed that SWCNT films prepared from three types of SWCNT made by CVD, laser ablation and arc discharge can have all high biocompatibility if the SWCNTs were sufficiently purified (Kalbacova et al., 2007).

2.4 Applications of the Carbon Biomaterials

The carbon-based materials are studied for construction of bone implants and biosensors. The variety of carbon allotropes and their mechanical and electrical properties give the scientists the possibility to choose the right material for a particular application.

2.4.1 Implants and Their Coating

Materials suggested and used for implantation to human body are required to have certain properties that can be classified in several categories like physical and chemical resistance or degradability, ability to integrate in the living tissue, toxicity and mechanical properties. Some of the properties depend on the role of the material in the body. Hard carbon based material like diamond is suitable for bone implant coating. The materials used for production of long term bone implants are fabricated from various corrosion resistant metal alloys or ceramic and polymer materials. Ceramics and polymers can resist the corrosive environment of the body, however their mechanical properties are not suitable for all implant types and components (Osman and Swain, 2015). The metal based implants are highly mechanically durable and can withstand high chronic mechanical stress; however, even the most resilient metal alloys can suffer severe corrosion after several years in body (Bhola et al., 2011; Fojt et al.; Hansen, 2008). The corrosion can release metal ions and other corrosion products into human body and can ultimately result in mechanical failure of the implant leading to urgent reoperations (Ricciardi et al., 2016).

Osseointegration is promoted using various bioactive coatings including bioceramics (Webster et al., 2000), hydroxyapatite – the inorganic component of the

bone ECM (Ripamonti et al., 2012), ECM proteins, adhesion peptides (Khatayevich et al., 2010) and growth factors (Dingal and Discher, 2014; Dyondi et al., 2012; Iwata et al., 2012). The osseointegration can be also improved by increasing the surface area of the implant where the ECM proteins and cells can attach to the implant. This modification can be done on the submicro- and nano-level using various types of etching and polishing. Some coating provides micro-pores for the living tissue to grow inside the implant surface (Chen et al., 2011). Results of animal *in vivo* studies indicate that submicro- and nano- roughness can improve the stability of bone implants. Shalabi et al. wrote a review of studies comparing the results of bone to implant contact, push-out and torque tests of experimental bone implants in relation to their surface roughness. The general conclusion of the review is that with rising surface roughness the bone-to-implant contact improves (Shalabi et al., 2006). Similar results came out of a study made on commonly used titanium alloys proved that the material roughness in the nano- and submicro-region improves the cell adhesion compared to the flat titanium surfaces (Khang et al., 2008).

The carbon materials excel in some mechanical properties like hardness and tensile strength; however, the low elasticity and high fragility of some carbon allotropes limit their utilization as materials for whole implants. Pure carbon material - pyrolytic carbon - was already used for construction of metacarpophalangeal and carpal joint substitutes (Cook et al., 1999; Daruwalla et al., 2012). However, the carbon-based materials can excel as implant coatings. Bone implant surface coatings are meant to solve two major problems of the implants – resistance to corrosive conditions of living body and osseointegration. The chemical stability predestines the carbon based materials to be excellent implant coating and several studies already investigated this possibility (Alakoski et al., 2008; Amaral et al., 2008b; Grabarczyk et al., 2007; Spear and Cameron, 2008; Sui and Cai, 2006; Sui et al., 2007). Good osseointegration is conditioned by no inflammation. Stable carbon based materials promise at least no chemical irritation of the close environment. The osseointegration of the carbon materials can be improved by surface modification e.g. nanostructuring and also surface atomic termination possibly improving cell-implant adhesion.

2.4.2 Carbon Based Biosensors

Biosensor is an analytical electronic apparatus gathering physiological or biochemical information through physicochemical interaction of a detector with a living or biological component (tissue, cell, protein etc.). The correct function of such devices relies on high sensitivity and low electrical noise. Many carbon allotropes are compatible with such demands due to their high conductivity and low electric resistance. Some carbon allotropes were already studied for construction of various biosensors. Although a pure diamond is normally highly electrically insulating, fabrication of surface electrical channels can be achieved through modification of surface termination. However, the surface termination also influences the interaction of the material with living cells and it can significantly influence the signal from the biosensor.

Diamond is a very promising material for construction of "bio-sensing" devices because of possible surface and bulk electrical conductivity modifications (Kromka et al., 2010; Nebel et al., 2006). Scientists try to functionalize this material in many ways. For example, Rubio-Retama et al. immobilized the horseradish peroxidase (HRP) on the NCD surface creating a biosensor capable of sensing the presence of H_2O_2 (Rubio-Retama et al., 2006). Due to the possibility of modification of surface electrical conductivity, the NCD is also often tested with neuronal cells. Despite results of other studies the study of Chen et al. proved that differentiation of stem cells to nervous tissue can occur even on a very stiff surface made from hydrogen and oxygen terminated UNCD (Chen et al., 2009). Moreover, Thalhammer et al. studied formation of functional neuronal networks cultivated on NCD substrate (Thalhammer et al., 2010). Regarding the cell attachment on diamond with various terminations, the affinity to the surface can influence the measurements done with these sensors. The study of Chong observed the detachment force of normal human dermal fibroblasts and pheochromocytoma (PC12) cells on hot filament CVD microcrystalline (grain size 100-300nm) and nanocrystalline (grain size 5-10nm) diamond using AFM cantilever (Chong et al., 2007). The diamond is normally hydrogen-terminated and the authors also prepared oxidized diamond by UV irradiation in normal atmosphere and diamond functionalized by undecylenic acid. Regarding the surface functionalization, the highest detachment force was observed on UV – irradiated (oxidized) diamond, whereas the normal hydrogen-

terminated diamond proved to be the worst for the cell attachment. The nano-crystalline diamond providing more specific area proved to be better for the cell adhesion than the micro-crystalline diamond. The study of Lechleitner determined the cell adhesion on NCD and diamond powder surfaces with glass and tissue culture polystyrene (TC PS) as references (Lechleitner et al., 2008). The study used human kidney HK-2 cell line. Especially NCD proved to be a material better for cell adhesion than the glass surface. The study also observed the influence of the surface termination (O, H). In this case, O-termination was incomparably better for the adhesion of the kidney cells than H-termination. The article of Ariano describes the *in vitro* biocompatibility of artificial diamonds prepared by hot filament CVD (Ariano et al., 2009). Surface termination of the diamond was modified by hydrogen and oxygen to simulate the conductive and insulating channels, respectively on the diamond surface. Cell line of hypothalamic neurons (GT1-7) was cultivated on the diamond surfaces. In comparison to the tissue culture plastic the number of cells on the diamond was significantly lower. Despite the article does not provide a good comparison of the cell number on O- and H-terminated surfaces, it can be concluded that they did not differ significantly. Study of Rezek preceding this thesis investigated the difference in adhesion of several cell lines on NCD- SAOS-2, HeLa, HPdLF (Rezek et al., 2009). The study was done on a NCD surface with photolithographically prepared alternating oxygen and hydrogen stripes of various widths 30-200nm This arrangement again creates electrically conductive and insulating surface channels simulating biosensor arrangement as in the previous study. It was found that all the cell lines tend to adhere to the oxygenated NCD rather than to the hydrogenated NCD. The fluorescence staining of the adhering cells after 48 h of cultivation proved that the cells tend to align along the termination stripes always preferring the oxygen termination. The study also shows other important details of the cell adhesion to the surfaces with different wettability. Although the cells prefer the oxygen termination, they will adhere and grow on the hydrogen termination if there is no free oxidized surface and if they are in relatively high amount. Therefore, the hydrogenated surface can support the cell adhesion and proliferation. And the final and also important result of this work tells us that the fetal bovine serum (FBS) plays an important role in the preference of the oxygenated surface as the cells are unable or less likely to form stripes in experiments where the FBS was not added in the initial period of cultivation (2 h). It was also found that the

cells tend to align along the termination stripes already during this initial 2 h period. The article also presents the topography images of the FBS layer on O-NCD and H-NCD acquired by the AFM. The FBS layer was adsorbed on the NCD samples after 10 min and then the AFM force spectroscopy measurement was done. These results were obtained by our colleagues at the Institute of Physics CAS but are of noticeable biological relevance. The results indicate that the FBS proteins are present on both terminations but the thickness of the layer and topography differs indicating either different conformation or different composition of the layer (Rezek et al., 2009).

2.5 Specific Cell Adhesion

Specific adhesion of human cells is a process of direct interaction between a cell and components of ECM or other cells or an artificial. It is an important source of information about physical, chemical and biological character of environment and an irreplaceable source of biochemical stimuli for cells. Without the adhesion, so called "anchorage-dependent" cells undergo a type of apoptosis called by Frisch and Francis *anoikis* – a state without a home (Frisch and Francis, 1994).

2.5.1 Cell Adhesion Molecules

The cells adhere to their environment through various cell adhesion molecules (CAMs) divided in several families – integrins, cadherins, selectins and syndecans. The most prominent CAMs are probably integrins that bind proteins of ECM and in some cases also CAMs of other cells. A whole chapter is dedicated to teir description later.

Cadherins are a superfamily of mostly transmembrane proteins binding to other cadherin molecules on other cells together forming adherent junctions (zonulae adherentes) or desmosomes (maculae adherentes). Cadherins need calcium ions for their proper function as is reflected in their name. Binding calcium has a allosteric effect on cadherins and changes their elasticity allowing them to achieve conformation in which cadherins can interact (Sotomayor and Schulten, 2008). Small intracellular domain of cadherins is connected to actin cytoskeleton through proteins α-actinin and vinculin. Vinculin plays also an important structural role in later described integrin mediated adhesion. There are several types of cadherins that are

mostly tissue specific. Amongst the most prominent are E-cadherin present in epithelia, N-cadherin of neurons and placental P-cadherin. To the cadherin protein family belong also desmogleins present in desmosomes present in desmosomes and protocadherins.

Selectins, as the name again suggests, is a type of lectin – protein binding carbohydrates. They belong to C-type lectins requiring calcium to bind. There are three cell specific members of selectin family. E-selectin is present in endothelial cells, L-selectin is expressed by leukocytes and P-lectin is on surface of platelets and endothelial cells. Selectins play important role in homing of leukocytes to sites of inflammation (Ley, 2003).

Syndecans are proteins acting like a backbone for several GAG (heparan sulfate, chondroitin sulfate) chains that are binding to ECM proteins like collagens and fibronectin. GAG chains of syndecans also function as coreceptors helping in binding of some growth factors (FGF, EGF, VEGF) to their receptors (Elfenbein and Simons, 2013).

2.5.2 Integrin Mediated Adhesion

Integrins are receptors providing mainly the adhesion with the surrounding ECM or its soluble components adsorbed on a surface e.g. *in vitro*. However, some types of integrins can also specifically attach to other CAMs exhibited on surfaces of certain cell types (Humphries, 2006; Luo et al., 2007). Integrins form heterodimers constituted from non-covalently bound α and β subunits. There are 18 α subunits and 8 β subunits known today in mammals (Barczyk et al., 2010; Hynes, 2002; Takada et al., 2007). The α subunits are responsible for the integrin specificity (Barczyk et al., 2010), whereas the β subunits play more important role in intracellular interaction with mechanotransducing proteins and signaling molecules.

Together with their anchoring function integrins are also involved in signaling. Integrins participate in both inside-out and outside-in cell signaling. Before the interaction with ECM the integrins are present in cell membrane in an inactive bent state. They are activated upon intracellular interaction with proteins like talin and kindlin. This activation is part of the inside-out integrin signaling because talin and kindlin change their affinity to the intracellular domains of integrins in dependence on other signaling cascades. (Calderwood et al., 2013; Critchley and

Gingras, 2008; Karakose et al., 2010). The integrin heterodimers depending on the type of integrin subunits then specifically recognize amino-acid sequences in proteins of the ECM or serum. The most prominent is probably RGD present in fibronectin or GFOGER in collagen (Barczyk et al., 2010; Knight et al., 1998). However, there are many other amino-acid sequences that have been studied as often tissue specific adhesion peptides (Deng et al., 2014). The integrin receptors form at least 24 known heterodimers with affinity to various substrates. Some integrin dimers are more universal - binding to a variety of commonly present substrates like collagens, fibronectin and vitronectin (αVβ1, αVβ3, α5β1) (Barczyk et al., 2010; Humphries, 2006). Others are specialized - found only in some cell types e.g. leukocytes that have a specific integrin dimers αLβ2, αMβ2 (Lahti et al., 2013). Upon binding to its substrate, the integrin molecules are in turn involved in outside-in signaling influencing the cell survival adhesion, actin contraction – motility, proliferation and differentiation.

As was already mentioned, the integrin receptors specifically recognize certain protein moieties and amino acid sequences present in ECM proteins. In *in vitro* conditions the integrin receptors of anchorage dependent cells bind to protein layer formed on the substrate (often TC PS or glass). The source of the adhesion proteins like fibronectin and vitronectin is FBS - a standard additive to tissue culture cultivation media. Precise composition and concentrations of proteins in a particular FBS lot is hard to determine since every source calf is different (Zheng et al., 2008). This fact can sometimes cause problems with experiment reproducibility. However, FBS is a hardly replaceable medium additive because it contains e.g. growth factors essential for maintaining cell signalization important for cell proliferation and survival.

2.5.3 Focal Adhesions

Focal adhesions (FA) are sites of attachment of cells to surrounding extracellular matrix. Upon the attachment to their extracellular protein ligand the integrin receptors can become part of FA. The FAs are multiprotein complexes composed of mechanotransducing, signaling and adaptor molecules. Nascent FAs are formed at the cell edge in protruding filopodia and lamellipodia. As the cell migrates over them, the focal adhesions grow and maturate. Some authors recognize three

distinguishable stages of FA maturation – 1) focal complexes, 2) focal adhesions *sensu stricto* and 3) fibrillar adhesions (Biggs et al., 2009; Parsons et al., 2010). These three FA types differ in size and cell localization. The focal complexes are small adhesions found at the cell edge, the focal adhesions *sensu stricto* are larger and in the cell periphery and the fibrillar adhesions are the largest adhesion sites often present more to the cell center. The integrin composition of these three stages also slightly differ. For example, the fibrillar adhesions have high content of α5β1 integrins binding fibronectin and intracellularly the protein tensin is more present (Biggs et al., 2009; Geiger et al., 2001). The complexity of molecular interactions within the focal adhesions was outlined already in 2001 in summarizing article of Zamir and Geiger (Zamir and Geiger, 2001) (Figure 2).

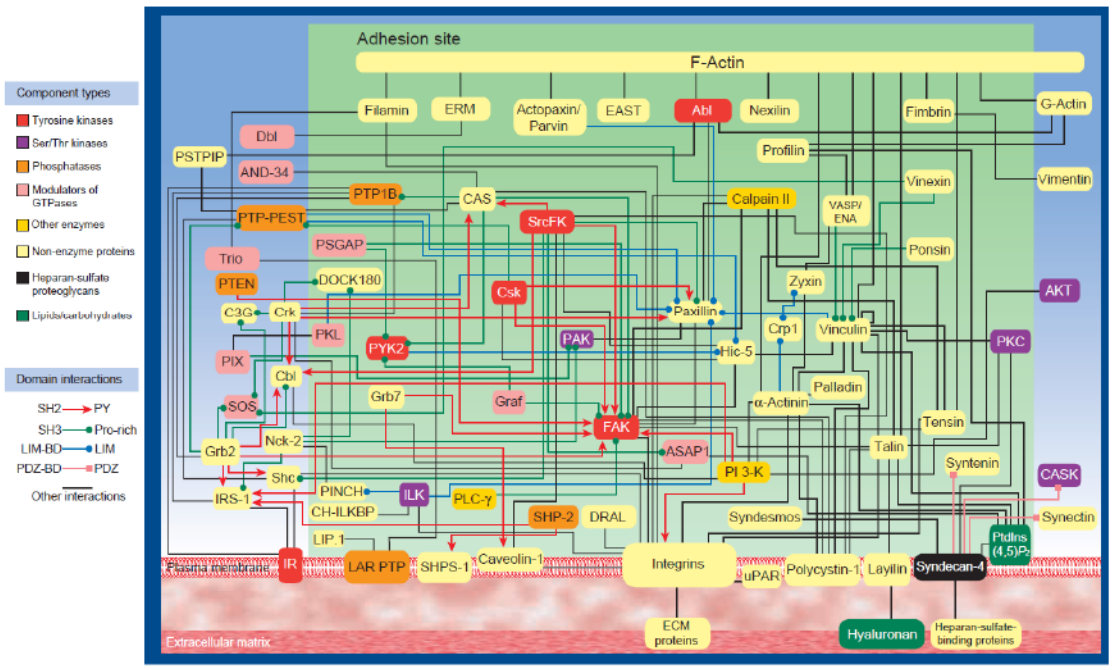

Figure 2: Scheme of molecular interactions in focal adhesion (Zamir and Geiger, 2001).

This review also pointed out the molecules with most interaction partners like mechanostransducing talin, vinculin and α-actinin and signaling protein tyrosine kinase 2 also called focal adhesion kinase (FAK). Three layers were later distinguished in the FA structure – integrin signaling layer, force transducing layer and actin regulatory layer (Kanchanawong et al., 2010) (Figure 3). The signaling layer is occupied by proteins like focal adhesion kinase (FAK) and signal transduction adaptor paxillin. The mechanotransducing molecules like talin and

vinculin transfer the tension from the integrin receptors to the actin cytoskeleton (Parsons et al., 2010). The actin regulatory layer is occupied by α-actinin crosslinking actin filaments and VASP protein promoting the filament elongation. The authors used interferometric photoactivated localization microscopy to identify the type and position of several FA associated proteins including integrin αV, vinculin, FAK, zyxin, talin, paxilin, α-actinin and actin.

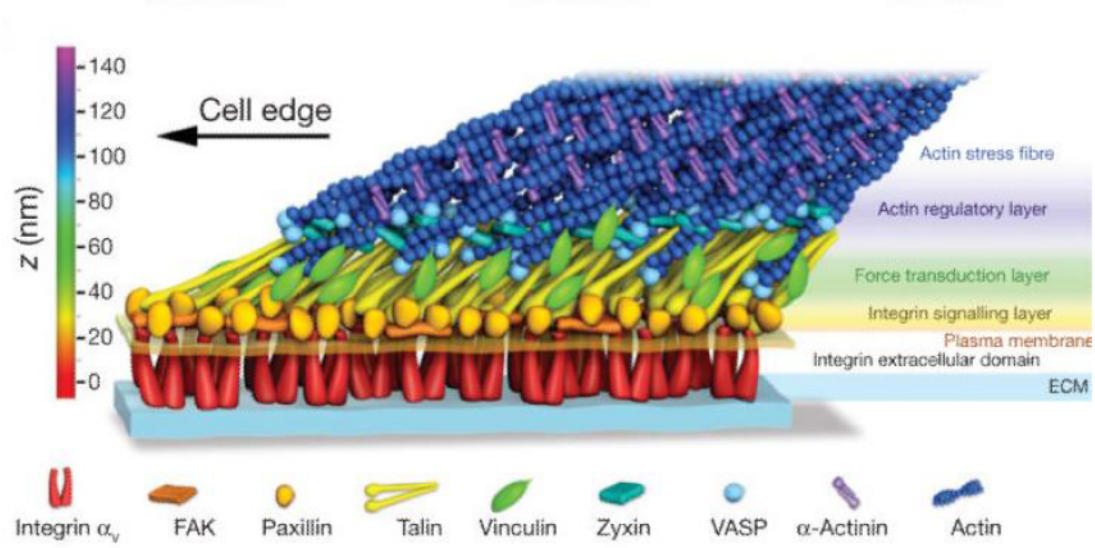

Figure 3 : Schematic model of focal adhesion molecular architecture, depicting experimentally determined protein positions. Note that the model does not depict protein stoichiometry (Kanchanawong, 2010).

2.6 Focal Adhesion Signaling, Substrate Sensing and Cell Fate Direction

The FA signaling is centered around two molecules - integrin-linked kinase (ILK) and already mentioned FAK. Recent results have proven that ILK which was originally described as a serine/threonine kinase (Hannigan et al., 1996) is actually a pseudokinase and acts more like an adaptor protein (Fukuda et al., 2011). The ILK can be part of various signaling pathways depending on which isoforms of other associated proteins like parvin or PINCH the ILK binds. The ILK signaling can e.g. influence the actin cytoskeleton organization through phosphorylation of cofilin and actomyosin contractility through ROCK signaling (Widmaier et al., 2012).

Nevertheless, most of the FA signaling is centered around the FAK. This cytoplasmic tyrosine kinase gets activated upon interaction with integrins by autophospholrylation on tyrosine residue (Y397) (Shi and Boettiger, 2003). However, FAK has several other phosphorylation sites propagating the signal to

various pathways (Schlaepfer et al., 1994). FAK functions not only as a signaling kinase but also as a scaffold or an adaptor (Schlaepfer et al., 2004) for other signaling molecules. Together with proteins like P130cas adaptor protein (Cary et al., 1998) and Src kinase stimulates a variety of signaling pathways. The interaction of FAK with PI3K is already known for at least two decades (Chen et al., 1996). PI3K is a key enzyme in Akt/PKB signaling pathway promoting cell survival and growth. FAK also influences signaling of receptor PTK (Schlaepfer et al., 1994). Several studies also proved that FAK plays important role in regulation of cell cycle and that disruption of the FAK function leads to the cell cycle arrest (Lim et al., 2008; Pirone et al., 2006; Zhao et al., 1998).

2.6.1 Cell Spreading and Motility

Upon the initial cell attachment to a substrate, the anchorage dependent cells start to spread on the substrate. Proper spreading is the indicator of good anchorage and adhesion to the surface. Cell spreading can be divided to "early" and "late" stages. The initial cell adhesion is driven probably exclusively by physicochemical interaction between the cell and substrate. It does not differ between cell types on wide variety of substrates and does not require any energy from the cells (Cuvelier et al., 2007). The late stage of cell spreading is typical by active membrane deformation driven by actin polymerization and myosin contraction requiring energy.

One of the most important functions of FA signaling is regulation of cell motility and cytoskeleton dynamics. However, the cell migration is a complicated process and its direction and speed can be also influenced by many external and internal factors. Amongst the most common mechanisms of cell migration is chemotaxis following the gradients of chemical attractants or repellents but also haptotaxis directed by the adhesiveness of underlying substrate (Charras and Sahai 2014). Several studies showed that the quality of the cell attachment to its surroundings (ECM or serum proteins) influences the speed of the cell migration - too firm or too weak cell adhesion can lead to poor cell motility (Palecek, Loftus et al. 1997, Gupton and Waterman-Storer 2006). There is also a difference between single cell migration and collective cell migration where the attaching cells migrate as a group in which every cell can have its own specialized role depending on the position of the cell inside the cell collective (Rorth 2009). Some studies proved that

the cells react to the micro- and nano-topographical features of the substrate - mostly oriented grooves and ridges - by polarization and elongation alongside the underlying features (Kim et al., 2009; Walboomers and Jansen, 2001). Even the migration speed can be controlled by the depth of the nanotopographic features. If the surface topography and chemistry allows the integrin bonding and assembly of a focal complex, the FAK then plays an important role in the actin cytoskeleton organization and action of the myosin molecular motors. The FAK signaling stimulates the actomyosin action through RhoA GTPase – ROCK signaling pathway (Mitra et al., 2005). By action of actin associated molecular motors – myosins activated by myosin light-chain kinase (MLCK) – cell expresses mechanical forces on the surface through FAs and migrates. Stimulation of Rho GTPase signaling also increases production of filopodia and lamellipodia which leads to promotion of cell migration.

2.6.2 Substrate Sensing and Differentiation

Cell fate and differentiation can be influenced not only by biochemical signals but also by mechanical and topographical properties of the cell niche (Murphy et al., 2014). Higher substrate stiffness results in higher isometric strain in FAs and actin cytoskeleton of anchorage dependent cells. It was proven that the cytoskeleton strain can influence the differentiation commitment of hMSCs through RhoA/ROCK signaling pathway (McBeath et al., 2004). The work of Engler et al. proved that the differentiation of hMSCs can be directed by the substrate stiffness (Engler et al., 2006). The expression profiles indicate that the low substrate stiffness (0,1 - 1 kPa) directed hMSCs towards neuronal differentiation, middle stiffness (11 kPa) towards muscle differentiation and high stiffness (34 kPa) towards the bone differentiation. The cytoskeleton of the cells was more ordered on stiffer substrate compared to the soft substrates indicating the bone differentiation. On the other hand, the cells cultivated on soft substrates had more intermediate neurofilaments indicating the neuronal differentiation.

The topography of the surface plays also an important role in the cell adhesion and differentiation. Solid nanotopographical features are present especially in connective tissues. For example, the bone cells adhere to ECM predominantly consisting of collagen fibers intertwined with the inorganic hydroxyapatite crystals forming an environment with nanotopographical features in order of magnitude of

tens of nanometers (Stevens and George, 2005). The study of Teo et al. demonstrated, that polydimethylsiloxane substrate nanograting with pitch 500 nm induced production of neurogenic and myogenic markers (Teo et al., 2013) in hMSC. On the other hand, Watari et al. found out that grating with pitch 400 nm in the same matrix induced osteogenic response in hMSC.

Other works investigating artificial adhesion nanodomains on non-adhesive matrix found that there is a distance between the adhesion sites inhibiting the cell adhesion around 70 nm (Cherniavskaya et al., 2005). This distance is probably based on the fact the length of talin protein connecting intracellularly the integrin dimers is around 50 nm. The work of Dalby et al. examined the influence of spacing and orderliness of nanoscale topography (nanopits in poly(methyl methacrylate) substrate) on the cell differentiation (Dalby et al., 2007). The study proved that the cell adhesion and production of bone differentiation markers osteocalcin and osteopontin was highest on a slightly disordered nanotopography pattern as opposed to a highly-ordered square or hexagonal grid of nanopits.

Direct mechanical influence on the cell nucleus plays also very important role. The work of Maniotis et al. proved that there is a direct connection between the integrin based adhesions and nucleoplasm (Maniotis et al., 1997). This connection is mediated by actin fibers and intermediate filaments. The connection between the cytoskeleton and the nuclear lamina is provided by LINC complex, namely nesprin and SUN-domain proteins (Dahl et al., 2008). The work of Gupta then proved that the actin dependent nucleus deformation influences the gene expression in T-cells (Gupta et al., 2012). Deligianni et al. proved that the hydroxyapatite polished by SiC paper with grit 1200 stimulated the activity of alkaline phosphatase (ALP) – a marker of osteo-differentiation – more compared to higher roughnesses (polished with paper 600, 180) (Deligianni et al., 2000). Mack et al. proved that the differentiation to smooth muscle is regulated through small GTPase RhoA signaling which is one of the pathways influenced by the FAK (Mack et al., 2001). Study of Avizienyte et al. indicates that Src and FAK integrate signaling from integrin mediated adhesions and cadherin and that both these molecules are involved in the epithelial-to-mesenchymal transition (Avizienyte and Frame, 2005). This suggest that the cell dedifferentiation can be also induced through the cell - matrix adhesion.

In *in vitro* conditions, differentiation media containing specific chemicals are used for artificial induction of differentiation of stem cells into various cell types. In

this study, the osteogenic differentiation medium in some experiments was used because the supposed utilization of the nanomaterials is in bone implants. The osteogenic differentiation medium contains three key compounds apart from standard cultivation medium – ascorbic acid, glycerolphosphate and dexamethasone. Ascorbic acid is a key compound needed as a cofactor for posttranslational modification by enzymes lysyl-hydroxylase and prolyl-hydroxylase, modifying respective amino-acids lysine and proline in collagen chain to hydroxylysine and hydroxyproline. Both modifications are important for creation of the triple helix structure of collagen molecule. Hydroxylysin residues are used by lysyl-oxidase for aldol condensation between collagen molecules creating collagen fibrils. On the other hand, hydroxyproline amino-acid twists the tropocollagen molecules allowing creation of typical collagen triple helix. Glycerolphosphate functions as a source of inorganic phosphate for creation of hydroxyapatite – the inorganic part of the bone matrix. Inorganic phosphate is also known to act as a signaling molecule promoting osteogenic differentiation. Finally, dexamethasone is a corticosteroid hormone penetrating due to its hydrophobic character the cell membrane and influencing expression of several genes promoting the osteogenic differentiation. Langenbach and Handschel summarized the osteogenic dexamethasone effect in their review (Langenbach and Handschel, 2013). Dexamethasone promotes transcription of three key genes: 1) Four and a half LIM-domain protein 2 (FHL2), 2) transcriptional coactivator with PDZ-binding motif (TAZ) and 3) mitogen-activated protein kinase phosphatase (MKP-1). FHL2 helps to transfer β-catenin to cell nucleus where it binds to LEF-1/TCF transcription factor and induces the transcription of Runt related transcription factor 2 (Runx2) gene. Runx2 is a key osteogenic transcription factor promoting production of collagen I, osteocalcin (OC), osteopontin (OP), fibronectin and bone sialoprotein II. MKP-1 modulates the phosphorylation of Runx2 protein and regulates its activity. TAZ protein in turn binds to Runx2 and helps to recruit core components of the transcriptional machinery and therefore helps to initiate Runx2 controlled transcription (Figure 4).

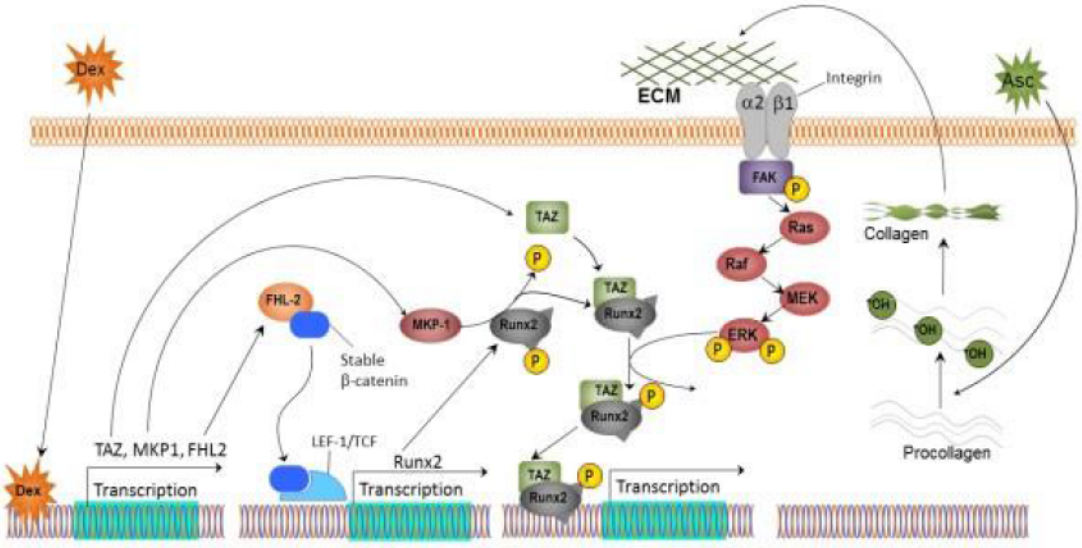

Figure 4: Scheme of osteogenic effect of dexamethasone. Dexamethasone directly promotes transcription of TAZ, MKP1 and FHL2 genes. FHL2 protein stabilizes the catenin molecule that in turn helps to promote the transcription of RUNX2 gene, one of the key osteogenic transcription factors. MKP1 dephosphorilates RUNX2 that in turn allows binding of the TAZ on RUNX2 that recruits transcriptional machinery and promotes RUNX2 controlled production of osteogenic markers like Col1A1 (Langenbach and Handschel, 2013).

2.7 Non-Specific Cell Adhesion

Eukaryotic cells as well as bacteria are surrounded by a "forest" of membrane glycoproteins, glycolipids and polysaccharides called glycocalyx. This glycan layer serves various purposes. It forms protection against chemically and biologically aggressive environment to enhancement of adhesion to various substrates and creation of suitable microenvironment. Some cell types, namely epithelial cells may have the layer more developed than other cells. The glycans constitutes 2 - 10 wt. % of their cytoplasmic membrane (Martins and Abairos, 2002). The non-specific initial cell adhesion is based on non-covalent bonds of these organic macromolecules on the cell surface with the substrate. The interaction is not necessarily mediated by the CAMs; however, they are certainly not excluded, as they are also highly glycosylated. The contribution of the non-specific interactions to overall adhesion strength can be significant. It plays an important role in early phase of the cell-substrate attachment *in vitro*. Lee et al. studied the cell detachment force using the AFM cantilever on alkylsilane self-assembled monolayers (SAM) with various terminal function groups (epoxide, COOH, NH_2, CH_3) (Lee et al., 2005). The highest detachment force was observed on the NH_2 terminated alkylsilanes. This adhesion force was probably even

greater than to surface with immobilized RGD peptides those were proved to be common and efficient adhesion peptide sequences. Moon et al. suggests that the adhesion mediated by heparansulfate proteoglycans on cell surface may constitute up to 33% of the adhesion force of endothelial cells (Moon et al., 2005). To similar results came the study of Loomis about adhesion of soil-living amoeba *Dictyostelium discoideum* (Loomis et al., 2012). This organism does not use the integrin mediated adhesion for attachment and migration in its environment. The study revealed that the cell adhesion is significantly weakened by addition of oligosaccharide cleaving alpha-mannosidase to the cultivation conditions. This again points on the surface glycans as important non-specific cell adhesion molecules. The authors also suggest that van der Waals force is the main interaction responsible for the non-specific adhesion. Important information about the issue of unspecific interaction of cells with substrate brought us the studies of Cohen and Zaidel-Bar (Cohen et al., 2003, 2006, 2007; Zaidel-Bar et al., 2004). The articles describe the integrin independent interaction of rat RCJ-P chondrocytes and A6 *Xenopus laevis* endothelial kidney cells based on interaction of GAG hyaluronan layer on the surface of the cells with substrate. The results suggest that the hyaluronan interaction with the substrate triggers outside-in signaling leading to the integrin based adhesion and inside-out signaling causing a thinning of the GAG layer.

3 Materials and Methods

3.1 Biomaterial Preparation

All the tested biomaterials were prepared by our colleagues at our cooperating institutions – Institute of Physics and Jaroslav Heyrovský Institute of Physical Chemistry both of the Czech Academy of Sciences. The preparation methods are described in detail in corresponding publications. A brief summary of material fabrication is written below.

3.1.1 Nanocrystalline Diamond

The NCD materials were grown by the microwave plasma chemical vapor deposition (MP CVD) method on silicone or transparent fused silica (for life-cell imaging) substrates using methane containing hydrogen atmosphere. Methane was the source of carbon for diamond growth. The surface topography was controlled by

polishing of the underlying silicone substrate or by dry ion etching using different masking materials (nickel, gold, diamond powder). The surface chemistry was modified by exposition to a plasma discharge in oxygen and hydrogen atmospheres resulting in different wettability and surface energy. Photolithography processing was in some experiments used for preparation of various surface termination patterns (Figure 5).

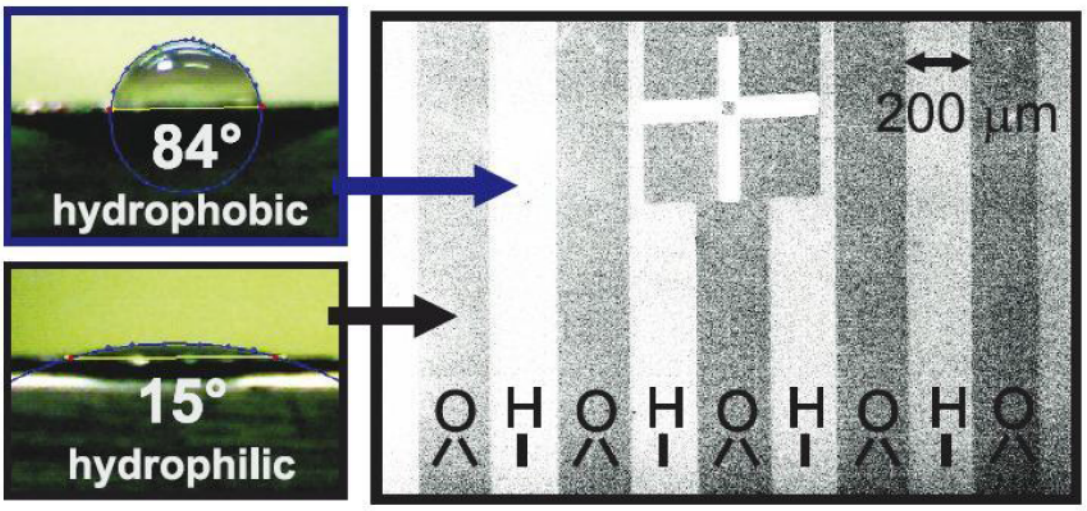

Figure 5: SEM image of a nanocrystalline diamond layer with 200-µm-wide stripes with alternating hydrogen and oxygen termination. Light stripes correspond to the hydrogen surface due to its low electron affinity. The cross in the upper part of the image is made up of a thin layer of gold and serves as a mark for the differentiation of particular stripes. Typical measurements of wetting angle on the two types of diamond surfaces (uniformly terminated) are shown along the left side of the SEM image (Rezek et al., 2011).

3.1.2 Graphene

The graphene layers were also fabricated by the CVD method. The graphene layer was deposited on a copper foil also from a methane containing hydrogen atmosphere. The copper foil was annealed in H_2 gas flow at 1000°C before the deposition then the foil was exposed to H_2 and CH_4 and the substrate was cooled down to 500°C. The graphene layer was transferred to Si/SiO_2 substrate using polymethylmethacrylate (PMMA) resist. The surface of the graphene was in the later studies treated with flow of O_2 gas (100sccm) or H_2 (250 sccm) + Ar (150 sccm) in 500°C to achieve oxidized hydrophilic surface (contact angle (CA) = 58°) or hydrogenated hydrophobic surface (CA = 90°) in order to influence the cell adhesion.

3.1.3 Single-Walled Carbon Nanotube Films

Super purified SWCNTs prepared by high pressure carbon monoxide (HiPCO) were used for the fabrication of SWCNTs films. The SWCNTs were sonicated in N-methylpyrrolidone, then filtered through a membrane filter and washed with ethanol and water. The film on the membrane filter was transferred onto a microscopic cover glass. The samples were heated at 450 °C in a flow of argon and hydrogen for 30 min. Their surface chemistry was then modified by plasma discharge in this case only by oxygen for three time periods – 1 min, 5 min, 30 min – resulting in surface oxidation and change in wettability (respective CA = 21°, 11°, 12°) and surface topography. The surface of SWCNT films without the oxygen treatment was hydrogenated and hydrophobic (CA = 100°).

3.2 Pre-Cultivation Material Treatment

Upon delivery from the manufacturing institutions the samples were held in dry state in containment vessels to avoid any unnecessary contamination. The samples were handled with care using sterile tweezers. Before any biological experiments, the materials were sterilized in 70% ethanol (in water) for 10 minutes. The samples were then washed by sterile water and let dry under sterile conditions.

3.3 Tissue Cultures

Because the tested biomaterials were often considered for an application in bone regeneration medicine, the adherent human osteoblast cell line SAOS-2 was used for most of the experiments. Several experiments were conducted using human bone marrow cells as a source of mesenchymal stem cells (hMSCs). The cells were cultivated and the experiments were performed under standard cultivation conditions 5% CO_2 atmosphere and 37°C in recommended cultivation media. The cells stocks were held in 25cm^2 and 75 cm^2 polystyrene culture flasks (TPP). The passage and harvest of the cells was performed using Trypsin in EDTA.

3.3.1 Osteoblast-Like Cell Line

SAOS – 2 is a human cell line derived from primary osteosarcoma of 11-years old Caucasian girl (Fogh et al., 1977; 1975). The doubling time of this cell line is about 43h. Stock cells were grown in McCoy's 5A medium (BioConcept - Amimed) with heat inactivated 15% fetal bovine serum (PAA). Freezing of SAOS-2 stocks was performed in McCoy's 5A medium with 25% FBS and 10% DMSO. The media were supplemented with Penicillin (20 U/ml) and Streptomycin (20 g/ml) (Sigma-Aldrich).

3.3.2 Primary Human Mesenchymal Stromal Cells

hMSCs for the experiment were provided by the Department of Hematology of the General Faculty Hospital in Prague. The hMSC were obtained with informed agreement from patients of the department. The patients had no diagnosed bone marrow disease. The cells used for the experiments were in the 2nd and 3rd passage. The hMSC were cultivated in AlphaMEM (Gibco) cultivation medium supplemented with 10% FBS. Storing and freezing of the hMSC stocks were performed in AlphaMEM medium with 20% FBS and 10% DMSO.

3.4 Fluorescence Staining

The fluorescence staining was done using standard protocol for this procedure. The stained cell compartments were cell nucleus stained by DAPI (Sigma-Aldrich) and actin cytoskeleton stained by phalloidin with Alexa Fluor 488 tag (Invitrogene). Immunofluorescence staining was targeted on:

1) **vinculin** - mouse monoclonal IgG1 (Sigma), dilution 1:150 with secondary antibody AlexaFluor 568 goat anti-mouse (Invitrogen), dilution 1:1000

2) **Y397 phosphorylated focal adhesion kinase** (pY397 FAK) - rabbit polyclonal (Invitrogen), dilution 1:100, with secondary antibody AlexaFluor 488, goat anti-rabbit (Invitrogen), dilution 1:1000

3) **osteocalcin** - mouse monoclonal, IgG1 (R&D Systems), dilution 1:150 with secondary antibody AlexaFluor 555 goat anti mouse IgG1 (Invitrogen), dilution 1:1000

The staining procedure was done according to the following protocol:

1) Fixation with 4% Paraformaldehyde for 10 minutes at room temperature
2) Wash with PBS
3) Permeabilization with 0,1% Triton X-100 in PBS
4) Wash with PBS
5) Block with 1% FBS and 0,05% Tween in PBS
6) Staining with primary antibody for 1 h, 37°C
7) Wash with PBS 3x
8) Staining with secondary antibody, DAPI and Phalloidin+AF488 for 1 h, 37°C
9) Wash with PBS 3x
10) Mount of the sample under cover glass and on the microscopy glass (Shandon Immumount Termo Scientific)

3.5 Fluorescence Microscopy

3.5.1 Widefield Fluorescence Microscopy

The fluorescence microphotographs were acquired on microscope systems of Nikon Corporation. The widefield images were photographed on fixed samples using Nikon E400 or Nikon TiS statives. The widefield images were photographed with objective Plan Achromat 40× (NA = 0.65). The fluorescence excitation source was Hg lamp.

3.5.2 Confocal Fluorescence Microscopy

The confocal scanning acquisition was done on Nikon TE 2000 E equipped with confocal scanning head C1si. For the confocal imaging an objective Apochromat TIRF 60× (NA = 1.49) was used. Excitation laser wavelengths used for confocal microscopy were 405nm (DAPI), 488 nm (Alexa Fluor 488), 543nm (Alexa Fluor 568).

3.6 Live-Cell Imaging

The life cell imaging of SAOS-2 cells adhering on NCD substrates with different surface termination was conducted under standard tissue cultures conditions. The cells were held in 37°C and 5% CO_2 atmosphere in OkoLab Bold Line Top Stage Incubator (type H301). The cells were photographed using objective Plan Fluor 4x (NA = 0.13) by phase contrast technique.

The acquired phase contrast image sequences were transformed to binary images using image thresholding in ImageJ (NIH) software. Dark cell nuclei became well distinguishable objects suitable for cell counting and tracking analysis. Cell number was counted from each image of the sequences using NIS-Elements (LIM) software. Growth curves of SAOS-2 cells on O-NCD and H-NCD were then plotted using the acquired cell number data. Doubling times for each experimental setup were then counted using Doubling Time Calculator (Roth, 2006).

The binary sequences were then analyzed using the Advanced Tracking Module (ATM) in NIS-Elements software. The ATM can track high number of objects in the image sequence. The ATM allowed to set various parameters of the tracking including maximum displacement of tracked object, maximum allowed variation of direction of object movement and tracking model (random/constant/circular movement).

From each cell track the starting and the end position of the track were acquired and the displacement of each cell was counted. The displacement vectors were then plotted using R statistical software with “splancs” library.

3.7 Computer Image Analysis

Computer image analysis was used in our studies in several cases. From fluorescence images of stained cells, the cell number and cell area on opaque samples (NCD, Graphene on Si wafer, SWCNT surfaces) was measured. Both parameters were automatically acquired from the images using freely available software Cell Profiler developed in Broad institute (MIT, USA). The software uses module based pipeline script structure for image adjustment and parameter measurement. The cell number was counted on the basis of DAPI stained nuclei using automatic thresholding based on the Otsu algorithm (Otsu, 1979) (Figure 6).

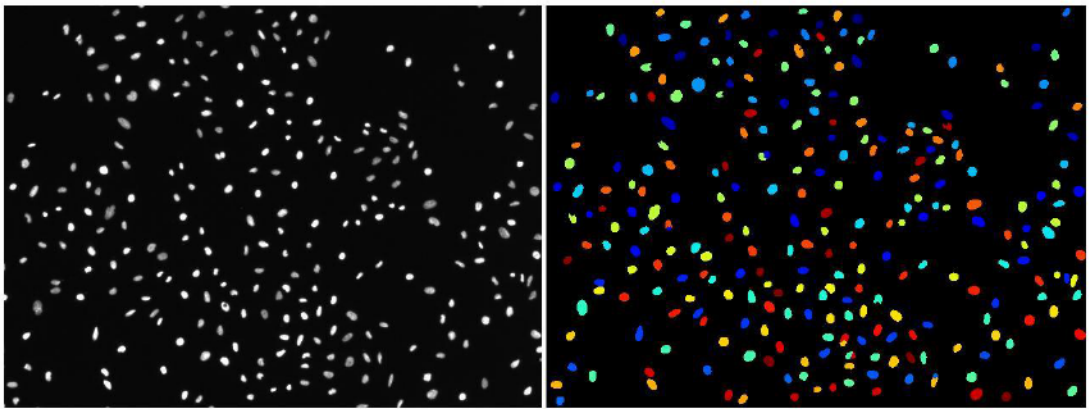

Figure 6: Cell counting: Left image – grayscale image of cell nuclei stained by DAPI. Right image – output from the cell counting in the Cell profiler application. Nuclei are distinguished by colors.

The cell area was measured on basis of actin staining. Each cell was recognized on the basis of DAPI stained nucleus and then the algorithm searched the surrounding for the actin staining (Figure 7).

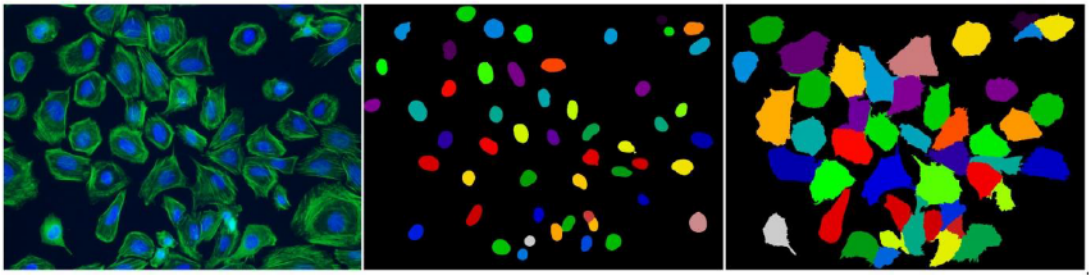

Figure 7: Cell size measurement: Left image – original 2-channel image (blue - nuclei, green – actin), Middle image –binary image of recognized cell nuclei, right image – binary image of recognized cells.

In some studies, the FA dimensions - long and short axes and FA area and number - were measured. Immunofluorescence staining of protein vinculin was used for visualization of FAs. Long and short axes of FAs were semi-manually measured using NIS-Elements (LIM).

For measurement of FA a self-made Java macro for open source ImageJ software was used. This macro automatically clears bright soluble vinculin background inside the cells by subtraction of background image created from the original image by sequence of minimum, maximum and Gaussian mathematical filters with radius size adjusted according to the searched object (FA) diameter. The

FAs were then localized by automatic thresholding with Otsu algorithm from the adjusted image and their area was measured by ImageJ (NIH) software (Figure 8).

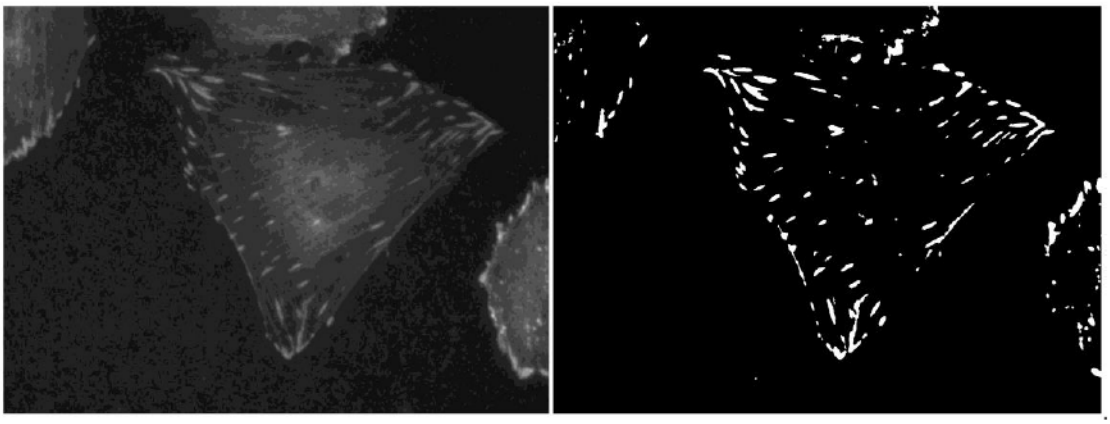

Figure 8: Focal adhesions highlighting for parameter measurements. Left image – grayscale image of vinculin staining. Right image – binary image of FAs.

Confocal images of triple-stained cells (nuclei/actin/vinculin) were deconvolved (each color channel separately) using Huygens Pro (Scientific Volume Imaging, Netherlands) software utilizing the classic maximum likelihood estimation algorithm with measured point spread function for each wavelength. The deconvolution was used to acquire sharper images with better resolution. The deconvolved images were then rendered using Imaris (Bitplane, Switzerland).

3.8 Statistical analysis

For finding of statistically significant differences in cell number, cell area, FA area on multiple samples (3 roughnesses, 3 nanostructures and controls etc.) Analysis of variance (ANOVA) and Kruskal-Wallis tests were used depending on the conditions for using the tests (data normality, same variance). The statistical analysis was done in software Statistica (Statsoft).

3.9 Test of Cell Metabolic Activity

The MTS test (Cell titer96®, Promega) is a procedure used for quantification of cell metabolic activity or an indirect measure of cell count. It is a colorimetric method based on the reduction of yellow MTS tetrazolium compound to dark red

Formazan by NADPH and NADH in cell mitochondria. The tetrazolium compound is added to a cultivation medium and poured in a cultivation chamber or well. The reaction time is at least 2h. The absorbance was measured on ELISA reader Synergy II (BioTek).

3.10 Scanning Electron Microscopy

Scanning electron microscopy was used for detailed observation of contact of cells with nanostructured NCD. The cells for scanning electron microscopy (SEM) were grown on nanostructured NCD samples under the standard cultivation conditions for 48h. The NCD samples with cells were fixed with 2,5% glutaraldehyde (GA) for 1h and then left in 0,25% GA for the next 24h. Then the samples were dehydrated in ethanol using 30% - 100% concentrations in ddH2O. The ethanol was exchanged for acetone (using 25%, 50%, 75% and 100% concentrations diluted in ethanol. The samples were finally dried in critical point dryer (Bal-Tec CPD 030) with CO_2. To make the samples electrically conductive, gold was sputtered on the sample using Bal-Tec SCD 050 sputter coater. The samples were observed on scanning electron microscope Jeol 6380 LV installed at the Laboratory of Electron Microscopy, Faculty of Science, Charles University. Magnification used for cell observation were 1500x and 10000x. Samples were observed using secondary electron imaging with acceleration voltage 20 kV, spot size: 38 nm (1500x), 35nm (10000x), working distance 11 mm.

4 Aims of the Thesis

1) Describe the adhesion, changes in metabolic activity and formation of focal adhesions of SAOS-2 cells and hMSC on NCD with different roughness.

2) Describe the adhesion and growth of SAOS-2 cells on NCD with various nanostructures prepared by dry ion etching.

3) Describe the adhesion and growth of SAOS-2 cells on NCD with oxygen and hydrogen surface termination regarding the presence of FBS in cultivation medium during cell seeding.

4) Describe the adhesion and growth of SAOS-2 cells and differentiation of hMSC on graphene with oxygen and hydrogen termination regarding the presence of FBS in cultivation medium during cell seeding.

5) Describe the adhesion and growth of SAOS-2 cells on SWCNT films with different times of oxygen plasma treatment.

5 Results

The presented articles describe *in vitro* testing of cell adhesion and growth of human osteoblastic cell line SAOS-2 and human mesenchymal stem cells using methods briefly described above. The comments to the results are categorized according to the studied materials and their surface modifications. The important figures and unpublished illustrations are presented in the main Results text. Most of the figures are referred to the included articles and are highlighted by *italic*.

The NCD was the first studied material with the most articles published. The articles presenting the results from NCD materials can be divided into two groups. The first group describes the cell response to materials with various nanotopographies while having the same oxygen surface termination. The oxygen termination proved to be supporting the cell adhesion. The second group of studies investigates two different NCD surface terminations – oxygen and hydrogen. The oxygen and hydrogen termination were studied as a possible tool for cell adhesion control on implants and for bio-electronic devices. Following the NCD studies, the studies about a novel carbon allotrope with excellent electrical properties – graphene were performed. Together with graphene one study done on related material single-walled carbon nanotubes was published widening our knowledge about the influence of surface termination on cell adhesion.

5.1 Nanocrystalline Diamond with Different Nanotopography

Two groups of NCD topographies possibly influencing the cell behavior were studied in the course of this thesis. The first group was NCD with different surface roughness and the second group was nanostructured NCD prepared by dry etching of the diamond substrate.

5.1.1 Article A: Strong Influence of Hierarchically Structured Diamond Nanotopography on Adhesion of Human Osteoblasts and Mesenchymal Cells

Antonin Broz, Veronika Baresova, Alexander Kromka, Bohuslav Rezek, and Marie Kalbacova (2009): Strong Influence of Hierarchically Structured Diamond Nanotopography on Adhesion of Human Osteoblasts and Mesenchymal Cells, Physica Status Solidi (A). 206, 9, 2038-2041. $IF_{2009} = 1.228$

The first topographical NCD study in this thesis investigated the influence of one type of topographical modification – the surface roughness. The NCD substrate roughness was described by *root mean square* (RMS) of the profile height deviations from the mean line, recorded within the evaluation length. Three NCD roughnesses were prepared for the experiment – 20 nm which was intrinsic to the NCD layer deposited on flat Si wafer. The other two surfaces with roughness of 270 nm and 500 nm were prepared by polishing of the underlying silicon substrate with subsequent NCD deposition (Figure 9). All the NCD surfaces were treated in inductively coupled radiofrequency oxygen plasma discharge to obtain a hydrophilic surface where the contact angle (CA) with water droplet was at most 35°. The plasma discharge changed only the surface chemistry and not the topography. Thus, the influence of only one parameter – topography - could be studied.

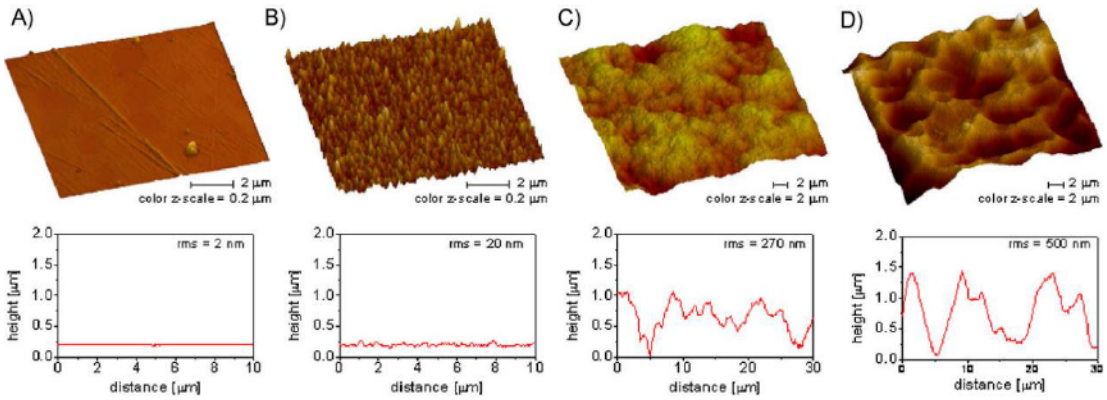

Figure 9: AFM images and surface profile graphs of A) polystyrene and Si substrates of different roughness with NCD coating – nanoroughness – B) RMS 20 nm, nano/microroughness – C) RMS 270 nm and D) RMS 500 nm (from included article A).

The study observed the activity of SAOS-2 cell line and primary hMSCs. The cells were cultivated for a short period of 1h to see the adhesion on NCD, and for 48 h to see their proliferation. The results from cell counting after 1 h indicate that both cell types adhere to the NCD surface in abundant numbers comparable with the TC PS (*Included article A, Fig. 2 A*). The comparison of SAOS-2 and hMSC adhesion was done in relative numbers because SAOS-2 cells are naturally smaller than hMSCs, thus more SAOS-2 cells is needed to cover the same area colonized by the hMSCs. SAOS-2 cells adhered to the diamond surface in higher numbers than to TC PS control whereas hMSCs adhered in numbers similar to TC PS control. Moreover, the number of SAOS-2 was significantly higher on NCD with RMS roughness 20 nm and 270 nm than on NCD with RMS 500 nm and TC PS. The metabolic activity was determined after 48h of cultivation (*Included article A, Fig. 2 B*). This parameter indicated how the cells prosper and proliferate on the surface. The test can be used as indirect measure of the cell number; however, it is also dependent on the activity of the mitochondrial metabolism. The results of this test indicated another interesting difference between SAOS-2 and hMSCs. HMSCs exhibited higher metabolic activity on NCD surfaces compared to TC PS control than SAOS-2. Though the differences were not significant the highest roughness (500 nm) induced slightly higher metabolic activity in hMSCs than the two lower roughnesses. In contrast, SAOS-2 metabolic activity was reduced and these results were significant when compared to TC PS control and the lowest NCD roughness (20 nm). Finally, the fluorescence images of adhering hMSCs stained for nuclei (blue – DAPI), actin (green – phalloidin + Alexa Fluor 488) and focal adhesions (anti-vinculin + Alexa Fluor 568)

indicate that the cell morphology of hMSCs differs significantly on the studied roughnesses early (1h) after the cell seeding (*Included article A, Fig. 3, rows A and B*). The cells beamed more lamellipodia with rising roughness reacting to the topography. The confocal images of focal adhesions visualized by vinculin staining of adhering SAOS-2 cells also reveal differences in formation of the focal adhesions on the three studied NCD roughness's (*Included article A, Fig. 3, row C*). The rougher the surface the more serrated was the cell edge with larger focal adhesions forming at the edge. In contrast, the cells on the NCD with the lowest roughness had a large amount of dispersed vinculin present in the center probably in the soluble form.

5.1.2 Article B: Fabrication of nano-structured diamond films for SAOS-2 cell cultivation; Article C: Study on cellular adhesion of human osteoblasts on nano-structured diamond films

Oleg Babchenko, Alexander Kromka, Karel Hruska, Marie Kalbacova, **Antonin Broz**, Milan Vanecek (2009): Fabrication of nano-structured diamond films for SAOS-2 cell cultivation, Physica Status Solidi (A) 206, 9, 2033-2037. $IF_{2009} = 1.228$

Marie Kalbacova, **Antonin Broz**, Oleg Babchenko, and Alexander Kromka (2009): Study on cellular adhesion of human osteoblasts on nano-structured diamond films, Physica Status Solidi (B) 246, 11-12, 2774-2777. $IF_{2009} = 1.15$

The study of the influence of NCD topography on the cell adhesion continued on unique newly prepared topographical modifications of NCD surface made by dry reactive ion etching (RIE). The article B is focused more on topography production process, whereas the article C describes the cell adhesion on NCD nanostructures in more detail. Using different masking materials - nickel, gold and diamond powder – preventing uniform etching of the NCD surface three different nanostructured surfaces were prepared by RIE. The nanostructures were named, nanocones (masked with diamond powder), ultrananocones (gold mask) and nanorods (nickel mask) and differed in their dimensions and shape (Figure 10).

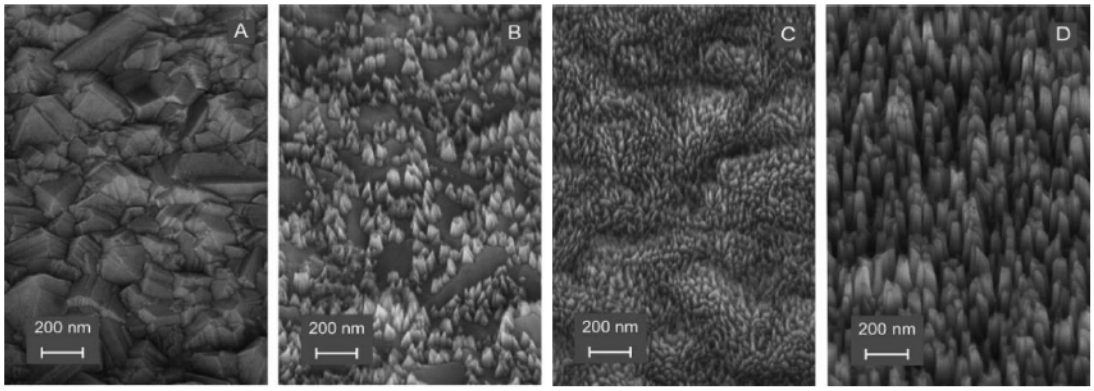

Figure 10: Nanostructured diamond topography (SEM) - tilted view (45◦) of A - as-deposited diamond and nanostructured diamonds: B - nanocones, C - ultrananocones, D - nanorods.

The nanorods made by using the nickel mask were the highest structures (120-200 nm) with diameter range between 20-40 nm. The nanocones were prepared using the diamond powder mask. The peaks of the relief were 5 – 100 nm above the base surface. The flat surface between the nanocones covered a significant part of the material. The ultrananocones were the smallest structures prepared on NCD with height ranging between 20 nm and 80 nm. The original relief of the NCD matrix is still visible in the ultrananocone structure. The surface of the NCD with these nanostructures was again oxidized by radiofrequency plasma treatment in oxygen atmosphere to prepare hydrophilic surface.

The published biological experiments on these surfaces were focused on the cell adhesion apparatus. The main difference was observed by immunofluorescence staining of vinculin after 1h and 48h of cultivation. The cells adhere on all surfaces in similar round shape; however, differences in formation of FAs at the cell edge could be already observed (*Included article C, Figure 2, A-C*). FAs of cell adhering on nanorods were longer and thinner and had lower signal intensity from the vinculin staining than on the other two surfaces. These differences in the organization of the adhesion apparatus persist through the cultivation up until the end of the experiment at 48 h (*Included article C, Figure 2, D-F*). The nanorods provided the cells with small adhesion areas on their tops with narrow and deep valleys in-between. The cells then formed thin and prolonged FAs. On the nanocones the cells formed largest FAs with pronounced vinculin staining. The cells formed FAs of normal size comparable to nanocones but located predominantly on the cell edge. These differences are perhaps even more visible on confocal images of vinculin staining presented in Figure 15. The cells were also immunofluorescently stained for

phosphorylated Y397 focal adhesion kinase (pFAK). The staining was also less pronounced on nanorods that could indicate an influence of the topography on the FA signaling that can be related to cell migration and proliferation. The NCD with nanorods provided the cells with small yet areas at the top of the nanostructure. Unpublished images from scanning electron microscopy in Figure 16 present SAOS-2 cells adhering in abundant numbers to all nanostructures. Zoomed images in Figure 17 also reveal numerous filopodia at the cell edges "touching" the nanostructure relief. From these observations, a simple model was proposed (Figure 18) indicating the relative size of FAs and where the cells interact with the surface nanostructures. The cells probably fully copy the surface relief of nanocones and ultrananocones and sit on top of nanorods.

5.1.3 Unpublished Results from Nanocrystalline Diamond with Different Topography

The hMSC cultivated on NCD with controlled nanoroughness were observed using confocal microscopy. The confocal images presented in the *included article A, Figure 3)* were only of SAOS-2 cells cultivated for 1 h on the NCD surfaces; however, confocal images of hMSC cultivated for 1h (Figure 11) and 48 h (Figure 12) were also acquired. The images in Figure 11 reveal different morphology of cells, their adhesion apparatus and actin cytoskeleton when adhering to different NCD topography. The cell cultivated on roughness RMS 20 nm adopts round shape. Well-developed focal adhesions are at least few microns behind the cell edge or under the cell, the cell was probing the environment with short arc lamellipodia. The cells cultivated on the sub-micron roughnesses (270nm, 500nm) have more irregular edge with protruding lamellipodia. The focal adhesions are present mostly at the cell edge in the tips of lamellipodia.

Already adhered cells in Figure 12 do not express any significant differences. The hMSCs adhering on 270 nm and 500 nm roughnesses have more prolonged shape and the polarized actin cytoskeleton, whereas the cell on 20 nm roughness is more rounded. Focal adhesions of cell on roughness 500 nm are more pronounced and shorter than on the other two surfaces.

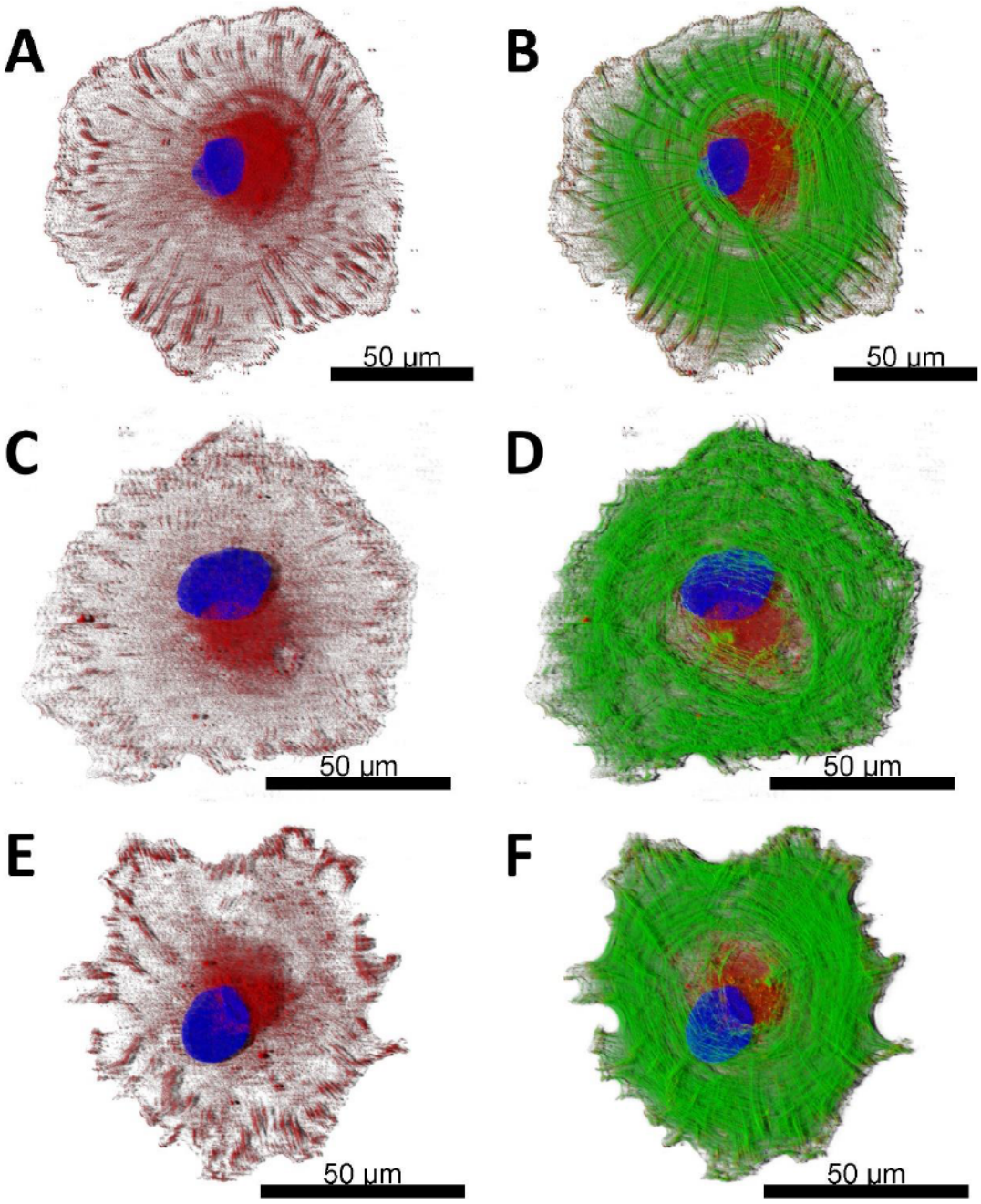

Figure 11: Deconvolved and rendered confocal microscopy immunofluorescence images of hMSCs cultivated on NCD for 1 h with different RMS roughnesses: A, B – RMS 20 nm; C, D – NCD RMS 270nm; E, F – RMS 500nm; blue – nucleus, green – actin, red – vinculin (focal adhesions).

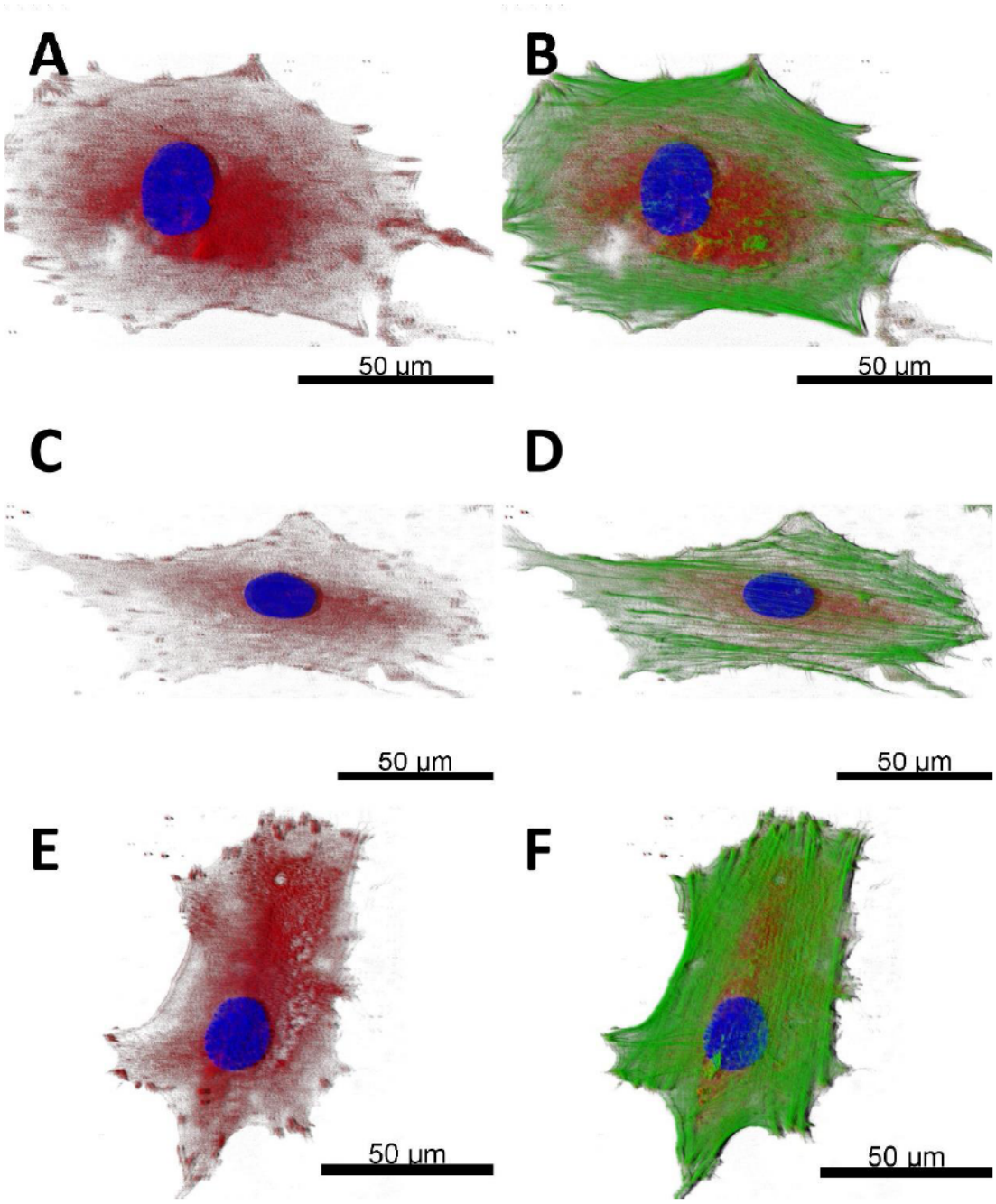

Figure 12: Deconvolved and rendered confocal microscopy immunofluorescence images of hMSCs cultivated on NCD for 48 h with different RMS roughnesses: A, B – RMS 20 nm; C, D – NCD RMS 270nm; E, F – RMS 500nm; blue – nucleus, green – actin, red – vinculin (focal adhesions).

The SAOS-2 cells were used for study of cell adhesion on NCD nanostructures (*included articles B and C*). The cell adhesion was also studied by cell counting (Figure 13) and measurement of the cell area (Figure 14). The results indicated no significant difference between the nanostructures and control unetched NCD surface and tissue culture polystyrene in both parameters. The highest number of cells adhered on ultrananocones (Au masking); however, the standard deviation of

the cell number measurement was high. This could indicate, that the cells tend to adhere in clusters on such surface.

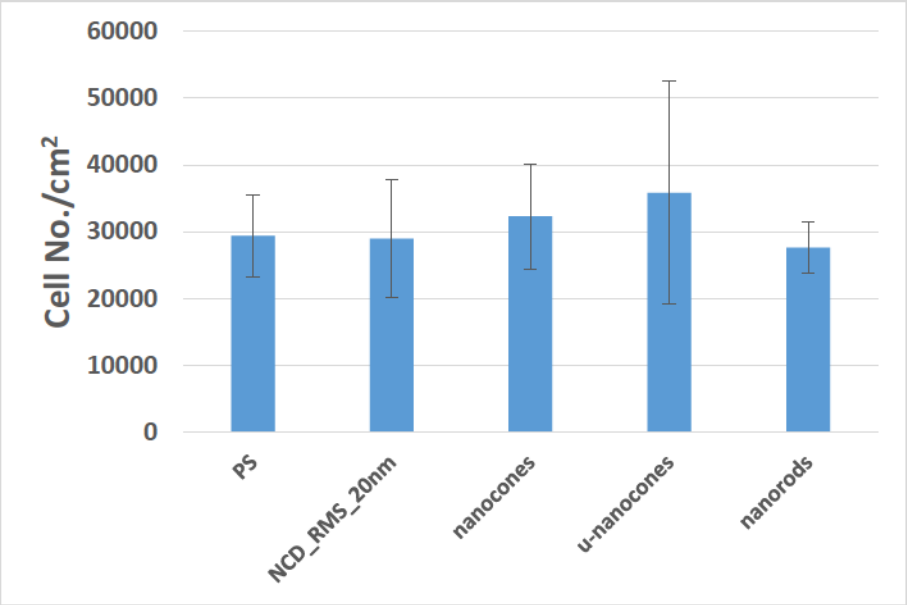

Figure 13: Cell number per cm^2 after 48h of cultivation on three different nanostructures (nanocones, u-nanocones, nanorods), un-etched NCD (NCD_RMS _20nm) and tissue culture polystyrene. (unpublished result).

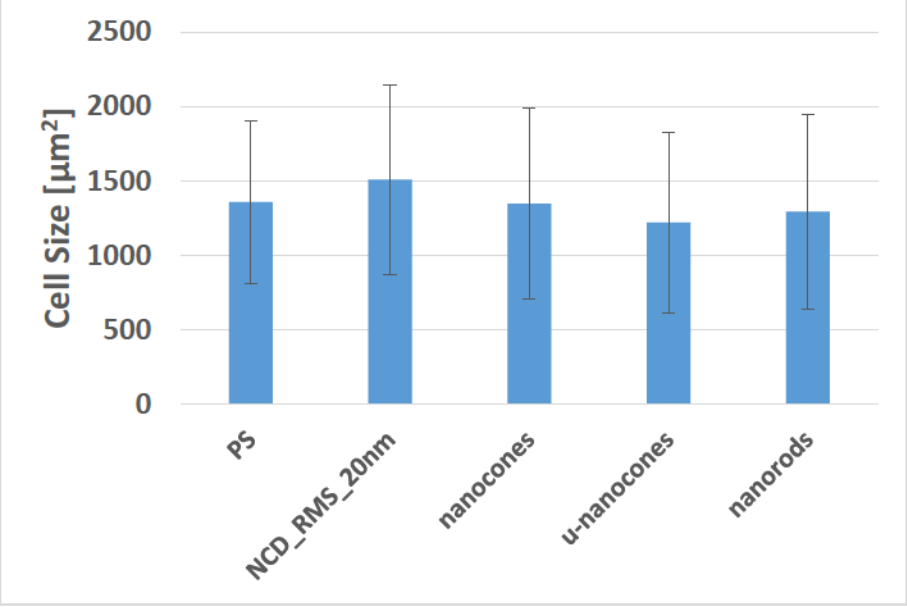

Figure 14: Cell size on three different nanostructures (nanocones, u-nanocones, nanorods), un-etched NCD (NCD_RMS _20nm) and tissue culture polystyrene. (unpublished result).

Focal adhesions (vinculin immunofluorescence staining) of cells cultivated on the NCD nanostructures were also observed by confocal microscopy (Figure 15). The images confirm the widefield observations and measurements. Thinner focal adhesions were observed on nanorods, larger adhesions were produced by cells on nanocones and ultrananocones.

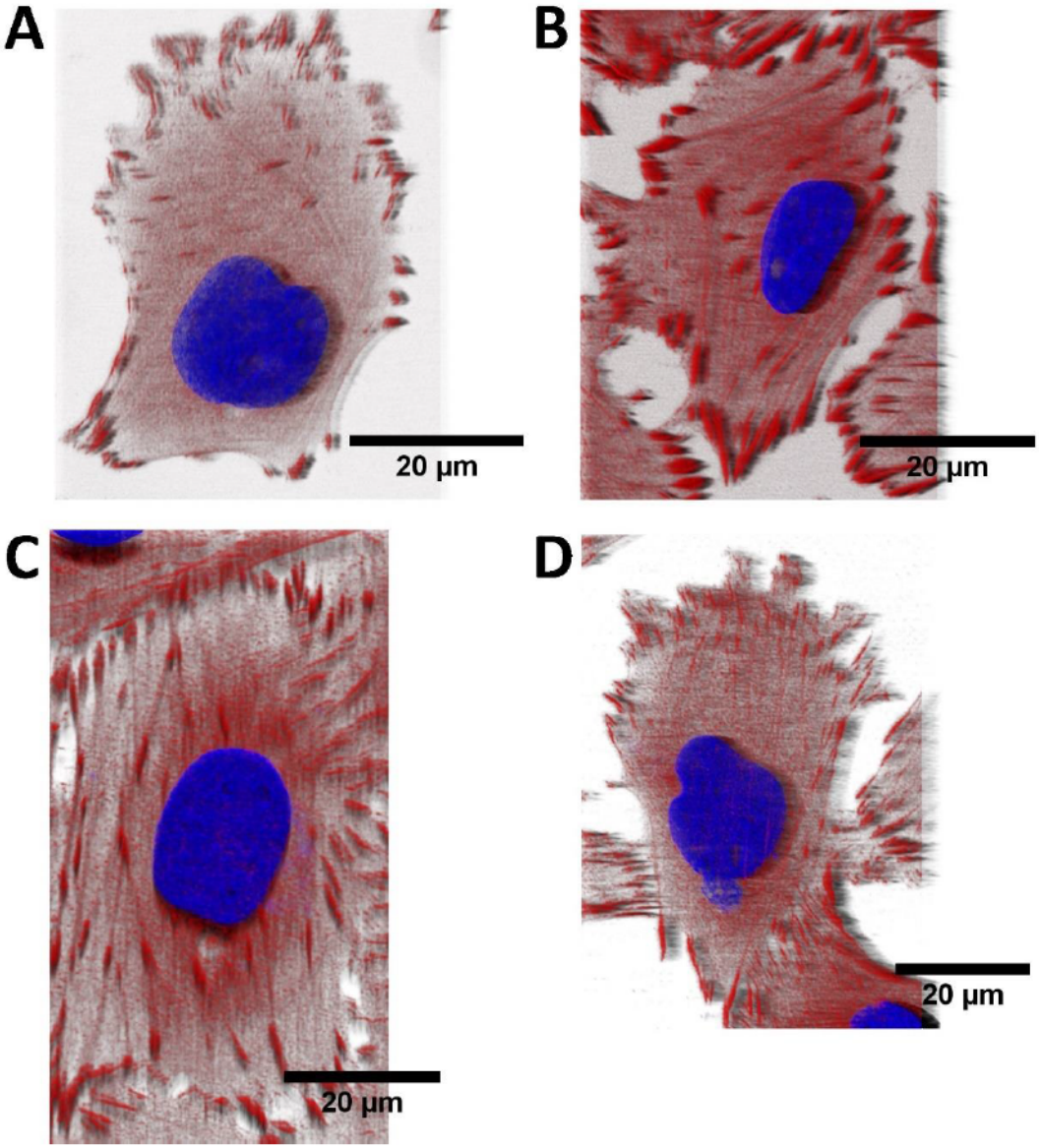

Figure 15: Confocal images of SAOS-2 cells adhering on A - non-etched NCD RMS 20nm, B - nanocones – mask diamond powder, C - ultrananocones – mask Au, D – nanorods mask Ni; blue – nucleus, red – vinculin (focal adhesions).

SAOS-2 cells were also observed by scanning electron microscopy. The SEM images confirmed high colonization of the nanostructured NCD surfaces (Figure 16). The SEM observations also revealed thin filopodia (few tenths of micrometers in

diameter) produced by the cells touching single or few NCD nanostructure features (Figure 17).

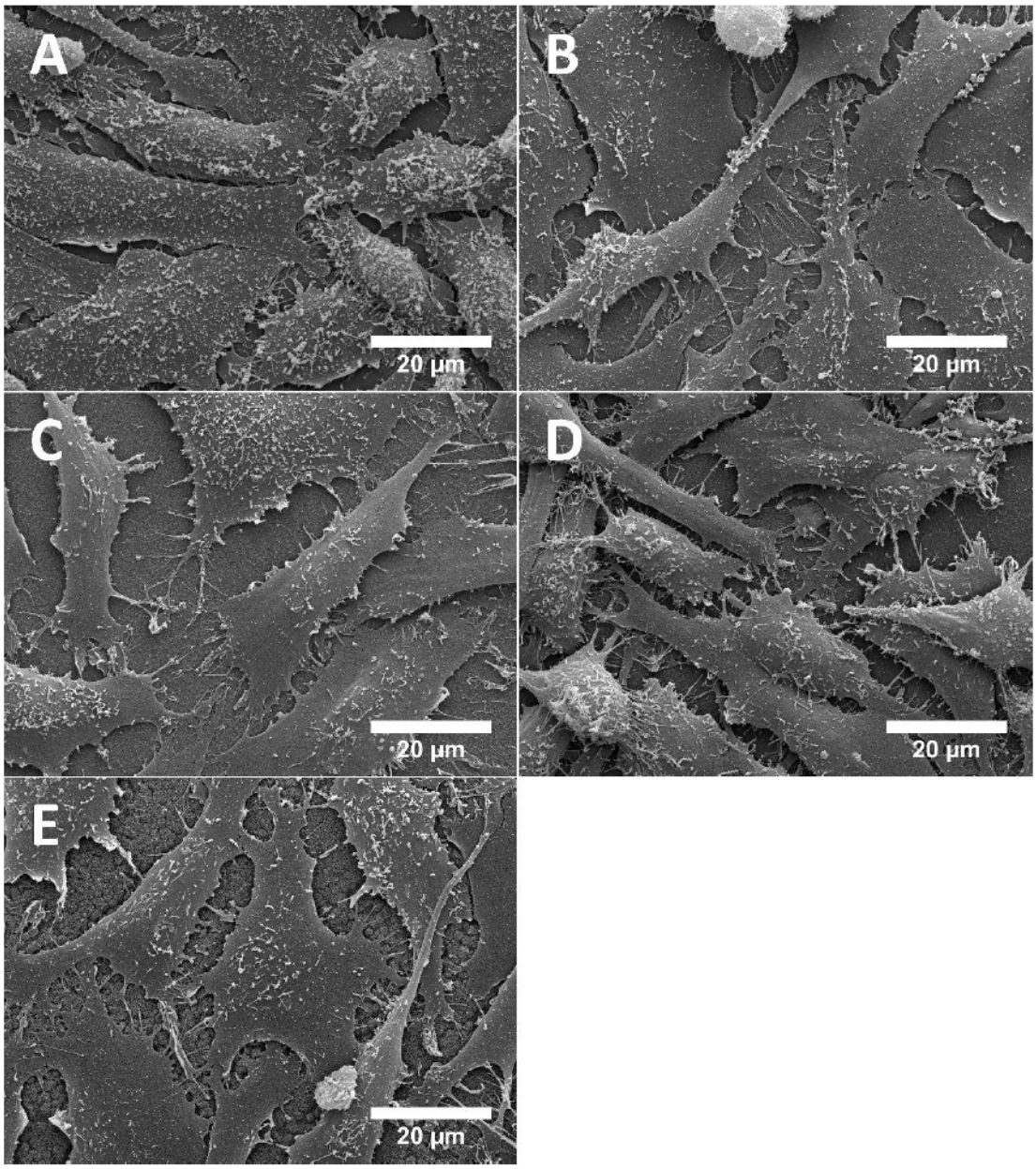

Figure 16: SEM images of SAOS-2 osteoblasts adhering on NCD nanostructures after 48h of cultivation in standard cultivation conditions, magnification 1500x: A) Glass control B) non-etched NCD - RMS = 20 nm, C – nanocones, D – ultrananocones, E – nanorods.

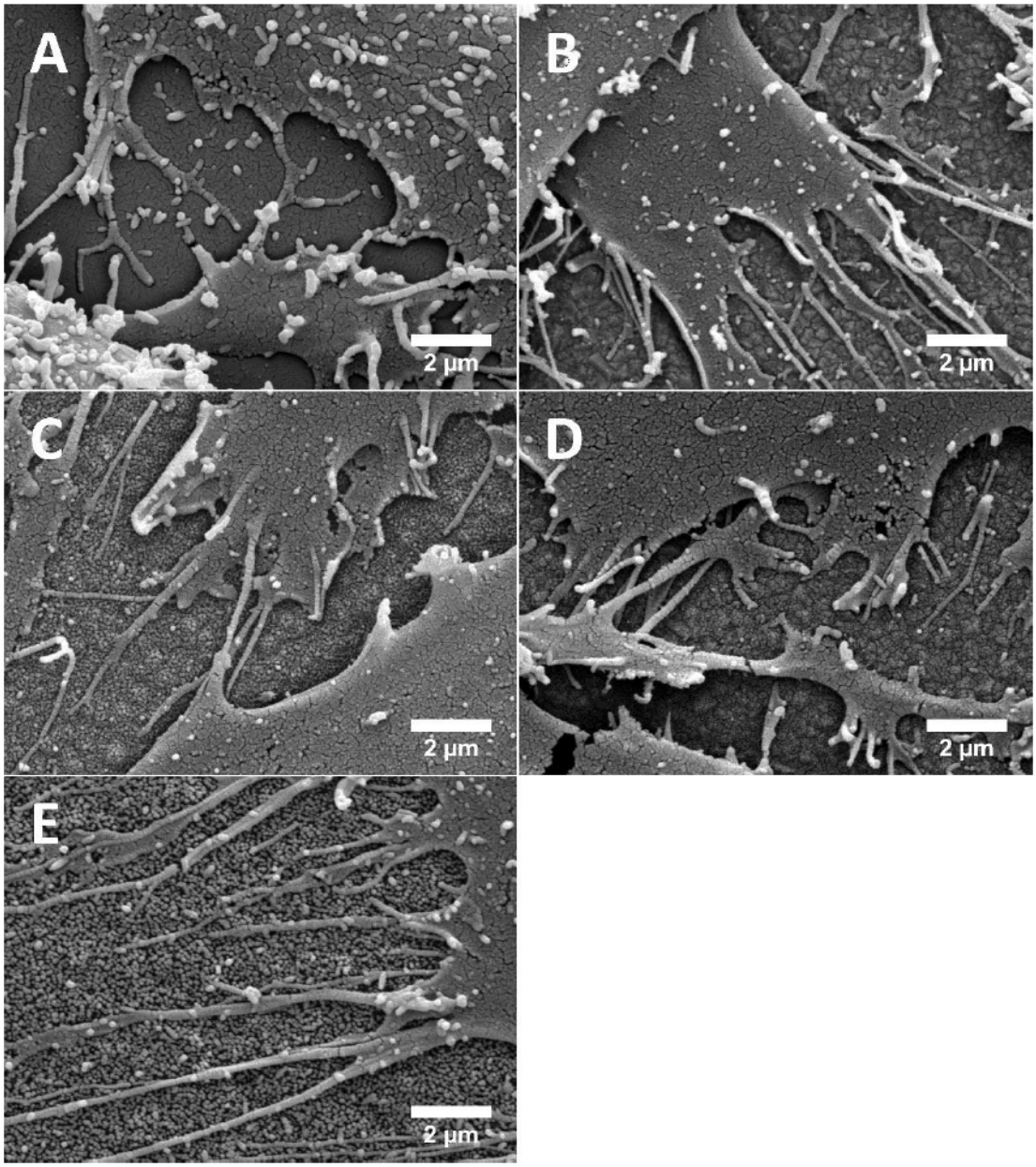

Figure 17: SEM images of SAOS-2 osteoblasts adhering on NCD nanostructures after 48h of cultivation in standard cultivation conditions, magnification 10000x: A) Glass control B) non-etched NCD - RMS = 20 nm, C) DP – nanocones, D) Au – ultrananocones, E) Ni – nanorods.

Figure 18 represents a simple model showing where the cells touch the nanotopographies. The largest adhesions were observed on nanocones and ultrananocones.

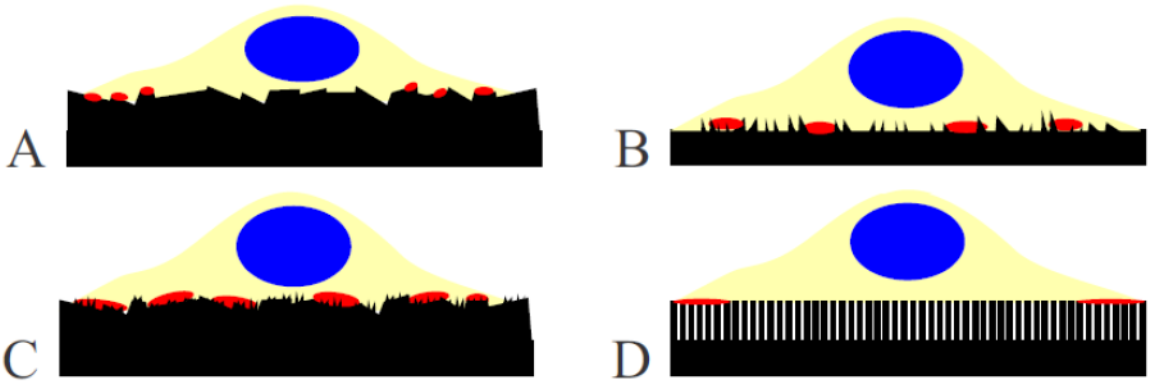

Figure 18: Model scheme of cells adhered on nanostructured NCD surfaces with indicated focal adhesions (red) and their relative size; A - non-etched NCD, B - nano-cones, C - ultra nanocones, D - nanorods.

We also conducted several attempts to investigate the influence of cell topography on osteogenic differentiation using the quantitative real time polymerase chain reaction (qRT-PCR) aiming on genes like osteocalcin, osteopontin, osteoprotegerin, bone sialoprotein, alkaline phosphatase, collagen I and RUNX 2 transcription factor. However, these attempts did not produce reproducible results that could be presented in thesis or a reviewed publication. A limited number and size of the NCD samples did not allowed for continuation and optimization of the qRT-PCR experiments.

5.2 Nanocrystalline Diamond with Different Surface Termination

The second branch of NCD studies was aimed on the differences in the cell adhesion on surface with the same topography (RMS roughness ca. 20 nm) and different surface termination – oxygen (O-NCD) and hydrogen (H-NCD). The oxygen and hydrogen terminations were prepared using radiofrequency and microwave plasma treatment. These two surfaces differ in several physical characteristics including water wettability (O-NCD CA = 15°-30°, H-NCD CA = 80°-100°), surface energy (Yang et al., 2012a) and surface electrical conductivity (Davydova et al., 2015; Liu et al., 2015; Sommer et al., 2007). As mentioned in the Introduction part, our research group already observed that cells can colonize NCD following the surface termination pattern (Rezek et al., 2009). Following this observation, we wanted to know why, when and how the cells align themselves.

5.2.1 Article D: Long-term adsorption of fetal bovine serum on H/O-terminated diamond studied in situ by atomic force microscopy

Egor Ukraintsev, Bohuslav Rezek, Alexander Kromka, **Antonin Broz**, and Marie Kalbacova (2009): Long-Term Adsorption of Fetal Bovine Serum on H/O-Terminated Diamond Studied in Situ by Atomic Force Microscopy, Physica Status Solidi (B) 246, 11–12, 2832–2835, $IF_{2009} = 1.15$

Firstly, we investigated the way of formation of FBS layer on oxidized and hydrogenated monocrystalline diamond (O-MCD, H-MCD) surface. Using the AFM, the differences in thickness of the FBS layer forming during 6 days of adsorption in McCoy's medium with 15% FBS content were studied. The measurements were done on a polished MCD surface because it is chemically identical to NCD and almost perfectly flat unlike the NCD. Therefore, the microscopic layers of FBS proteins can be easily observed using AFM without any interference from the NCD topography. The results show that FBS forms two mechanically distinct layers during 6 days on both O-MCD and H-MCD (*Included article D, Figure 2, 6*). The first layer is formed rather quickly in a matter of seconds or minutes and it differed in its thickness on both terminations (4 ± 2nm on O-MCD, 1,5 ± 2 nm on H-MCD) (*Included article D, Figure 1*). The thickness of FBS deposit does not change on H-MCD for about a day and then starts to grow from few nm to several tens of nm up to the 6th day. The 2nd layer on O-MCD starts to grow much later (4 days) and does not reach the thickness of the layer on H-MCD (*Included article D, Figure 3, 6*). AFM tapping mode technique proved that the FBS layers on O- and H-MCD have very different mechanical properties and adherence to the diamond substrate (*Included article D, Figure 4*). The FBS layer was easily scratched off the H-MCD surface by AFM cantilever but not from O-MCD surface. The secondary FBS layer formed after 6 days on H-MCD can be also easily peeled off the primary FBS layer whereas the primary and secondary FBS layers on O-MCD stay compact. These mechanical and special characteristics of the protein layers on different surfaces have a very important effect on the initial cell adhesion and further cultivation and migration of the cells cultivated on diamonds with such terminations. In addition, we wanted to know whether different times of incubation with FBS have some influence on the differential cell adhesion. Therefore, we seeded NCD samples either without any

FBS preadsorption or incubated for 5 days in FBS containing medium prior to the cell seeding. The cells were then incubated on these samples for 48 h days. The immunofluorescence images indicate that the cell adhered preferentially on the oxidized diamond irrespective to the time of FBS protein preadsorption and FBS layer thickness (*included article D, Figure 5*).

5.2.2 Article E: Assembly of osteoblastic cell micro-arrays on diamond guided by protein pre-adsorption

Bohuslav Rezek, Egor Ukraintsev, Alexander Kromka, Martin Ledinský, **Antonín Brož**, Lenka Nosková, Hana Hartmannová, and Marie Kalbacova (2010): Assembly of Osteoblastic Cell Micro-Arrays on Diamond Guided by Protein Pre-Adsorption, Diamond and Related Materials 19, 2–3, 153–57, $IF_{2010} = 1.913$

Further investigation of the dependence of the cell adhesion on the diamond termination was performed using shaking of NCD samples with adhered cells for controlled amount of time after 2 h of cultivation. The shaking proved that the cell adherence on H-NCD is reduced as was suspected from the previous experiments (*Included article E, Figure 2*). The results of the previous study indicated that the FBS proteins are crucial for the cell adhesion. Therefore, the shaking experiments were also conducted in media without FBS so the cells could adhere directly onto NCD surface and not onto FBS layer formed on NCD. Interestingly, the experiments proved that when the cells adhere on "naked" H-NCD surface the adhesion is much stronger than the adhesion on FBS covered H-NCD. The cell adhesion on O-NCD with and without FBS was similar. The study also investigated which of FBS proteins has a major effect on cell adhesion. Three candidate proteins were chosen from the literature: albumin, fibronectin and vitronectin. Albumin is the most abundant protein in the FBS, known as a "cell repellent" (Kaji et al., 2005; Okuyama et al., 2010) and the latter two are proteins often reported to be responsible for the cell adhesion (Grinnell and Feld, 1982; Grinnell and Phan, 1983; Underwood and Bennett, 1989). The single proteins were preadsorbed on NCD surfaces with striped termination pattern for direct visualization of the difference on O and H termination.

The cells were then seeded in FBS-free cultivation medium for the first 2 h and then cultivated on the samples in already fully supplemented medium for 48 h. Fluorescence images of the fixed samples showed that fibronectin is very probably the protein most responsible for the differential cell adhesion on O-NCD and H-NCD (*Included article E, Figure 4*), because the pattern formed by cells was similar to pattern formed on FBS. The study also presents another AFM method of the protein layer quality characterization – nanoshaving. The method was again used on MCD surface with oxygen and hydrogen termination with preadsorbed FBS layer. This procedure uses the oscillating AFM cantilever to peel or shave the surface FBS layer. By controlling the loading force on AFM cantilever pressing on FBS layer surface we could determine the force necessary to remove the layer. The force applied on FBS layer to remove it from O-NCD was 10 nN and from H-NCD 5nN. The result tells us that FBS layer on O-MCD adheres with double the force of the FBS layer on H-MCD. The Raman spectroscopy of FBS layers done by our colleagues at the Institute of Physics indicated presence of albumin - the most abundant protein in FBS - on the MCD surface. No fibronectin or vitronectin were detected with this method. However, the method sensitivity can be dubious when detecting low concentration proteins in a mixture of many other proteins.

5.2.3 Article F: Function of thin film nanocrystalline diamond–protein SGFET independent of grain size

Marie Krátká, Alexander Kromka, Egor Ukraintsev, Martin Ledinský, **Antonín Brož**, Marie Kalbacova, and Bohuslav Rezek (2012): Function of Thin Film Nanocrystalline Diamond–protein SGFET Independent of Grain Size, Sensors and Actuators B: Chemical, 166–167, 239–245. $IF_{2012} = 3.535$

This article followed the studies of cell adhesion on O/H-NCD. The study investigated the dependence of transfer characteristics of the solution gated field-effect transistors (SG FET) fabricated on the surface of NCD using electrically conductive hydrogen termination and insulating oxygen termination. The results of this study were again measured in cooperation with the Institute of Physics. The

results tell us that the transfer characteristic of SG FET change upon protein adsorption as well as cell adhesion and therefore such prototype is applicable as a functional optically transparent biosensor. This work was further developed in the work of Ižák et al. by creating NCD based impedance sensor with interdigitating H-termination electrodes (Ižák et al., 2013) in cooperation with the Department of Biomaterials and Tissue Engineering of Institute of Physiology, CAS.

5.2.4 Article G: Osteoblast adhesion, migration and proliferation variations on chemically patterned nanocrystalline diamond films evaluated by live-cell imaging.

Antonin Broz, Egor Ukraintsev, Alexander Kromka, Bohuslav Rezek, and Marie Hubalek Kalbacova (2017): Osteoblast Adhesion, Migration, and Proliferation Variations on Chemically Patterned Nanocrystalline Diamond Films Evaluated by Live-Cell Imaging, Journal of Biomedical Materials Research Part A 105, 5, 1469–78, $IF_{2015} = 3.263$

Cell adhesion on O/H-NCD termination was further investigated by live-cell imaging. As we have found in the previous studies, the cells tend to adhere to the O-NCD rather than H-NCD. This could significantly influence e.g. the output of NCD based biosensors and it also has its relevance in the control of cell adhesion on implants with NCD passivation. The experiments were conducted on NCD samples with the "striped" (biosensor-like) termination pattern and on "halved" samples with only one O/H termination border. The NCD was deposited on transparent fused silica that allowed the observation of cells using an inverted microscope with phase contrast. We already knew that the effect of FBS on the cell adhesion is important so we included this variable in the experiment setups. The cells were for 48 h in controlled cultivation conditions and from the acquired pictures, the growth curves and migration maps were obtained so we could decide what is the main contributing factor of the cell alignment along the termination pattern on the FET-like striped pattern. The results of this study indicated that after pouring the cell suspension on the sample the non-adhered cells tend to drift on the surface of NCD if FBS is present in the medium (*included article G, Figure 2*). In the FBS-free medium the

cells anchored on one spot and did not move. This observation is in accord with the shaking experiment presented in the *included article E,* where the cells seeded without the FBS were not detached by the shaking. The other important information from the initial period of cultivation was the speed of adhesion on H-NCD and O-NCD. The cells tend to adhere on O-NCD faster than on H-NCD in both FBS-free and FBS-supplemented medium. Together, the drift on FBS layer and faster cell adhesion on O-NCD caused in the experiments with the FBS on the striped pattern an initial shift of cell distribution towards O-NCD. In the experiments without FBS the cell distribution was initially more even but during the cultivation thanks to the faster cell adhesion and also the cell migration and proliferation the cells also tend to align on O-NCD surface of the striped samples (*included article G, Figure 3*). The results from the halved samples confirmed that the cells are able to adhere and grow on H-NCD surface if there is no O-NCD in the near vicinity. The adhesion on the H-NCD is slower and the cell migration is probably slightly faster when compared to the O-NCD. This fact could contribute to the cell distribution shift on the striped samples as well. The cell doubling times of cells on H- and O- terminations were another measured factor that could explain the cell distribution differences. The doubling times observed on the halved samples were similar on both terminations; however, the initial difference in the number of adhered cells or the difference in the speed of cell adhesion in the beginning of the experiment caused persisting difference in absolute cell numbers despite the similar doubling times. Interestingly, the doubling times on the striped samples were very different, the proliferation on H-NCD surface almost stopped. This was observed in experiments with and without FBS in cultivation medium and it is certainly one of the major aspects influencing the final cell distribution on the two surface terminations on striped samples.

5.2.5 Article H: Stochastic model explains formation of cell arrays on H/O-diamond patterns

Egor Ukraintsev, **Antonin Broz**, Marie Hubalek Kalbacova, Alexander Kromka, and Bohuslav Rezek (2015): Stochastic Model Explains Formation of Cell Arrays on H/O-Diamond Patterns, Biointerphases 10, 4, 041006-1-9, $IF_{2015} = 3.374$

Some of the results of the live-cell experiments gave also basis for in silico work of Egor Ukraintsev. The study result is a stochastic mathematical model that is proposed as a possible explanation of the alignment of the cells on 200μm O-NCD/H-NCD alternated surfaces. The model uses three parameters - speed of cell movement before adhesion and probabilities of cell adhesion and cell division. The model revealed that the most important factors for alignment of the cells along the termination pattern are the speed of the cell movement before adhesion (drift) and probability i.e. speed of cell adhesion on each surface.

5.3 Graphene

Graphene is a nanomaterial that was originally prepared by exfoliation or delamination method (Novoselov et al., 2004). Other methods were developed since then. The graphene used in this thesis was prepared by chemical vapor deposition at the Department of Low-dimensional Systems of the Heyrovský Institute of Physical Chemistry, CAS (Li et al., 2009). This method allows preparation of large graphene sheets suitable for *in vitro* experiments. Its mechanical and electrical properties as well as possible surface modifications promised interesting utilizations in various scientific fields including cell biology.

5.3.1 Article I: Graphene substrates promote adherence of human osteoblasts and mesenchymal stromal cells

Marie Kalbacova, **Antonin Broz**, Jing Kong, and Martin Kalbac (2010): Graphene Substrates Promote Adherence of Human Osteoblasts and Mesenchymal Stromal Cells, Carbon 48, 15, 4323–4329, $IF_{2010} = 4.893$

Our first work published on graphene was also one of the first studies investigating the cell adhesion on graphene sheets ever and it is still an important work in graphene field of study despite its simple experimental setup. The Institute of Physical Chemistry, CAS was at that time one of the few institutions able to prepare graphene sheets in size and quality suitable for tissue culture experiments. The work studied the possibility of cell (SAOS-2 and hMSCs) cultivation on this surface and its eventual possibility to lead the hMSC towards differentiation. The fluorescence staining of cells grown on the substrate for 48 h indicate, that untreated CVD graphene layer is suitable for cell adhesion and growth. The comparison with the underlying Si substrate with SiO_2 surface layer showed better dispersion of the cells on the graphene layer. The silicon is a typical semiconductor material used for construction of electronic devices and therefore using these materials was useful for good comparison regarding graphene utilization as biosensor. The cells growing on SiO_2 surface layer of Si substrate tend to cluster which is not dissimilar to what we could see on normal microscope glass slide. From detailed view on the graphene/Si/SiO_2 substrate border (*included article I, Figure 3*) we could see that the cells align along the border on the graphene and do not migrate on the Si/SiO_2 which indicates that the adhesion on the graphene is different and better than on Si/SiO_2. The cell morphology and formation of the adhesion apparatus was studied further using immunofluorescence staining of vinculin. The detailed look on the confocal immunofluorescence (*included article I, Figure 5*) images indicated changes possibly leading to different cell fate on each substrate. The cells on the graphene were probably in more proliferative state whereas the cells on Si/SiO_2 were more quiescent and clumped together. More profound quantitative studies regarding the cell growth and adhesion were complicated by still very small (c.a. 2x3 mm) and undefined size of the graphene sheets prepared at that time.

5.3.2 Article J: Influence of the fetal bovine serum proteins on the growth of human osteoblast cells on graphene

Marie Kalbacova, **Antonin Broz**, and Martin Kalbac (2012): Influence of the Fetal Bovine Serum Proteins on the Growth of Human Osteoblast Cells on Graphene, Journal of Biomedical Materials Research Part A 100A, 11, 3001–3007. IF_{2012} = 2.834

The previous pioneering study was followed by work focused on FBS influence on the cell adhesion on graphene. The study compared untreated H-terminated graphene with the underlying Si/SiO_2 substrate and standard TC PS. From the previous studies on NCD we already knew that FBS can significantly influence the cell adhesion, therefore we conducted also experiments investigating FBS absence in the first 2 h of cultivation (*included article J, Figure 2*). The main studied parameters were cell number and single cell area (*included article J, Figure 3*), cell morphology and adhesion apparatus. The study results indicate that the cells spread on the graphene surface in a similar way as on TC PS. Si/SiO_2 surface was less suitable than both graphene and TC PS. The cell number on surfaces seeded with FBS after 48 h of cultivation was similar on TC PS and graphene. Si/SiO_2 was significantly behind these two surfaces. If we did not add FBS for the first 2 h of the experiment the cell number dropped significantly on the TC PS surface even below Si/SiO_2 surface. Interestingly the cell number remained unchanged on the graphene surface. The cell area was again smallest on Si/SiO_2 indicating problems in the cells adhesion. In the presence of FBS, the cells on TC PS and graphene were of similar size. Without the FBS during seeding, the cell area was following the pattern TC PS > graphene > Si/SiO_2. This was also presented in the cell area distribution graph (*included article J, Figure 4*). The immunofluorescence images of focal adhesions (vinculin staining) show well-formed focal adhesions on graphene with and without FBS after 48 h of incubation. Interestingly, on Si/SiO_2 the cells formed more FAs without FBS whereas on TC PS FAs were well formed in both cases (*included article J, Figure 5*).

5.3.3 Article K: Influence of oxygen and hydrogen treated graphene on cell adhesion in the presence or absence of fetal bovine serum

Martina Verdanova, **Antonin Broz**, Martin Kalbac, and Marie Kalbacova (2012): Influence of Oxygen and Hydrogen Treated Graphene on Cell Adhesion in the Presence or Absence of Fetal Bovine Serum, Physica Status Solidi (B) 249, 12, 2503–2506, $IF_{2012} = 1.489$

The electrically conductive graphene is a material that could be used as a basis for construction of a biosensor. With this on mind and thanks to our previous experiments with the NCD we investigated also different surface termination of graphene as a main variable in our experiments. The controlled surface termination of the graphene layer was done by treatment in heated (500°C) oxygen and hydrogen atmospheres resulting in different wettabilities - on O-graphene CA was 58°, on hydrogenated graphene (H-graphene) CA was 90°. A plasma discharge used for the modification of NCD termination would easily destroy this single atom thick layer of carbon. The study again investigated FBS influence on the cell adhesion. In this study, the cell adhesion was observed just 2 h after the cell seeding therefore the direct effect of FBS absence could be observed. The study also describes the adhered cell number and cell size (*included article K, Figure 2*). Without FBS cells adhered to H-graphene and O-graphene in higher numbers and spread more than with FBS in the medium during the 2h after seeding. Surprisingly, the best adhesion was observed on H-terminated graphene without FBS. The larger area of cells on surfaces without FBS is caused by protruding lamellipodia. Interesting observation was made from the immunofluorescence staining of FA protein vinculin (*included article K, Figure 1*). Although the cells adhered to the graphene and control TC PS without FBS, the vinculin staining did not reveal any distinct vinculin containing FAs. This observation gives us another clue that confirms hypothesis that without FBS proteins present the cell adhesion is mediated not only by integrin molecules but also with other moieties.

5.3.4 Article L: Modulated surface of single-layer graphene controls cell behavior

Marie Hubalek Kalbacova, Martina Verdanova, **Antonin Broz**, Aliaksei Vetushka, Antonin Fejfar, and Martin Kalbac (2014) Modulated Surface of Single-Layer Graphene Controls Cell Behavior, Carbon 72, 207–214, $IF_{2014} = 6.196$

The plasma untreated graphene in the *included article L* was specified as "single layered graphene" (1-LG) due to new publications about so called double layered graphene (Yan et al., 2011). The oxidized graphene was denoted as 1-LG-O. This article expanded the knowledge obtained in the previous article (*incluced article K*) for AFM measurements of graphene topography that were not published before, because of not yet developed technique for such measurement at that time (2012) (*included article L, Figure 1*). Graphene was automatically considered as strictly flat. However, AFM uncovered that the graphene surfaces are covered with small ridges up to couple of nm above the bottom. These ridges are less pronounced on 1-LG-O than on 1-LG. The biology experiments expanded the results from the *included article K* for measurements of cell number and cell size also after 48 h cultivation (seeding with and without FBS) on 1-LG and 1-LG-O. The results indicate that more cells tend to adhere onto both 1-LG-O and 1-LG seeded without FBS than on graphene seeded with FBS (*included article L, Figure 5*). This difference is still noticeable after 48 h; however, it is only significant on O-graphene. The cell number is significantly higher on 1-LG than on 1-LG-O (seeded with and without FBS). Therefore, the best surface for cell cultivation is 1-LG seeded without FBS. The cell area results copy the cell number results (*included article L, Figure 6*). On surfaces with higher cell number cells are also more spread and these tendencies also persist after 48 h of cultivation. The highest spreading rate (cell area after 48 h /cell area after 2 h) was observed for cells seeded on 1-LG in the presence of FBS. Whereas, the lowest spreading rate was observed on 1-LG seeded without FBS (included article L, Figure 6 B). This illustrates the initial inhibiting influence of FBS on cell adhesion that is later compensated on 1-LG. The article also shows evaluation of FA number per cell and FA area (included article L, Figure 7). Again, the number of FA per cell is higher in cases when cells are seeded without FBS. More FAs are found on

1-LG than on 1-LG-O. The area of FAs is prominently high in experiments on 1-LG-O with FBS. That is also experiment with the lowest number of FAs.

5.3.5 Article M: Nanocarbon Allotropes - Graphene and Nanocrystalline Diamond - Promote Cell Proliferation

Martina Verdanova, Bohuslav Rezek, **Antonin Broz**, Egor Ukraintsev, Oleg Babchenko, Anna Artemenko, Tibor Izak, Alexander Kromka, Martin Kalbac, and Marie Hubalek Kalbacova (2016): Nanocarbon Allotropes-Graphene and Nanocrystalline Diamond-Promote Cell Proliferation, *Small* 12, 18, 2499–2509, $IF_{2014} = 8.368$

Finally, the last included article compares the results obtained on graphene and NCD and control TC PS. The article contains a topographical comparison of all nanomaterials including SEM images and 2D profiles (*included article M, Figure 1*) and Raman and X-ray photoelectron (XPS) spectra illustrating the quality and composition of the materials (*included article M, Figures 2, 3*). The cell adhesion statistics is compiled from immunofluorescence images of cells stained for actin (*included article M, Figure 4*) and the cell number and cell area in 2 h and 48 h intervals. The results are at first presented regardless of material termination and only with FBS (*included article M, Figure 5*). The graphs of cell number are showing that initially (2h) NCD is generally better material for cell adhesion than graphene. However, this difference is leveled at 48h. The cell area is again larger on NCD than on graphene after 2 h but this difference persists to the 48 h (*included article M, Figure 5*). If we pay attention to the material termination the results reveal that O-termination of graphene hinders the cell adhesion, whereas H-termination of graphene improves the cell adhesion even more than O-NCD previously considered as the best of the studied surfaces for the cell adhesion (*included article M, Figure 7*).

5.3.6 Unpublished Graphene Results

The samples of graphene for cell cultivation were delivered deposited on small chips of Si/SiO_2 wafer. The graphene flakes themselves were 4 – 6 mm^2 in size. Figure 19 shows hMSC cultivated for 21 days on graphene flake on the Si/SiO_2 wafer. The cells were washed away from the Si/SiO_2 surface during the staining procedure, whereas the cells adhered on graphene stayed on the sample. Clear edge was formed at the lower and right side of the confluent cell layer. The image therefore shows better cell adhesion on graphene than on the supporting substrate.

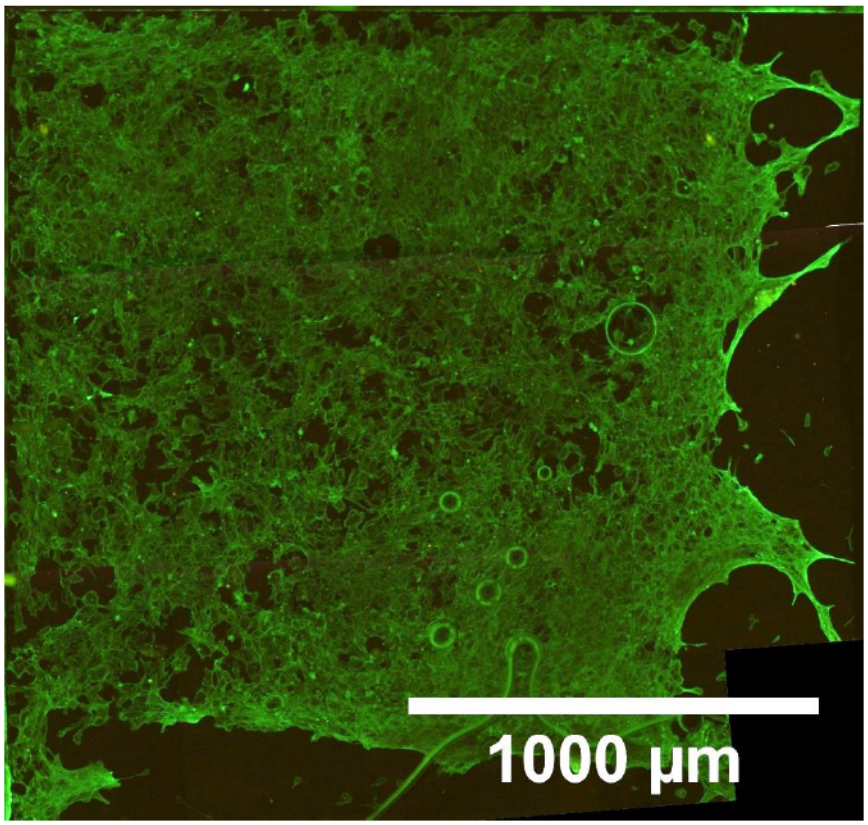

Figure 19: hMSCs cultivated for 21 days on graphene supported by Si/SiO_2 wafer. Fluorescence staining for actin (phalloidin + Alexa Fluor 488). Image contains the whole graphene flake. No graphene was deposited in the lower and right edge of the image. The cells are present only on the graphene flake.

Graphene was also tested for its possibility to induce differentiation of hMSC; however, the results were insignificant and therefore not published. The hMSC cultivated on graphene, Si/SiO2 substrate and polystyrene were immunofluorescently stained for osteocalcin (OC) deposits and histologically stained for alkaline phosphatase (ALP). The ALP staining experiments were cultivated for 14 days in

differentiation medium containing the beta-glycerolphophate and ascorbic acid. The influence of dexamethasone as a compound known to induce the osteogenic differentiation was also investigated.

It is apparent from the images of ALP staining that the cells cultivated without dexamethasone retained spindle-like prolonged shape (Figure 20), whereas the cells cultivated with dexamethasone adopted a star-like or polygonal-shape (Figure 21). The ALP staining itself shows no visible difference in ALP content between the cells cultivated with and without dexamethasone.

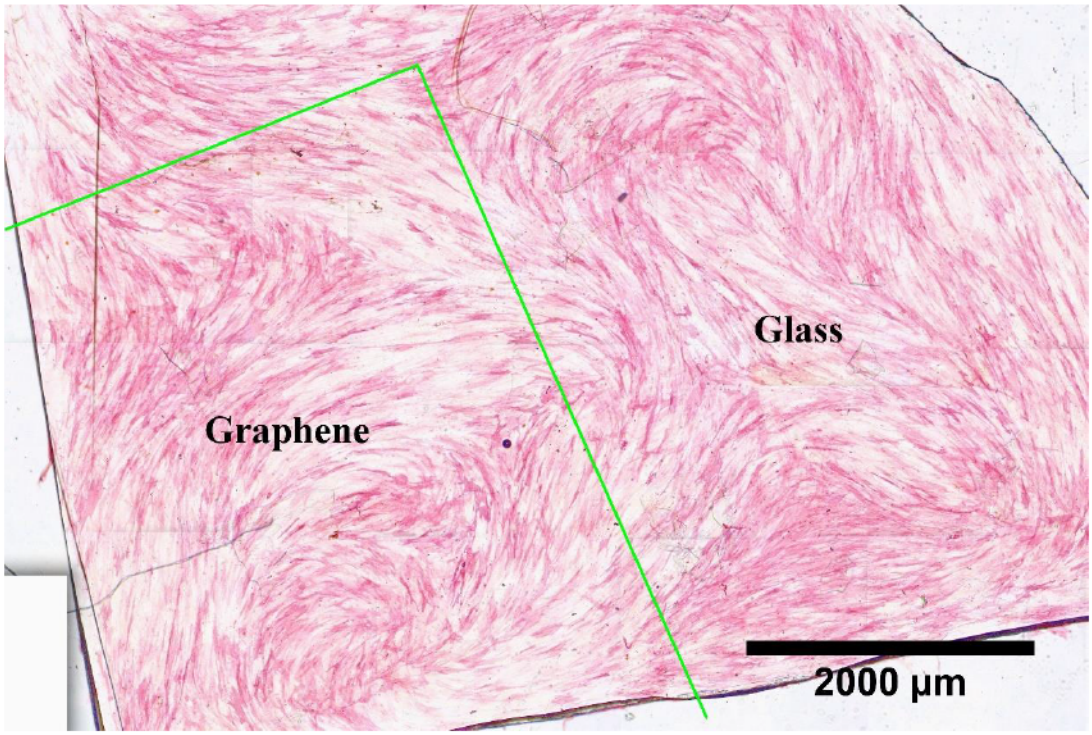

Figure 20: Brightfield microscopy image of hMSC cultivated on quarter of microscopy cover glass with deposited graphene (border marked with the free line). The cells were cultivated with β-glycerolphosphate and ascorbic acid and without dexamethasone in cultivation medium for 14 days. The cells were stained for alkaline phosphatase (red coloring).

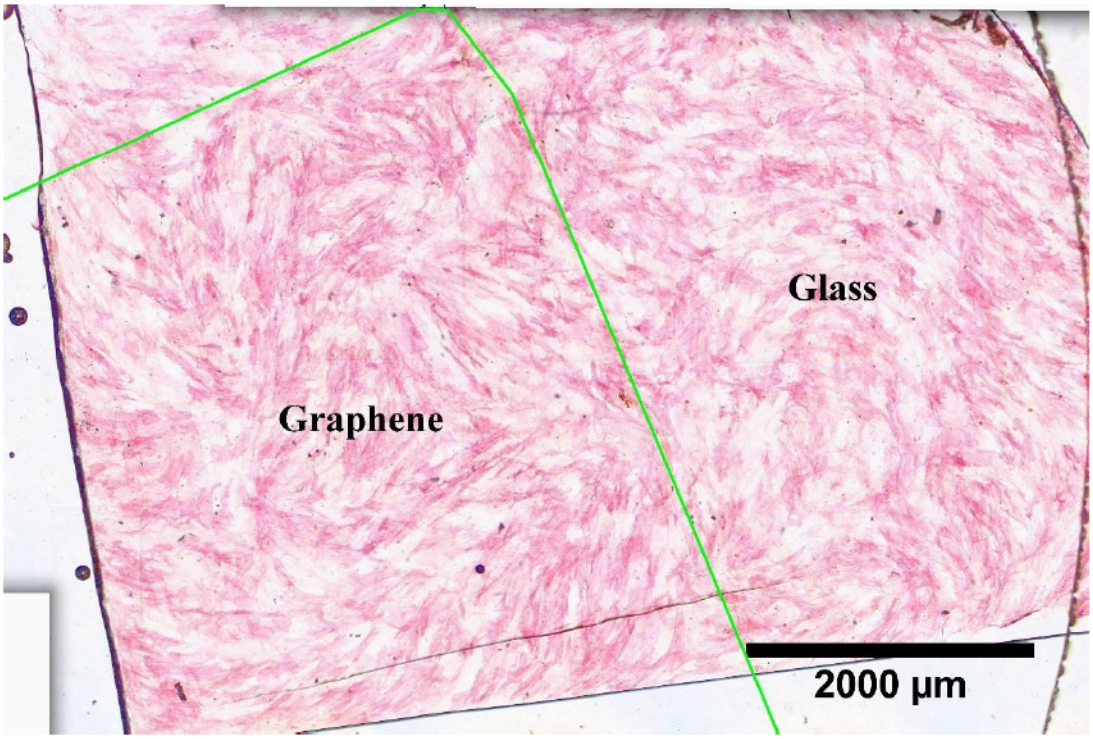

Figure 21: Brightfield microscopy image of hMSC cultivated on quarter of microscopy cover glass with deposited graphene (border marked with the free line). The cells were cultivated with β-glycerolphosphate and ascorbic acid and dexamethasone in cultivation medium for 14 days. The cells were stained for alkaline phosphatase (red coloring) .

The OC staining also revealed the influence of dexamethasone on the cell shape (Figure 22). The photos indicate some clusters containing higher amount of OC in the dexamethasone samples. No marked osteogenic effect of the graphene layer was observed.

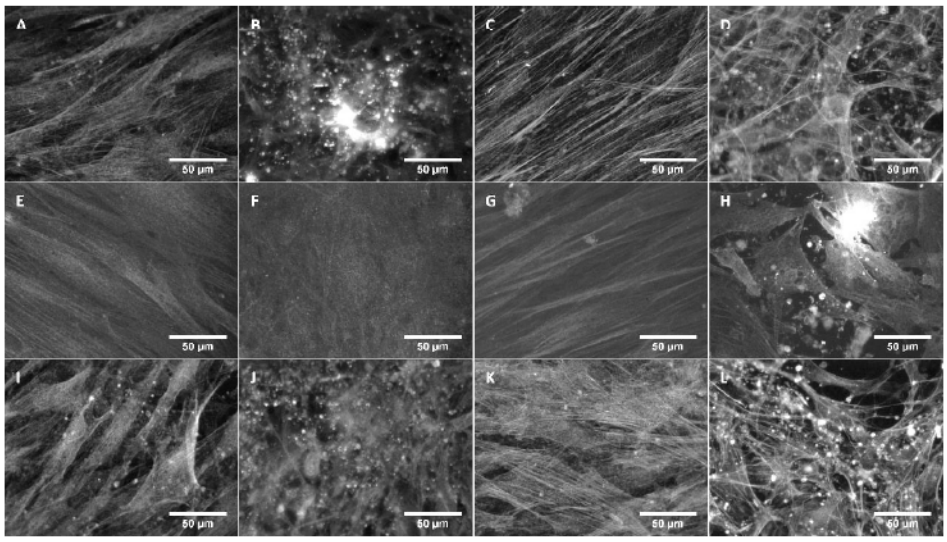

Figure 22: hMSC cells cultivated on graphene (A, B, C, D), PS (E, F, G, H) and Si (I, J, K, L,) for 14 days (A, B, E, F, I, J) and 21 days (C, D, G, H, K, L,) in osteogenic medium with dexamethasone (B, F, J, D, H, L) and without dexamethasone (A, E, I, C, G, K).

5.4 Single-Walled Carbon Nanotube Films

5.4.1 Article N: Controlled oxygen plasma treatment of single-walled carbon nanotube films improves osteoblastic cells attachment and enhances their proliferation

Marie Kalbacova, **Antonin Broz**, Alexander Kromka, Oleg Babchenko, and Martin Kalbac (2011): Controlled Oxygen Plasma Treatment of Single-Walled Carbon Nanotube Films Improves Osteoblastic Cells Attachment and Enhances Their Proliferation. *Carbon* 49, 9, 2926–2934. $IF_{2011} = 5.378$

The last studied carbon material was single-walled carbon nanotube (SWCNTs) film. The study was based on previously published works (Kalbacova et al., 2006, 2007). The biocompatibility of this artificial carbon allotrope has been often questioned. In contrast to many studies investigating the SWCNT biocompatibility in a colloid we decided to look on the cell adhesion on a layer of SWCNT prepared from HiPCO SWCNTs. In addition to the previously mentioned studies we also wanted to see the difference in the cell adhesion on SWCNT layer with different terminations. These SWCNT layers were exposed to oxygen plasma discharge for different time intervals - 1, 5 and 30 minutes. The sample without the plasma treatment was considered as hydrogen terminated. The obtained samples differed in CA – no treatment – 100° ± 5°, 1-minute O – 21° ± 5°, 5-minute O – 11° ± 3°, 30-minute O – 12° ± 3°. The oxygen plasma treatment resulted in significant topographical changes of the layer which were visualized by SEM (*included article N, Figure 1*). The most significant topographical changes were on 30 min treated sample as expected. The SWCNT were probably slowly degrading under the plasma exposition. Differences in the cell coverage could be observed already from low magnification microscopy images (*included article N, Figure 3*). The cell adhesion was quantified using the cell counting from fluorescence images (*included article N, Figure 4*) and by immunofluorescence staining of vinculin in FAs (*included article N, Figure 5*). The FAs are oblong structures therefore we measured their long and short axis to quantify their shape and size (*included article N, Figure 6*). The results suggest that 5 min oxygen treatment (changing hydrophobic to hydrophilic character

of the surface) creates the most suitable SWCNT surface for the cell adhesion. The cell number on this surface was twice higher than on the other surfaces and the FAs formed by the cells were present on the whole bottom of the cell in contrast with other surfaces. The cells adhering on 30 min treated SWCNT layer had clearly very different morphology and formation of the adhesion apparatus suggesting worse adhesion conditions. The size of the FAs was decreasing with the oxygenation of the SWCNT surface. In case of 1 and 5 minutes O-treated sample the size of the FAs was very similar. However, the cell number was very different and the localization of the FAs also suggested that the cell adhesion was the best on 5 minutes treated sample.

5.4.2 Unpublished SWCNT Results

The size of the single cell was also measured; however, this result was not published (Figure 23). The smallest cells were observed on the 5 minutes O-treated sample; however, it was only because of the full confluency of the cell layer. The cells had no room to spread already after 48 h of cultivation on this sample. The cells on the other samples were significantly larger. There was no difference in the cell size on no treated (H) sample and 1 minute O-treated sample; however, the size of the cells on 30 minutes O-treated sample was smaller than H and 1 minute O-treated sample even though the cells were not confluent. This again points to a compromised cell adhesion on the 30 minutes O-treated sample.

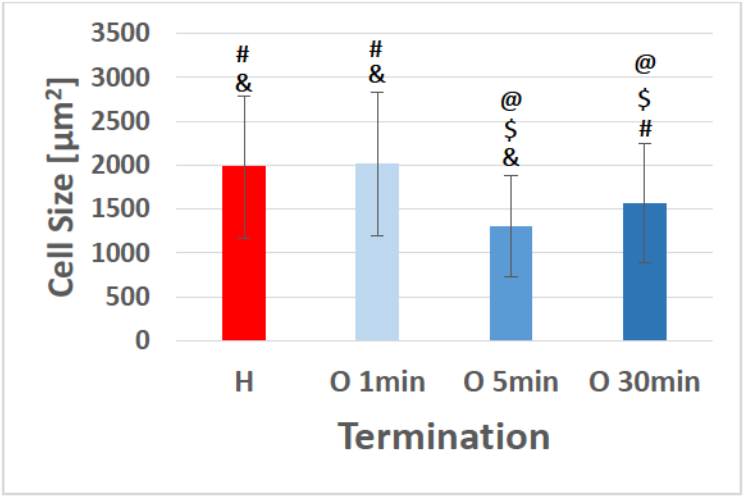

Figure 23: Size of cells cultivated for 48 h on SWCNT surfaces with different termination (H – hydrogen, O – oxygen) and with different oxygen plasma treatment times, significant difference to: @ - H, $ - O 1min, # - O 5min, & - O 30min, p-value = 0,01 in all cases.

6 Discussion

6.1 Nanocrystalline Diamond with Different Nanotopographies

The first topographical study (*included article A*) described the cell adhesion and metabolic activity on NCD of various roughnesses. Its uniqueness lay in the comparison of the response of two cell types – non-differentiated primary hMSCs and differentiated SAOS-2 human cell line on three nanocrystalline diamond roughnesses. The results confirmed that NCD surface is suitable for cultivation of both cell types as was already published (Bajaj et al., 2007; Rubio-Retama et al., 2006). However, the cell response to the nanomaterial topography differs. The decreasing roughness of NCD surface supports the early adhesion of differentiated SAOS-2, whereas the speed of adhesion of hMSC does not change with the roughness of the surface. On the other hand, the metabolic activity of the undifferentiated cells after 48 h of cultivation is increased (although insignificantly) with the growing RMS roughness, whereas the metabolic activity of SAOS-2 cells is significantly decreased. Yang et al. published study describing differentiatedhuman fetal osteoblast adhesion on NCD (grain size 30-100 nm), submicron crystalline diamond (SMCD, grain size 100-600 nm) with RMS roughness 19,8 nm and 56,3 nm respectively and flat silicone (Yang et al., 2009). The cell adhesion in this case also proved to be the worst on SMCD surface and surprisingly the best adhesion was observed on Si substrate. Si wafers proved to be worse substrates for cell adhesion in other graphene studies done in our group. In the study of Yang at al. the cell adhesion was probably negatively influenced by the hydrogen termination of the diamond surfaces. H-NCD substrates were observed to be worse in comparison to O-NCD in our studies. We speculate that in our study the adhesion and metabolic activity of both cell types (SAOS-2 and hMSCs) was different due to their differentiation states. The hard diamond surface with nanoroughness was recognized by SAOS-2 cells as familiar environment therefore they adhere to such surface more willingly as is demonstrated by the number of adhered cells after 1 h. However, undifferentiated hMSCs used to softer niche of bone marrow could be driven by the harder material towards higher activity. This speculation could be supported by review of Shyh-Chang et al. describing the changes in energy metabolism of stem

cells depending on which differentiation path they take. The review shows that the oxidative phosphorylation is increased in hMSC that differentiate into osteoblasts (Shyh-Chang et al., 2013). Since MTS transition to formazan on which is the metabolic test based is supposed to be mediated by reduced form of nicotinamide adenine dinucleotide (NADH) which is needed for the oxidative phosphorylation to take place we suggest that hMSCs in our experiment have been also driven to the osteogenic differentiation. The influence of surface topography and mechanical properties on adhesion was observed in work of Chen et al. The authors prepared smooth (1 nm) and nanorough (70 and 150 nm) glass surfaces by lithography process and proved that the preference of human embryonal stem cells (hESC) and differentiated fibroblasts (NIH/3T3) to those surfaces was opposite (Chen et al., 2012). hESC adhered better on smooth surfaces and were driven towards differentiation by the nanorough surfaces. In contrast the differentiated fibroblasts NIH/3T3 adhered on the rough surfaces and did not adhere to the smooth surfaces. The work of Watari found that hMSCs cultivated on perpendicular submicron (400nm) ridges on Si substrate deposit more Ca and have increased expression of RUNX2 gene – a marker of osteoblastic differentiation (Watari et al., 2012). The work of Vandrovcova was studying cell adhesion of MG63 human osteoblast cell line on nanorough TiO_2 (0 nm , 40 nm, 100 nm, 170 nm) and glass surfaces (Vandrovcova et al., 2012). Cell adhesion on particular roughness differs on both materials. After 1 day of cultivation the roughnesses 0 nm and 170 nm supported the adhesion of MG63 osteoblasts on TiO_2 whereas on the glass surface the best cell adhesion was in the middle range (40 nm 100 nm). This proves that the cell adhesion is a complicated phenomenon ruled by both chemical and topographical cues.

The other two topographical studies focused on unique nanostructures fabricated on NCD by ion etching and the formation of cell adhesion apparatus on these surfaces. These nanostructures were in their dimensions roughly one order of magnitude smaller than the nanodiamond crystals of the original matrix. Our studies demonstrated that the focal adhesions size and amount of signaling proteins (pFAK) in the adhesion sites can be manipulated by nanostructuring of the surface topography. Even though the surface structures were covered with serum proteins the formation of thinner adhesion was observed on the nanorods compared to the other surfaces. The cells were able to adhere probably only on the tips of nanorods and not

in between them. Whereas on nanocones and ultrananocones the cells were able to touch even the basis of NCD matrix as is illustrated by the proposed model (Figure 18). The ultrananocones surface features were perhaps so miniscule for the cells to perceive on the fine surface topography that was also covered with the FBS proteins from the cultivation medium. However, very well-formed focal adhesions were observed on this surface. The size and shape of sites available for cells to adhere can therefore influence the cell fate in many various ways as focal adhesion signaling influence the cell proliferation, migration and differentiation.

Prepared nanostructures, especially the nanorods, can be compared to surfaces investigated in the work of Yang (Yang et al., 2010). The nanostructures were prepared from silicon by wet etching. Two different kinds of silane compounds were deposited on the surface modifying its wettability. CHO cells were used for biocompatibility tests. Unlike the NCD nanorods, the nanostructuring of the silicon substrate influenced the cell adhesion clearly negatively. However, the study also proved that the deposited silanes and wettability of the surface could significantly influence cell adhesion both positively and negatively. The quality of the cell adhesion is therefore orchestrated by both substrate topography and substrate chemistry. Oxidizing of the NCD nanostructures could also significantly improve the cell adhesion as is disscused in the next chapter.

6.2 Nanocrystalline Diamond with Different Surface Terminations

The first studies investigating the NCD surface termination (*included articles D and E*) confirmed that the hydrophilic oxygen termination of NCD promotes the cell adhesion more than the hydrophobic H termination. Similar observations were already done in studies on other materials like self-assembled monolayers from alkylthiols (Barrias et al., 2009; Lopez et al., 1993; Scotchford et al., 2002) and silanes (Healy et al., 1996; Ishizaki et al., 2010; McFarland et al., 2000). The surface chemical termination can be used as a tool for controlling the cell adhesion e.g. on implants as well as for fabrication of biosensing devices which was confirmed in the *included article F*. Same principle was then used for construction of impedance biosensor (Izak et al., 2014).

Our studies also indicate that FBS and the proteins contained in it are an important factor influencing the speed and strength of the cell adhesion. FBS proteins

adsorb on almost any surface before the cells touch it. The results obtained by our colleagues from the Institute of Physics using AFM (*included articles D and E*) suggested that the protein layer formed on H-NCD is less stable than the layer on O-NCD. The experiments with shaking of the adhering SAOS-2 cells revealed that the weakest cell adhesion after 2 h was in FBS-containing medium on H-NCD. That confirmed AFM observations of protein layer. The observations of cells adhering on samples with striped termination pattern indicated that O-NCD is preferred by the cells on samples with preadsorbed FBS proteins. This reveals that the positive effect of the O termination "radiates" even through a thick FBS layer as was described in an classical review of Schakenraad and Busscher (Schakenraad and Busscher, 1989). Microscopy observation of cells adsorbed on samples with preadsorbed chosen FBS proteins albumin (most abundant), fibronectin and vitronectin strongly indicated that the protein most responsible for the termination selectivity is fibronectin, although Raman spectroscopy at the Institute of Physics was not sensitive enough to detect it on the diamond surface. Important aspect of the adsorbed FBS proteins can be their conformation as is indicated in a work of Gugutkov et al. that revealed that cell adhesion is dependent on the density of hydroxyl (oxygen containing) groups of acrylate copolymers coated by fibronectin (Gugutkov et al., 2010). Scotchford and Keselowsky studied how alkylthiol SAM surface functional groups (-COOH, -OH, CH_3, -NH_2) influence the adsorption and conformation of serum proteins (fibronectin in particular) (Scotchford et al., 2002). Oxygen containing groups (carboxyl and hydroxyl) were promoting the cell adhesion in comparison to methyl and amino groups. Oxidized NCD surface may have a variety of oxygen function groups attached on the surface including carboxyl, carbonyl and hydroxyl groups.

The experiments presented in the *included articles G* confirmed that the cells are indeed adhering faster on O-NCD and without FBS in the cultivation medium. The life-cell imaging experiments confirmed that FBS layer acts as a barrier slowing the cell attachment and adhesion and allows the cells to move on the substrate up to several minutes before adhesion. This phenomenon allows the cells to encounter the more suitable O-NCD surface and adhere there. This in turn creates cell coverage according to the termination pattern. However, the presence of FBS proteins is certainly not required for cell adhesion as was also observed in our previous experiments. That means that the cell adhesion *in vitro* does not depend on certain specific proteins or protein moieties or peptides. Several studies on various

eukaryotic organisms discovered that cell adhesion may be strongly depending on proteoglycans and glycoproteins present on cell surface (Loomis et al., 2012; Moon et al., 2005). The studies of Cohen and Zaidel-bar describe the adhesion of chondroblasts and endothelial cells to ECM (Cohen et al., 2003, 2006, 2007; Zaidel-Bar et al., 2004). Cohens study from the year 2003 describes a similar drift phenomenon observed in the *included article G* of cells under sheer stress before full adhesion; however, this drift is not present in endothelial cells with thinner hyaluronan layer. This kind of layer, if present also in SAOS-2 adhesion, can be important for explanation of the variances in SAOS-2 adhesion on O-NCD and H-NCD.

Based on our results and results found in the literature, we suggest that the initial non-specific contact of the cell proteoglycan and glycosaminoglycan coat decides where the cell will adhere based on the substrate electrochemical properties and the presence of serum proteins in certain composition amount and conformation. The cell drift allowed by FBS layer at the beginning of the experiment and faster adhesion of the cells onto O-NCD could significantly shift the distribution of the cells in favor of O-NCD early in the experiment, especially on the samples with microscopic termination stripes.

6.3 Graphene

The studies on graphene were truly pioneering the field of biocompatibility of this unique material. They proved that this material despite its thickness can affect the cell adhesion mostly in positive manner. It is hard to compare this material to any other due to its dimensional and physical properties. However, we were able to conduct experiments that probed the influence of oxygen and hydrogen surface modification of this material on the cell adhesion as on the NCD. The first study of graphene (*included article I*) discovered that macroscopic untreated graphene flakes are suitable for the cell adhesion. The adhesion was improved when compared to the Si/SiO_2 - substrate used to support the graphene sheet, although silicone is considered to be material with a good biocompatibility (Berry et al., 2004).

In the next study (*included article J*), we tried to quantify the difference in cell adhesion represented by cell number and cell area between graphene, its underlying substrate Si/SiO_2 and TC PS as a commonly used reference. We also

included FBS presence/absence during the cell seeding (2 h) as another experiment variable. The results confirmed that the cells adhere and grow on graphene significantly better than on the underlying Si substrate. The results from the serum-free experiments revealed that the cell adhesion on graphene was not affected by the initial absence of the serum as was observed on TC PS. Further studies (*included articles K and L*) expanded the experimental variables again for the oxygen and hydrogen surface terminations of the graphene as was done on NCD. On graphene, O- and H-treatment was done using only increased temperature in respective atmospheres. The results indicated that the presence of serum is surely inhibiting the cell adhesion (cell number and cell size) as was observed on NCD. However, surprising observation was that the early cell adhesion is significantly improved on more hydrophobic H-termination and not on hydrophilic O-termination as was on NCD. The second study added to the previous results the measurements done after 48 h of cultivations and measurements of focal adhesion dimensions. The results also confirmed the previous observations from 2 h interval and indicated that after addition of FBS the differences in cell number and cell is slowly equalizing. Still, after 48 h of cultivation the differences between experiments with FBS in medium and FBS-free experiments persist. The H-terminated graphene (1-LG) was again observed to be the most suitable surface for cell adhesion. Several studies revealed that the graphene electrical properties can by modified by chemical composition (Cupolillo et al., 2015), nanotopography (Lee and Kim, 2012) and mechanical strain (Lee et al., 2013) of the underlying substrate supporting the graphene sheet . We can therefore speculate that since graphene is a single atom thick nanomaterial, the different adhesion of the SAOS-2 cells on same termination on graphene and NCD can be perhaps explained by influence of the Si/SiO_2 substrate on the electrochemistry of the graphene layer.

The last publication (*included article M*) compared the results obtained on graphene with the results from NCD with O and H termination. The materials have the same composition and surface termination. The contact angles indicated that the H-termination is making the surface of diamond and graphene hydrophobic and the oxidation creates hydrophilic surface. The SEM and AFM images indicated that the topography of the oxidized and hydrogenated graphene is different. The hydrogenated graphene carries nanowrinkles few nanometers in size, whereas the oxidized graphene was much smoother. Generally, the results indicate that NCD and

graphene are similarly good for cell adhesion comparable to tissue culture polystyrene. If not disturbed, the cells adhered to O-NCD and H-NCD in similar numbers after certain time. However, there is a marked difference in cell adhesion between oxidized graphene and hydrogenated graphene in favor of the hydrogen termination as was observed in our previous works. The worse adhesion to O-graphene can be explained by possible toxic effect of the oxidized graphene. However, enhanced H-graphene is probably explainable only through the nanotopography that is not present on O-graphene. Better cell adhesion on H-graphene can make the graphene a better choice for construction of biosensors than NCD because O-termination makes from the graphene an insulator (Gómez-Navarro et al., 2007) as is in the case of NCD.

6.4 Single-Walled Carbon Nanotubes

The only study in this chapter was aimed on description of the influence of exposition time of SWCNT films to oxygen plasma on the cell. The work was inspired by the unique electrical SWCNTs properties that can be, similarly to graphene, utilized for the construction of biosensors (Balasubramanian and Burghard, 2006; Yang et al., 2015). The majority of the SWCNT studies aim on toxicity (Lam et al., 2006; Movia et al., 2011; Wang et al., 2011) issues or utilization in targeted therapies (Iancu et al., 2011; Markovic et al., 2011; Yang et al., 2012b). However, the work of Akasaki investigated the cell adhesion of SAOS-2 cells on SWCNT and MWCNT films prepared by sedimentation and drying on non-adhesive non-treated polystyrene. The results indicate that the cell adhesion was indeed improved by addition of the SWCNT on the surface.

The SWCNT film in our work was prepared by a simple procedure resulting in relatively stable substrate. The uniqueness of the work was in using of oxygen plasma exposure for three different times allowing us to choose the optimal period of plasma treatment. The plasma processing in the oxygen atmosphere led to change in the surface wettability as was observed on to the NCD. However, the surface morphology was also markedly changed as this material is certainly not as resilient to the plasma exposure as the NCD. The SWCNTs were slowly burned by the oxygen plasma. The prolonged exposition the oxygen plasma (30-minutes treatment)

ultimately resulted in damage of the SWCNT layer and in significant deterioration of the cell colonization of the surface back on the level of pristine SWCNT film.

The fluorescence microscopy images indicated a different confluency of the SAOS-2 cells on samples with different plasma treatment times. The confluency on 5 minutes O-treated sample was close to 100% and the cell counting indeed confirmed that for the best cell adhesion the optimal oxygen plasma exposure of SWCNT film is 5 minutes. The sample had twice the number of cells than all the other surfaces including the hydrogenated SWCNT. The O5 sample had also the lowest contact angle with water droplet, i.e. with the best wettability. However, the difference in wettability between samples treated for 5 and 30 minutes was negligible. The cell adhesion must be therefore influenced also by factors like topography and SWCNT structural degradation and creation of more toxic products.

Immunofluorescence staining of the vinculin protein again confirmed that the 5-minute exposure is the best for the cell adhesion as FAs can be observed not only at the edges of the cells but also in the cell center. The vinculin staining of cells cultivated on O30 sample was aggregated in very small FAs as is illustrated by the FA axes measurements. The significant deterioration of the cell adhesion on O30 sample can be explained by several ways including surface stability, surface topography, composition/conformation of the adsorbed proteins and CNT induced oxidative stress (Hsieh et al., 2014; Manke et al., 2013).

7 Conclusions

1) We described the cell adhesion and changes in metabolic activity of differentiated SAOS-2 osteoblast cell line and hMSC on NCD. SAOS-2 cells tend to adhere to solid NCD substrate in higher numbers than hMSCs. Moreover, lower RMS roughness was more suitable for SAOS-2 cell adhesion. HMSC tend to adhere in similar numbers to all NCD roughnesses. The highest metabolic activity of hMSC was observed on samples with the highest roughness (500 nm). This could indicate a tendency towards differentiation. The cells adopted different shapes and produced lamellipodia in dependence on the surfaces topography. The cells cultivated on smoother surfaces with 20 nm RMS roughness were round after 2 h of adhesion. Higher roughness (270 nm and 500 nm) caused formation of lamellipodia on the cell edges. The cells are probably forced to search for suitable places for optimal anchoring.

2) We described the cell adhesion and growth of SAOS-2 cells on oxidized nanostructured NCD surfaces prepared by dry ion etching. The cells adhere to all surfaces in similar numbers and shape. However, the formation of the adhesion apparatus differs depending on the topography feature shape. The thinnest focal adhesions were observed on high and thin nanorods, larger focal adhesions were observed on nanocones and ultrananocones.

3) We described the differences of adhesion of SAOS-2 cells on hydrophilic oxidized O-NCD and hydrophobic hydrogenated H-NCD used for preparation of biosensor. The cells tend to adhere faster on O-NCD surfaces resulting in preferential colonization of O-NCD in the vicinity of H-NCD area. FBS plays an important role in cell adhesion on these surface terminations. It slows down the cell anchorage and adhesion allowing the cells to drift and distribute themselves especially on samples with termination pattern. Without FBS, the cells tend to adhere on spot where they touch the surface regardless its termination. However, the adhesion on O-NCD is still faster than on H-NCD even without FBS. Migration of SAOS-2 cells on H-NCD is faster than on O-NCD, which in turn helps to distribute the cells in favor of O-NCD during further cultivation again.

Field effect transistor on basis of O-NCD and H-NCD was prepared at the Institute of Physics CAS. Its ability to detect adsorbed protein layer and adhered cells was confirmed.

4) We described the adhesion and proliferation of SAOS-2 cells on graphene. Graphene turned out to be better substrate for cell cultivation than undelaying Si/SiO_2. Proliferation of SAOS-2 cells is improved, in particular, by hydrophobic hydrogenated graphene, whereas the oxidation of graphene turned out to be hindering the cell adhesion and growth. This is in contrast to the results seen on NCD. Moreover, improved cell adhesion and proliferation on graphene is independent of presence of FBS proteins in the cultivation medium. AFM revealed a large number of "nanowrinkles" on hydrogenated graphene that are not present on oxidized graphene. This nanotopography difference can be related to the observed difference in cell adhesion. No differentiation tendencies of hMSC cultivated on graphene were observed.

5) We described the adhesion and growth of SAOS-2 cells on SWCNT films with different times of oxygen plasma treatment. The most suitable time of oxygen treatment for cell adhesion and proliferation was 5 minutes. Prolonged 30-minute plasma treatments damaged SWCNT film and worsen the cell adhesion back to the level of the untreated sample with pristine (hydrogenated) SWCNTs. The wettability of the sample could not be improved with 30-minute oxygen treatment. Interestingly the focal adhesions on 30 minutes oxygen-treated sample were the smallest of all the studied SWCNT films. Largest focal adhesions were in contrast on the pristine SWCNT film. The adhesions were present at the edges of cell filopodia. However, the best formation of focal adhesion apparatus was observed on the 5 minutes O-treated sample, where the FAs were distributed under the whole cell.

All studied carbon based nanomaterials proved to support cell adhesion and growth. Their surface topography and chemistry of the materials can be modified to control cell adhesion and proliferation.

8 List of Abbreviations

A6 – *Xenopus laevis* kidney epithelial cells

AFM – atomic force microscopy

ARPE-19 - human retina pigment epithelium cells

ATM – advanced tracking module for NIS-Elements software

BMP – bone morphogenic protein

CA – contact angle with water droplet, a measure of surface wettability

CAM – cell adhesion molecule

CAS – Czech Academy of Sciences

CHO – Chinese hamster ovary epithelial cells

CVD – chemical vapor deposition

DAPI – 4',6-diamidino-2-phenylindole, fluorescent dye for DNA staining

ddH2O – deionized and distilled water

DLC – diamond-like carbon, one of many carbon allotropes

DWCNT – double-walled carbon nanotube

FBS – fetal bovine serum

GAG – glycosaminoglycan

GFOGER – peptide glycine, phenylalanine, hydroxyproline, glycine, glutamic acid, arginine

HeLa – human cervical carcinoma cell line

hESC – human embryonal stem cells

HF CVD hot filament chemical vapor depostion

HK-2 – human kidney cortex cell line

H-NCD – hydrogen terminated NCD

HPdLF – human periodontal ligament fibroblasts

LINC – protein complex - linker of nucleoskeleton and cytoskeleton

MG63 – human osteoblast cell line

MCD – monocrystalline diamond

MP CVD – microwave plasma induced chemical vapor deposition

MSC – mesenchymal stem cells

MTS – 3-(4,5-dimethylthiazol-2-yl)-5-(3-carboxymethoxyphenyl)-2-(4-sulfophenyl)-2H-tetrazolium – a compound used for metabolic activity test

MWCNT – multi-walled carbon nanotube

NA – numerical aperture

NADH – nicotinamide adenine dinucleotide

NADPH – nicotinamide adenine dinucleotide phosphate

NCD – nanocrystalline diamond

NIH/3T3 – mouse embryo fibroblast cell line

O-NCD – oxygen terminated NCD

PBS – phosphate buffered saline – a standard buffer used in cell biology applications

PC12 – cell line derived from pheochromocytoma of rat adrenal medulla

pFAK – phosphorylated focal adhesion kinase

PI3K – phosphoinositide 3-kinase

PS – polystyrene – a polymer used for manufacturing of standard cultivation flasks, petri dishes and plates.

PMMA – poly (methyl methacrylate)

RCJ-P – rat chondrocytes from fetal calvaria

RGD – peptide arginine, glycine, aspartic acid

RhoA – Ras homolog member A, small GTPase

RIE – reactive ion etching

RMS – root mean square – a statistical value also used as a measure of surface roughness.

ROCK – Rho-associated protein kinase

RUNX2 – Runt-related transcription factor 2

SAM – self-assembled monolayer

SAOS-2 – human osteosarcoma cell line (SArcoma OSteogenic)

SEM – scanning electron microscopy

SG FET – solution gated field effect transistor

SMCD – submicrocrystalline diamond

SWCNT – single-walled carbon nanotubes

TC PS tissue culture polystyrene

UNCD – ultra nanocrystalline diamond

9 References

Abbaschian, R., Zhu, H., and Clarke, C. (2005). High pressure–high temperature growth of diamond crystals using split sphere apparatus. Diam. Relat. Mater. *14*, 1916–1919.

Agarwal, S., Zhou, X., Ye, F., He, Q., Chen, G.C.K., Soo, J., Boey, F., Zhang, H., and Chen, P. (2010). Interfacing Live Cells with Nanocarbon Substrates. Langmuir *26*, 2244–2247.

Ai, J., Kiasat-Dolatabadi, A., Ebrahimi-Barough, S., Ai, A., Lotfibakhshaiesh, N., Norouzi-Javidan, A., Saberi, H., Arjmand, B., and Aghayan, H.R. (2013). Polymeric Scaffolds in Neural Tissue Engineering: A Review. Arch. Neurosci. *1*, 15–20.

Akhavan, O., and Ghaderi, E. (2010). Toxicity of Graphene and Graphene Oxide Nanowalls Against Bacteria. ACS Nano *4*, 5731–5736.

Akhtar, M.J., Ahamed, M., Kumar, S., Khan, M.M.A., Ahmad, J., and Alrokayan, S.A. (2012). Zinc oxide nanoparticles selectively induce apoptosis in human cancer cells through reactive oxygen species. Int. J. Nanomedicine *7*, 845–857.

Alakoski, E., Tiainen, V.-M., Soininen, A., and Konttinen, Y.T. (2008). Load-bearing biomedical applications of diamond-like carbon coatings-current status. Open Orthop. J. *2*, 43.

Amaral, M., Dias, A.G., Gomes, P.S., Lopes, M.A., Silva, R.F., Santos, J.D., and Fernandes, M.H. (2008a). Nanocrystalline diamond: In vitro biocompatibility assessment by MG63 and human bone marrow cells cultures. J. Biomed. Mater. Res. A *87A*, 91–99.

Amaral, M., Gomes, P.S., Lopes, M.A., Santos, J.D., Silva, R.F., and Fernandes, M.H. (2008b). Nanocrystalline Diamond as a Coating for Joint Implants: Cytotoxicity and Biocompatibility Assessment. J. Nanomater. *2008*, 1–9.

Arash, B., Wang, Q., and Varadan, V.K. (2014). Mechanical properties of carbon nanotube/polymer composites. Sci. Rep. *4*, 6479.

Ariano, P., Budnyk, O., Dalmazzo, S., Lovisolo, D., Manfredotti, C., Rivolo, P., and Vittone, E. (2009). On diamond surface properties and interactions with neurons. Eur. Phys. J. E Soft Matter *30*, 149–156.

Avizienyte, E., and Frame, M.C. (2005). Src and FAK signalling controls adhesion fate and the epithelial-to-mesenchymal transition. Curr. Opin. Cell Biol. *17*, 542–547.

Bajaj, P., Akin, D., Gupta, A., Sherman, D., Shi, B., Auciello, O., and Bashir, R. (2007). Ultrananocrystalline diamond film as an optimal cell interface for biomedical applications. Biomed. Microdevices *9*, 787–794.

Balasubramanian, K., and Burghard, M. (2006). Biosensors based on carbon nanotubes. Anal. Bioanal. Chem. *385*, 452–468.

Barczyk, M., Carracedo, S., and Gullberg, D. (2010). Integrins. Cell Tissue Res. *339*, 269–280.

Barrias, C.C., Martins, M.C.L., Almeida-Porada, G., Barbosa, M.A., and Granja, P.L. (2009). The correlation between the adsorption of adhesive proteins and cell behaviour on hydroxyl-methyl mixed self-assembled monolayers. Biomaterials *30*, 307–316.

Berry, C.C., Campbell, G., Spadiccino, A., Robertson, M., and Curtis, A.S.G. (2004). The influence of microscale topography on fibroblast attachment and motility. Biomaterials *25*, 5781–5788.

Bethune, D.S., Klang, C.H., de Vries, M.S., Gorman, G., Savoy, R., Vazquez, J., and Beyers, R. (1993). Cobalt-catalysed growth of carbon nanotubes with single-atomic-layer walls. Nature *363*, 605–607.

Bhola, R., Bhola, S.M., Mishra, B., and Olson, D.L. (2011). Corrosion in titanium dental implants/prostheses–a review. Trends Biomater. Artif. Organs *25*, 34–46.

Biggs, M.J.P., Richards, R.G., Gadegaard, N., McMurray, R.J., Affrossman, S., Wilkinson, C.D.W., Oreffo, R.O.C., and Dalby, M.J. (2009). Interactions with nanoscale topography: Adhesion quantification and signal transduction in cells of osteogenic and multipotent lineage. J. Biomed. Mater. Res. A *91A*, 195–208.

Bronikowski, M.J., Willis, P.A., Colbert, D.T., Smith, K.A., and Smalley, R.E. (2001). Gas-phase production of carbon single-walled nanotubes from carbon monoxide via the HiPco process: A parametric study. J. Vac. Sci. Technol. Vac. Surf. Films *19*, 1800–1805.

Calderwood, D.A., Campbell, I.D., and Critchley, D.R. (2013). Talins and kindlins: partners in integrin-mediated adhesion. Nat. Rev. Mol. Cell Biol. *14*, 503–517.

Cary, L.A., Han, D.C., Polte, T.R., Hanks, S.K., and Guan, J.-L. (1998). Identification of p130Cas as a mediator of focal adhesion kinase–promoted cell migration. J. Cell Biol. *140*, 211–221.

Chen, D., Bertollo, N., Lau, A., Taki, N., Nishino, T., Mishima, H., Kawamura, H., and Walsh, W.R. (2011). Osseointegration of porous titanium implants with and without electrochemically deposited DCPD coating in an ovine model. J. Orthop. Surg. *6*, 56.

Chen, H.-C., Appeddu, P.A., Isoda, H., and Guan, J.-L. (1996). Phosphorylation of tyrosine 397 in focal adhesion kinase is required for binding phosphatidylinositol 3-kinase. J. Biol. Chem. *271*, 26329–26334.

Chen, W., Villa-Diaz, L.G., Sun, Y., Weng, S., Kim, J.K., Lam, R.H.W., Han, L., Fan, R., Krebsbach, P.H., and Fu, J. (2012). Nanotopography Influences Adhesion, Spreading, and Self-Renewal of Human Embryonic Stem Cells. ACS Nano *6*, 4094–4103.

Chen, Y.-C., Lee, D.-C., Hsiao, C.-Y., Chung, Y.-F., Chen, H.-C., Thomas, J.P., Pong, W.-F., Tai, N.-H., Lin, I.-N., and Chiu, I.-M. (2009). The effect of ultra-nanocrystalline diamond films on the proliferation and differentiation of neural stem cells. Biomaterials *30*, 3428–3435.

Cherniavskaya, O., Chen, C.J., Heller, E., Sun, E., Provezano, J., Kam, L., Hone, J., Sheetz, M.P., and Wind, S.J. (2005). Fabrication and surface chemistry of nanoscale bioarrays designed for the study of cytoskeletal protein binding interactions and their effect on cell motility. J. Vac. Sci. Technol. B Microelectron. Nanometer Struct. *23*, 2972.

Chong, K.F., Loh, K.P., Vedula, S.R.K., Lim, C.T., Sternschulte, H., Steinmüller, D., Sheu, F., and Zhong, Y.L. (2007). Cell Adhesion Properties on Photochemically Functionalized Diamond. Langmuir *23*, 5615–5621.

Cohen, M., Klein, E., Geiger, B., and Addadi, L. (2003). Organization and adhesive properties of the hyaluronan pericellular coat of chondrocytes and epithelial cells. Biophys. J. *85*, 1996–2005.

Cohen, M., Kam, Z., Addadi, L., and Geiger, B. (2006). Dynamic study of the transition from hyaluronan-to integrin-mediated adhesion in chondrocytes. EMBO J. *25*, 302–311.

Cohen, M., Joester, D., Sabanay, I., Addadi, L., and Geiger, B. (2007). Hyaluronan in the pericellular coat: an additional layer of complexity in early cell adhesion events. Soft Matter *3*, 327.

Cook, S.D., Beckenbaugh, R.D., Redondo, J., Popich, L.S., Klawitter, J.J., and Linscheid, R.L. (1999). Long-Term Follow-up of Pyrolytic Carbon Metacarpophalangeal Implants*. J. Bone Jt. Surg. *81*, 635–48.

Critchley, D.R., and Gingras, A.R. (2008). Talin at a glance. J. Cell Sci. *121*, 1345–1347.

Cupolillo, A., Politano, A., Ligato, N., Cid Perez, D.M., Chiarello, G., and Caputi, L.S. (2015). Substrate-dependent plasmonic properties of supported graphene. Surf. Sci. *634*, 76–80.

Cuvelier, D., Théry, M., Chu, Y.-S., Dufour, S., Thiéry, J.-P., Bornens, M., Nassoy, P., and Mahadevan, L. (2007). The Universal Dynamics of Cell Spreading. Curr. Biol. *17*, 694–699.

Dahl, K.N., Ribeiro, A.J.S., and Lammerding, J. (2008). Nuclear Shape, Mechanics, and Mechanotransduction. Circ. Res. *102*, 1307–1318.

Dalby, M.J., Gadegaard, N., Tare, R., Andar, A., Riehle, M.O., Herzyk, P., Wilkinson, C.D.W., and Oreffo, R.O.C. (2007). The control of human mesenchymal cell differentiation using nanoscale symmetry and disorder. Nat. Mater. *6*, 997–1003.

Daruwalla, Z., Davies, K., Shafighian, A., and Gillham, N. (2012). Early results of a prospective study on the pyrolytic carbon (pyrocarbon) Amandys® for osteoarthritis of the wrist. Ann. R. Coll. Surg. Engl. *94*, 496–501.

Davydova, M., Kulha, P., Babchenko, O., and Kromka, A. (2015). Hydrogen-Terminated Diamond Surface as Gas Sensing Layer Working at Room Temperature. In Nanocon, (Brno, Czech Republic: Tanger)

Deligianni, D.D., Katsala, N.D., Koutsoukos, P.G., and Missirlis, Y.F. (2000). Effect of surface roughness of hydroxyapatite on human bone marrow cell adhesion, proliferation, differentiation and detachment strength. Biomaterials *22*, 87–96.

Deng, Y., Zhang, X., Zhao, Y., Liang, S., Xu, A., Gao, X., Deng, F., Fang, J., and Wei, S. (2014). Peptide-decorated polyvinyl alcohol/hyaluronan nanofibers for human induced pluripotent stem cell culture. Carbohydr. Polym. *101*, 36–39.

Dingal, P.D.P., and Discher, D.E. (2014). Combining insoluble and soluble factors to steer stem cell fate. Nat. Mater. *13*, 532–537.

Du, Y., Zhang, W., and Wang, M. (2016). Sensing of Salivary Glucose Using Nano-Structured Biosensors. Biosensors *6*, 10.

Dyondi, Webster, and Banerjee, R. (2012). A nanoparticulate injectable hydrogel as a tissue engineering scaffold for multiple growth factor delivery for bone regeneration. Int. J. Nanomedicine 47.

Elfenbein, A., and Simons, M. (2013). Syndecan-4 signaling at a glance. J. Cell Sci. *126*, 3799–3804.

Engler, A.J., Sen, S., Sweeney, H.L., and Discher, D.E. (2006). Matrix Elasticity Directs Stem Cell Lineage Specification. Cell *126*, 677–689.

Faklaris, O., Joshi, V., Irinopoulou, T., Tauc, P., Sennour, M., Girard, H., Gesset, C., Arnault, J.-C., Thorel, A., Boudou, J.-P., et al. (2009). Photoluminescent Diamond Nanoparticles for Cell Labeling: Study of the Uptake Mechanism in Mammalian Cells. ACS Nano *3*, 3955–3962.

Feng, L., Chen, Y., Ren, J., and Qu, X. (2011). A graphene functionalized electrochemical aptasensor for selective label-free detection of cancer cells. Biomaterials *32*, 2930–2937.

Feng, L., Wu, L., and Qu, X. (2013). New Horizons for Diagnostics and Therapeutic Applications of Graphene and Graphene Oxide. Adv. Mater. *25*, 168–186.

Fogh, J. (1975). Human Tumor Cells in Vitro (Boston, MA: Springer US).

Fogh, J., Wright, W.C., and Loveless, J.D. (1977). Absence of HeLa cell contamination in 169 cell lines derived from human tumors. J. Natl. Cancer Inst. *58*, 209–214.

Fojt, J., Šmatová, S., Joska, L., and Hnilica, F. Corrosion Behaviour of Ti-39Nb Alloy Prepared by Powder Metallurgy. Metal 2012, (Brno, Czech Republic: Tanger)

Frank, I.W., Tanenbaum, D.M., van der Zande, A.M., and McEuen, P.L. (2007). Mechanical properties of suspended graphene sheets. J. Vac. Sci. Technol. B Microelectron. Nanometer Struct. *25*, 2558.

Frisch, S.M., and Francis, H. (1994). Disruption of epithelial cell-matrix interactions induces apoptosis. J. Cell Biol. *124*, 619–626.

Fucikova, A., Valenta, J., Pelant, I., Kalbacova, M.H., Broz, A., Rezek, B., Kromka, A., and Bakaeva, Z. (2014). Silicon nanocrystals and nanodiamonds in live cells: photoluminescence characteristics, cytotoxicity and interaction with cell cytoskeleton. RSC Adv *4*, 10334–10342.

Fukuda, K., Knight, J.D.R., Piszczek, G., Kothary, R., and Qin, J. (2011). Biochemical, Proteomic, Structural, and Thermodynamic Characterizations of Integrin-linked Kinase (ILK): Cross-Validation of the Pseudokinase. J. Biol. Chem. *286*, 21886–21895.

Geckeler, K.E., and Nishide, H. (2009). Advanced Nanomaterials (Weinheim, Germany: Wiley-VCH Verlag GmbH & Co. KGaA).

Geiger, B., Bershadsky, A., Pankov, R., and Yamada, K.M. (2001). Transmembrane crosstalk between the extracellular matrix--cytoskeleton crosstalk. Nat. Rev. Mol. Cell Biol. *2*, 793–805.

Geim, A.K., and Novoselov, K.S. (2007). The rise of graphene. Nat. Mater. *6*, 183–191.

Gómez-Navarro, C., Weitz, R.T., Bittner, A.M., Scolari, M., Mews, A., Burghard, M., and Kern, K. (2007). Electronic Transport Properties of Individual Chemically Reduced Graphene Oxide Sheets. Nano Lett. *7*, 3499–3503.

Grabarczyk, J., Batory, D., Louda, P., Couvrat, P., Kotela, I., and Bakowicz-Mitura, K. (2007). Carbon coatings for medical implants. J. Achiev. Mater. Manuf. Eng. *20*, 107–110.

Grinnell, F., and Feld, M.K. (1982). Fibronectin adsorption on hydrophilic and hydrophobic surfaces detected by antibody binding and analyzed during cell adhesion in serum-containing medium. J Biol Chem *257*, 4888–4893.

Grinnell, F., and Phan, T.V. (1983). Deposition of fibronectin on material surfaces exposed to plasma: Quantitative and biological studies. J. Cell. Physiol. *116*, 289–296.

Gugutkov, D., Altankov, G., RodrÃ-guez HernÃ¡ndez, J.C., MonleÃ³n Pradas, M., and SalmerÃ³n SÃ¡nchez, M. (2010). Fibronectin activity on substrates with controlled ï£¿OH density. J. Biomed. Mater. Res. A *92A*, 322–331.

Gupta, S., Marcel, N., Sarin, A., and Shivashankar, G.V. (2012). Role of Actin Dependent Nuclear Deformation in Regulating Early Gene Expression. PLoS ONE *7*, e53031.

Hannigan, G.E., Leung-Hagesteijn, C., Fitz-Gibbon, L., Coppolino, M.G., Radeva, G., Filmus, J., Bell, J.C., and Dedhar, S. (1996). Regulation of cell adhesion and anchorage-dependent growth by a new [beta]1-integrin-linked protein kinase. Nature *379*, 91–96.

Hansen, D.C. (2008). Metal corrosion in the human body: the ultimate bio-corrosion scenario. Electrochem. Soc. Interface *17*, 31.

Healy, K.E., Thomas, C.H., Rezania, A., Kim, J.E., McKeown, P.J., Lom, B., and Hockberger, P.E. (1996). Kinetics of bone cell organization and mineralization on materials with patterned surface chemistry. Polym. Scaffolding Hard Tissue Eng. *17*, 195–208.

Hench, L.L. (2002). Third-Generation Biomedical Materials. Science *295*, 1014–1017.

Hsieh, H.-S., Wu, R., and Jafvert, C.T. (2014). Light-Independent Reactive Oxygen Species (ROS) Formation through Electron Transfer from Carboxylated Single-Walled Carbon Nanotubes in Water. Environ. Sci. Technol. *48*, 11330–11336.

Hu, W., Peng, C., Luo, W., Lv, M., Li, X., Li, D., Huang, Q., and Fan, C. (2010). Graphene-Based Antibacterial Paper. ACS Nano *4*, 4317–4323.

Huang, H.-H., Ho, C.-T., Lee, T.-H., Lee, T.-L., Liao, K.-K., and Chen, F.-L. (2004). Effect of surface roughness of ground titanium on initial cell adhesion. Biomol. Eng. *21*, 93–97.

Humphries, J.D. (2006). Integrin ligands at a glance. J. Cell Sci. *119*, 3901–3903.

Hynes, R.O. (2002). Integrins: bidirectional, allosteric signaling machines. Cell *110*, 673–687.

Iancu, C., Constantin, Cornel, C., Flaviu, Rares, Ariana, Cristian, Dana, Florin, Mocan, T., et al. (2011). Enhanced laser thermal ablation for the in vitro treatment of liver cancer by specific delivery of multiwalled carbon nanotubes functionalized with human serum albumin. Int. J. Nanomedicine 129, 129-141.

Ishizaki, T., Saito, N., and Takai, O. (2010). Correlation of Cell Adhesive Behaviors on Superhydrophobic, Superhydrophilic, and Micropatterned Superhydrophobic/Superhydrophilic Surfaces to Their Surface Chemistry. Langmuir *26*, 8147–8154.

Iwata, K., Asawa, Y., Nishizawa, S., Mori, Y., Nagata, S., Takato, T., and Hoshi, K. (2012). The development of a serum-free medium utilizing the interaction between growth factors and biomaterials. Biomaterials *33*, 444–454.

Ižák, T., Novotná, K., Kopová, I., Bačáková, L., Rezek, B., and Kromka, A. (2013). H-terminated diamond as optically transparent impedance sensor for real-time monitoring of cell growth: H-terminated diamond as optically transparent impedance sensor. Phys. Status Solidi B *250*, 2741–2746.

Izak, T., Novotná, K., Kopová, I., Bačáková, L., Varga, M., Rezek, B., and Kromka, A. (2014). Hydrogen-Terminated Diamond Sensors for Electrical Monitoring of Cells. Key Eng. Mater. *605*, 577–580.

Jayaswal, G.P., Dange, S.P., and Khalikar, A.N. (2010). Bioceramic in dental implants: A review. J. Indian Prosthodont. Soc. *10*, 8–12.

Jha, A.K., Xu, X., Duncan, R.L., and Jia, X. (2011). Controlling the adhesion and differentiation of mesenchymal stem cells using hyaluronic acid-based, doubly crosslinked networks. Biomaterials *32*, 2466–2478.

Kairdolf, B.A., Smith, A.M., Stokes, T.H., Wang, M.D., Young, A.N., and Nie, S. (2013). Semiconductor quantum dots for bioimaging and biodiagnostic applications. Annu. Rev. Anal. Chem. Palo Alto Calif *6*, 143-162.

Kaji, H., Tsukidate, K., Hashimoto, M., Matsue, T., and Nishizawa, M. (2005). Patterning the Surface Cytophobicity of an Albumin-Physisorbed Substrate by Electrochemical Means. Langmuir *21*, 6966–6969.

Kalbacova, M., Kalbac, M., Dunsch, L., Kataura, H., and Hempel, U. (2006). The study of the interaction of human mesenchymal stem cells and monocytes/macrophages with single-walled carbon nanotube films. Phys. Status Solidi B *243*, 3514–3518.

Kalbacova, M., Kalbac, M., Dunsch, L., Kromka, A., Vaněček, M., Rezek, B., Hempel, U., and Kmoch, S. (2007). The effect of SWCNT and nano-diamond films on human osteoblast cells. Phys. Status Solidi B *244*, 4356–4359.

Kanchanawong, P., Shtengel, G., Pasapera, A.M., Ramko, E.B., Davidson, M.W., Hess, H.F., and Waterman, C.M. (2010). Nanoscale architecture of integrin-based cell adhesions. Nature *468*, 580–584.

Kane, R., and Ma, P.X. (2013). Mimicking the nanostructure of bone matrix to regenerate bone. Mater. Today *16*, 418–423.

Karakose, E., Schiller, H.B., and Fassler, R. (2010). The kindlins at a glance. J. Cell Sci. *123*, 2353–2356.

Khachatryan, A.K., Aloyan, S.G., May, P.W., Sargsyan, R., Khachatryan, V.A., and Baghdasaryan, V.S. (2008). Graphite-to-diamond transformation induced by ultrasound cavitation. Diam. Relat. Mater. *17*, 931–936.

Khang, D., Lu, J., Yao, C., Haberstroh, K.M., and Webster, T.J. (2008). The role of nanometer and sub-micron surface features on vascular and bone cell adhesion on titanium. Biomaterials *29*, 970–983.

Khatayevich, D., Gungormus, M., Yazici, H., So, C., Cetinel, S., Ma, H., Jen, A., Tamerler, C., and Sarikaya, M. (2010). Biofunctionalization of materials for implants using engineered peptides. Acta Biomater. *6*, 4634–4641.

Kim, D.-H., Han, K., Gupta, K., Kwon, K.W., Suh, K.-Y., and Levchenko, A. (2009). Mechanosensitivity of fibroblast cell shape and movement to anisotropic substratum topography gradients. Biomaterials *30*, 5433–5444.

Knight, C.G., Morton, L.F., Onley, D.J., Peachey, A.R., Messent, A.J., Smethurst, P.A., Tuckwell, D.S., Farndale, R.W., and Barnes, M.J. (1998). Identification in collagen type I of an integrin α2β1-binding site containing an essential GER sequence. J. Biol. Chem. *273*, 33287–33294.

Kong, J., Cassell, A.M., and Dai, H. (1998). Chemical vapor deposition of methane for single-walled carbon nanotubes. Chem. Phys. Lett. *292*, 567–574.

Kromka, A., Babchenko, O., Kozak, H., Hruska, K., Rezek, B., Ledinsky, M., Potmesil, J., Michalka, M., and Vanecek, M. (2009). Seeding of polymer substrates for nanocrystalline diamond film growth. Diam. Relat. Mater. *18*, 734–739.

Kromka, A., Grausova, L., Bacakova, L., Vacik, J., Rezek, B., Vanecek, M., Williams, O.A., and Haenen, K. (2010). Semiconducting to metallic-like boron doping of nanocrystalline diamond films and its effect on osteoblastic cells. Diam. Relat. Mater. *19*, 190–195.

Krüger, A., Kataoka, F., Ozawa, M., Fujino, T., Suzuki, Y., Aleksenskii, A.E., Vul', A.Y., and Ōsawa, E. (2005). Unusually tight aggregation in detonation nanodiamond: Identification and disintegration. Carbon *43*, 1722–1730.

Kulkarni, M., Mazare, A., Schmuki, P., Iglic, A., and Seifalian, A. (2014). Biomaterial surface modification of titanium and titanium alloys for medical applications. Nanomed. *111*, 111-136.

Lahti, M., Heino, J., and Käpylä, J. (2013). Leukocyte integrins αLβ2, αMβ2 and αXβ2 as collagen receptors—Receptor activation and recognition of GFOGER motif. Int. J. Biochem. Cell Biol. *45*, 1204–1211.

Lam, C., James, J.T., McCluskey, R., Arepalli, S., and Hunter, R.L. (2006). A Review of Carbon Nanotube Toxicity and Assessment of Potential Occupational and Environmental Health Risks. Crit. Rev. Toxicol. *36*, 189–217.

Langenbach, F., and Handschel, J. (2013). Effects of dexamethasone, ascorbic acid and β-glycerophosphate on the osteogenic differentiation of stem cells in vitro. Stem Cell Res. Ther. *4*, 117.

Lechleitner, T., Klauser, F., Seppi, T., Lechner, J., Jennings, P., Perco, P., Mayer, B., Steinmüller-Nethl, D., Preiner, J., Hinterdorfer, P., et al. (2008). The surface properties of nanocrystalline diamond and nanoparticulate diamond powder and their suitability as cell growth support surfaces. Biomaterials *29*, 4275–4284.

Lee, Y.-H., and Kim, Y.-J. (2012). Electrical and lattice vibrational behaviors of graphene devices on flexible substrate under small mechanical strain. Appl. Phys. Lett. *101*, 83102.

Lee, C., Wei, X., Kysar, J.W., and Hone, J. (2008). Measurement of the Elastic Properties and Intrinsic Strength of Monolayer Graphene. Science *321*, 385–388.

Lee, J.-K., Yamazaki, S., Yun, H., Park, J., Kennedy, G.P., Kim, G.-T., Pietzsch, O., Wiesendanger, R., Lee, S., Hong, S., et al. (2013). Modification of Electrical Properties of Graphene by Substrate-Induced Nanomodulation. Nano Lett. *13*, 3494–3500.

Lee, J.-U., Yoon, D., and Cheong, H. (2012). Estimation of Young's Modulus of Graphene by Raman Spectroscopy. Nano Lett. *12*, 4444–4448.

Lee, M.H., Brass, D.A., Morris, R., Composto, R.J., and Ducheyne, P. (2005). The effect of non-specific interactions on cellular adhesion using model surfaces. Biomaterials *26*, 1721–1730.

Ley, K. (2003). The role of selectins in inflammation and disease. Trends Mol. Med. *9*, 263–268.

Li, J., Guo, D., Wang, X., Wang, H., Jiang, H., and Chen, B. (2010). The Photodynamic Effect of Different Size ZnO Nanoparticles on Cancer Cell Proliferation In Vitro. Nanoscale Res. Lett. *5*, 1063–1071.

Li, M., Liu, Q., Jia, Z., Xu, X., Cheng, Y., Zheng, Y., Xi, T., and Wei, S. (2014). Graphene oxide/hydroxyapatite composite coatings fabricated by electrophoretic nanotechnology for biological applications. Carbon *67*, 185–197.

Li, N., Xia, T., and Nel, A.E. (2008). The role of oxidative stress in ambient particulate matter-induced lung diseases and its implications in the toxicity of engineered nanoparticles. Free Radic. Biol. Med. *44*, 1689–1699.

Li, X., Cai, W., An, J., Kim, S., Nah, J., Yang, D., Piner, R., Velamakanni, A., Jung, I., Tutuc, E., et al. (2009). Large-Area Synthesis of High-Quality and Uniform Graphene Films on Copper Foils. Science *324*, 1312–1314.

Lim, S.-T., Chen, X.L., Lim, Y., Hanson, D.A., Vo, T.-T., Howerton, K., Larocque, N., Fisher, S.J., Schlaepfer, D.D., and Ilic, D. (2008). Nuclear FAK Promotes Cell Proliferation and Survival through FERM-Enhanced p53 Degradation. Mol. Cell *29*, 9–22.

Liu, F.B., Jing, B., Cui, Y., Di, J.J., and Qu, M. (2015). Voltammetric and impedance behaviours of surface-treated nano-crystalline diamond film electrodes. AIP Adv. *5*, 41306.

Liu, X., Zhao, X., Fu, R.K.Y., Ho, J.P.Y., Ding, C., and Chu, P.K. (2005). Plasma-treated nanostructured TiO2 surface supporting biomimetic growth of apatite. Biomaterials *26*, 6143–6150.

Loomis, W.F., Fuller, D., Gutierrez, E., Groisman, A., and Rappel, W.-J. (2012). Innate non-specific cell substratum adhesion. PloS One *7*, e42033.

Lopez, G.P., Albers, M.W., Schreiber, S.L., Carroll, R., Peralta, E., and Whitesides, G.M. (1993). Convenient methods for patterning the adhesion of mammalian cells to surfaces using self-assembled monolayers of alkanethiolates on gold. J. Am. Chem. Soc. *115*, 5877–5878.

Luo, B.-H., Carman, C.V., and Springer, T.A. (2007). Structural basis of integrin regulation and signaling. Annu. Rev. Immunol. *25*, 619-647.

Ma, L., and Wen, J. (2008). Biocomposite of double-walled carbon nanotube-doped alginate gel for biomaterial immobilization. Compos. Sci. Technol. *68*, 1297–1303.

Mack, C.P., Somlyo, A.V., Hautmann, M., Somlyo, A.P., and Owens, G.K. (2001). Smooth Muscle Differentiation Marker Gene Expression Is Regulated by RhoA-mediated Actin Polymerization. J. Biol. Chem. *276*, 341–347.

Maniotis, A.J., Chen, C.S., and Ingber, D.E. (1997). Demonstration of mechanical connections between integrins, cytoskeletal filaments, and nucleoplasm that stabilize nuclear structure. Proc. Natl. Acad. Sci. *94*, 849–854.

Manke, A., Wang, L., and Rojanasakul, Y. (2013). Mechanisms of Nanoparticle-Induced Oxidative Stress and Toxicity. BioMed Res. Int. *2013*, 1–15.

Mao, H., Kawazoe, N., and Chen, G. (2013). Uptake and intracellular distribution of collagen-functionalized single-walled carbon nanotubes. Biomaterials *34*, 2472–2479.

Markovic, Z.M., Harhaji-Trajkovic, L.M., Todorovic-Markovic, B.M., Kepić, D.P., Arsikin, K.M., Jovanović, S.P., Pantovic, A.C., Dramićanin, M.D., and Trajkovic, V.S. (2011). In vitro comparison of the photothermal anticancer activity of graphene nanoparticles and carbon nanotubes. Biomaterials *32*, 1121–1129.

Martins, M. de F., and Abairos, V. (2002). Glycocalyx of lung epithelial cells. In International Review of Cytology, (Academic Press), pp. 131–173.

Matthews, J.A., Wnek, G.E., Simpson, D.G., and Bowlin, G.L. (2002). Electrospinning of Collagen Nanofibers. Biomacromolecules *3*, 232–238.

McBeath, R., Pirone, D.M., Nelson, C.M., Bhadriraju, K., and Chen, C.S. (2004). Cell shape, cytoskeletal tension, and RhoA regulate stem cell lineage commitment. Dev. Cell *6*, 483–495.

McFarland, C.D., Thomas, C.H., DeFilippis, C., Steele, J.G., and Healy, K.E. (2000). Protein adsorption and cell attachment to patterned surfaces. J. Biomed. Mater. Res. *49*, 200–210.

Mitra, S.K., Hanson, D.A., and Schlaepfer, D.D. (2005). Focal adhesion kinase: in command and control of cell motility. Nat. Rev. Mol. Cell Biol. *6*, 56–68.

Moon, J.J., Matsumoto, M., Patel, S., Lee, L., Guan, J.-L., and Li, S. (2005). Role of cell surface heparan sulfate proteoglycans in endothelial cell migration and mechanotransduction. J. Cell. Physiol. *203*, 166–176.

Movia, D., Prina-Mello, A., Bazou, D., Volkov, Y., and Giordani, S. (2011). Screening the Cytotoxicity of Single-Walled Carbon Nanotubes Using Novel 3D Tissue-Mimetic Models. ACS Nano *5*, 9278–9290.

Murphy, W.L., McDevitt, T.C., and Engler, A.J. (2014). Materials as stem cell regulators. Nat. Mater. *13*, 547–557.

Namekawa, K., Tokoro Schreiber, M., Aoyagi, T., and Ebara, M. (2014). Fabrication of zeolite–polymer composite nanofibers for removal of uremic toxins from kidney failure patients. Biomater. Sci. *2*, 674.

Nebel, C.E., Kato, H., Rezek, B., Shin, D., Takeuchi, D., Watanabe, H., and Yamamoto, T. (2006). Electrochemical properties of undoped hydrogen terminated CVD diamond. Diam. Relat. Mater. *15*, 264–268.

Neves, N.M., Campos, R., Pedro, A.J., Cunha, J., Macedo, F., and Reis, R.L. (2007). Patterning of polymer nanofiber meshes by electrospinning for biomedical applications. Int. J. Nanomedicine *2*, 433–448.

Nikolaev, P., Bronikowski, M.J., Bradley, R.K., Rohmund, F., Colbert, D.T., Smith, K.A., and Smalley, R.E. (1999). Gas-phase catalytic growth of single-walled carbon nanotubes from carbon monoxide. Chem. Phys. Lett. *313*, 91–97.

Novoselov, K.S., Geim, A.K., Morozov, S.V., Jiang, D., Zhang, Y., Dubonos, S.V., Grigorieva, I.V., and Firsov, A.A. (2004). Electric Field Effect in Atomically Thin Carbon Films. Science *306*, 666–669.

Novoselov, K.S., Geim, A.K., Morozov, S.V., Jiang, D., Katsnelson, M.I., Grigorieva, I.V., Dubonos, S.V., and Firsov, A.A. (2005). Two-dimensional gas of massless Dirac fermions in graphene. Nature *438*, 197–200.

Okuyama, T., Yamazoe, H., Mochizuki, N., Khademhosseini, A., Suzuki, H., and Fukuda, J. (2010). Preparation of arrays of cell spheroids and spheroid-monolayer cocultures within a microfluidic device. J. Biosci. Bioeng. *110*, 572–576.

Olivas-Armendariz, I., Martel-Estrada, S.A., Mendoza-Duarte, M.E., Jiménez-Vega, F., García-Casillas, P., and Martínez-Pérez, C.A. (2013). Biodegradable Chitosan/Multiwalled Carbon Nanotube Composite for Bone Tissue Engineering. J. Biomater. Nanobiotechnology *4*, 204–211.

Osman, R., and Swain, M. (2015). A Critical Review of Dental Implant Materials with an Emphasis on Titanium versus Zirconia. Materials *8*, 932–958.

Otsu, N. (1979). A Threshold Selection Method from Gray-Level Histograms. IEEE Trans. Syst. Man Cybern. *9*, 62–66.

Ozawa, M., Inaguma, M., Takahashi, M., Kataoka, F., Krüger, A., and Ōsawa, E. (2007). Preparation and Behavior of Brownish, Clear Nanodiamond Colloids. Adv. Mater. *19*, 1201–1206.

Parsons, J.T., Horwitz, A.R., and Schwartz, M.A. (2010). Cell adhesion: integrating cytoskeletal dynamics and cellular tension. Nat. Rev. Mol. Cell Biol. *11*, 633–643.

Peña, B., Martinelli, V., Jeong, M., Bosi, S., Lapasin, R., Taylor, M.R.G., Long, C.S., Shandas, R., Park, D., and Mestroni, L. (2016). Biomimetic Polymers for Cardiac Tissue Engineering. Biomacromolecules *17*, 1593–1601.

Pinto, A.M., Gonçalves, I.C., and Magalhães, F.D. (2013). Graphene-based materials biocompatibility: A review. Colloids Surf. B Biointerfaces *111*, 188–202.

Pirone, D.M., Liu, W.F., Ruiz, S.A., Gao, L., Raghavan, S., Lemmon, C.A., Romer, L.H., and Chen, C.S. (2006). An inhibitory role for FAK in regulating proliferation: a

link between limited adhesion and RhoA-ROCK signaling. J. Cell Biol. *174*, 277–288.

Popov, C., Kulisch, W., Reithmaier, J.P., Dostalova, T., Jelinek, M., Anspach, N., and Hammann, C. (2007). Bioproperties of nanocrystalline diamond/amorphous carbon composite films. Diam. Relat. Mater. *16*, 735–739.

Potocky, S., Kromka, A., Potmesil, J., Remes, Z., Polackova, Z., and Vanecek, M. (2006). Growth of nanocrystalline diamond films deposited by microwave plasma CVD system at low substrate temperatures. Phys. Status Solidi A *203*, 3011–3015.

Raffa, V., Taccola, L., Cristina Riggio, Vittorio, O., Iorio, M.C., Pietrabissa, A., and Cuschieri, A. (2011). Zinc oxide nanoparticles as selective killers of proliferating cells. Int. J. Nanomedicine 1129.

Ramanathan, T., Abdala, A.A., Stankovich, S., Dikin, D.A., Herrera-Alonso, M., Piner, R.D., Adamson, D.H., Schniepp, H.C., Chen, X., Ruoff, R.S., et al. (2008). Functionalized graphene sheets for polymer nanocomposites. Nat. Nanotechnol. *3*, 327–331.

Reed, M., Randall, J., Aggarwal, R., Matyi, R., Moore, T., and Wetsel, A. (1988). Observation of discrete electronic states in a zero-dimensional semiconductor nanostructure. Phys. Rev. Lett. *60*, 535–537.

Rezek, B., Michalíková, L., Ukraintsev, E., Kromka, A., and Kalbacova, M. (2009). Micro-Pattern Guided Adhesion of Osteoblasts on Diamond Surfaces. Sensors *9*, 3549–3562.

Rezek, B., Krtk, M., Ukraintsev, E., Babchenko, O., Kromka, A., Bro, A., and Kalbacov, M. (2011). Diamond as functional material for bioelectronics and biotechnology. In New Perspectives in Biosensors Technology and Applications, P.A. Serra, ed. (InTech), p.

Ricciardi, B.F., Nocon, A.A., Jerabek, S.A., Wilner, G., Kaplowitz, E., Goldring, S.R., Purdue, P.E., and Perino, G. (2016). Histopathological characterization of corrosion product associated adverse local tissue reaction in hip implants: a study of 285 cases. BMC Clin. Pathol. *16*.

Ripamonti, U., Roden, L.C., and Renton, L.F. (2012). Osteoinductive hydroxyapatite-coated titanium implants. Biomaterials *33*, 3813–3823.

Roth, V. (2006). Doubling Time Calculator.

Rubio-Retama, J., Hernando, J., López-Ruiz, B., Härtl, A., Steinmüller, D., Stutzmann, M., López-Cabarcos, E., and Antonio Garrido, J. (2006). Synthetic Nanocrystalline Diamond as a Third-Generation Biosensor Support. Langmuir *22*, 5837–5842.

Salah, N., Habib, Khan, Memic, Azam, Al-Hamedi, Zahed, and Habib (2011). High-energy ball milling technique for ZnO nanoparticles as antibacterial material. Int. J. Nanomedicine 863–869.

Samavedi, S., Whittington, A.R., and Goldstein, A.S. (2013). Calcium phosphate ceramics in bone tissue engineering: A review of properties and their influence on cell behavior. Acta Biomater. *9*, 8037–8045.

Schakenraad, J.M., and Busscher, H.J. (1989). Cell—polymer interactions: The influence of protein adsorption. Sel. Pap. Symp. Surf. Transfort Phenom. Bioparticle Adhes. Held Third Chem. Congr. N. Am. *42*, 331–343.

Schlaepfer, D.D., Hanks, S.K., Hunter, T., and van der Geer, P. (1994). Integrin-mediated signal transduction linked to Ras pathway by GRB2 binding to focal adhesion kinase. Nature *372*, 786–791.

Schlaepfer, D.D., Mitra, S.K., and Ilic, D. (2004). Control of motile and invasive cell phenotypes by focal adhesion kinase. Biochim. Biophys. Acta BBA - Mol. Cell Res. *1692*, 77–102.

Schliephake, H., and Scharnweber, D. (2008). Chemical and biological functionalization of titanium for dental implants. J. Mater. Chem. *18*, 2404.

Scotchford, C.A., Gilmore, C.P., Cooper, E., Leggett, G.J., and Downes, S. (2002). Protein adsorption and human osteoblast-like cell attachment and growth on alkylthiol on gold self-assembled monolayers. J. Biomed. Mater. Res. *59*, 84–99.

Shalabi, M.M., Gortemaker, A., Hof, M.A.V., Jansen, J.A., and Creugers, N.H.J. (2006). Implant Surface Roughness and Bone Healing: a Systematic Review. J. Dent. Res. *85*, 496–500.

Shao, Y., Wang, J., Wu, H., Liu, J., Aksay, I.A., and Lin, Y. (2010). Graphene Based Electrochemical Sensors and Biosensors: A Review. Electroanalysis *22*, 1027–1036.

Shi, Q., and Boettiger, D. (2003). A novel mode for integrin-mediated signaling: tethering is required for phosphorylation of FAK Y397. Mol. Biol. Cell *14*, 4306–4315.

Shih, Y.-R.V., Chen, C.-N., Tsai, S.-W., Wang, Y.J., and Lee, O.K. (2006). Growth of Mesenchymal Stem Cells on Electrospun Type I Collagen Nanofibers. Stem Cells *24*, 2391–2397.

Shyh-Chang, N., Daley, G.Q., and Cantley, L.C. (2013). Stem cell metabolism in tissue development and aging. Development *140*, 2535–2547.

Singh, Z.S. (2016). Applications and toxicity of graphene family nanomaterials and their composites. Nanotechnol. Sci. Appl. 15, 15-28.

Sisson, K., Zhang, C., Farach-Carson, M.C., Chase, D.B., and Rabolt, J.F. (2010). Fiber diameters control osteoblastic cell migration and differentiation in electrospun gelatin. J. Biomed. Mater. Res. *94*, 1312-1320

Sommer, A.P., Zhu, D., and Brühne, K. (2007). Surface Conductivity on Hydrogen-Terminated Nanocrystalline Diamond: Implication of Ordered Water Layers. Cryst. Growth Des. *7*, 2298–2301.

Sotomayor, M., and Schulten, K. (2008). The Allosteric Role of the Ca2+ Switch in Adhesion and Elasticity of C-Cadherin. Biophys. J. *94*, 4621–4633.

Spear, R.L., and Cameron, R.E. (2008). Carbon nanotubes for orthopaedic implants. Int. J. Mater. Form. *1*, 127–133.

Stevens, M.M., and George, J.H. (2005). Exploring and engineering the cell surface interface. Science *310*, 1135–1138.

Sui, J.H., and Cai, W. (2006). Formation of diamond-like carbon (DLC) film on the NiTi alloys via plasma immersion ion implantation and deposition (PIIID) for improving corrosion resistance. Appl. Surf. Sci. *253*, 2050–2055.

Sui, J.H., Gao, Z.Y., Cai, W., and Zhang, Z.G. (2007). Corrosion behavior of NiTi alloys coated with diamond-like carbon (DLC) fabricated by plasma immersion ion implantation and deposition. Mater. Sci. Eng. A *452–453*, 518–523.

Sundaramurthi, D., Krishnan, U.M., and Sethuraman, S. (2014). Electrospun Nanofibers as Scaffolds for Skin Tissue Engineering. Polym. Rev. *54*, 348–376.

Takada, Y., Ye, X., and Simon, S. (2007). The integrins. Genome Biol *8*, 215.

Tang, L., Tsai, C., Gerberich, W.W., Kruckeberg, L., and Kania, D.R. (1995). Biocompatibility of chemical-vapour-deposited diamond. Biomaterials *16*, 483–488.

Teo, B.K.K., Wong, S.T., Lim, C.K., Kung, T.Y.S., Yap, C.H., Ramagopal, Y., Romer, L.H., and Yim, E.K.F. (2013). Nanotopography Modulates Mechanotransduction of Stem Cells and Induces Differentiation through Focal Adhesion Kinase. ACS Nano *7*, 4785–4798.

Thalhammer, A., Edgington, R.J., Cingolani, L.A., Schoepfer, R., and Jackman, R.B. (2010). The use of nanodiamond monolayer coatings to promote the formation of functional neuronal networks. Biomaterials *31*, 2097–2104.

Thess, A., Lee, R., Nikolaev, P., Dai, H., Petit, P., Robert, J., Xu, C., Lee, Y.H., Kim, S.G., Rinzler, A.G., et al. (1996). Crystalline Ropes of Metallic Carbon Nanotubes. Science *273*, 483–487.

Underwood, P.A., and Bennett, F.A. (1989). A comparison of the biological activities of the cell-adhesive proteins vitronectin and fibronectin. J. Cell Sci. *93*, 641–649.

Van Vlierberghe, S., Dubruel, P., and Schacht, E. (2011). Biopolymer-Based Hydrogels As Scaffolds for Tissue Engineering Applications: A Review. Biomacromolecules *12*, 1387–1408.

Vandrovcova, M., Hanus, J., Drabik, M., Kylian, O., Biederman, H., Lisa, V., and Bacakova, L. (2012). Effect of different surface nanoroughness of titanium dioxide films on the growth of human osteoblast-like MG63 cells. J. Biomed. Mater. Res. A *100A*, 1016–1032.

Walboomers, X.F., and Jansen, J.A. (2001). Cell and tissue behavior on micro-grooved surfaces. Odontology *89*, 2–11.

Wang, J., Sun, P., Bao, Y., Liu, J., and An, L. (2011). Cytotoxicity of single-walled carbon nanotubes on PC12 cells. Toxicol. In Vitro *25*, 242–250.

Watari, S., Hayashi, K., Wood, J.A., Russell, P., Nealey, P.F., Murphy, C.J., and Genetos, D.C. (2012). Modulation of osteogenic differentiation in hMSCs cells by submicron topographically-patterned ridges and grooves. Biomaterials *33*, 128–136.

Webster, T.J., Ergun, C., Doremus, R.H., Siegel, R.W., and Bizios, R. (2000). Specific proteins mediate enhanced osteoblast adhesion on nanophase ceramics. J. Biomed. Mater. Res. *51*, 475–483.

Wendel, H.P., and Ziemer, G. (1999). Coating-techniques to improve the hemocompatibility of artificial devices used for extracorporeal circulation. Eur. J. Cardiothorac. Surg. *16*, 342–350.

Widmaier, M., Rognoni, E., Radovanac, K., Azimifar, S.B., and Fassler, R. (2012). Integrin-linked kinase at a glance. J. Cell Sci. *125*, 1839–1843.

Wildöer, J.W., Venema, L.C., Rinzler, A.G., Smalley, R.E., and Dekker, C. (1998). Electronic structure of atomically resolved carbon nanotubes. Nature *391*, 59–62.

Williams, D.F. (1987). Definitions in Biomaterials: Proceedings of a Consensus Conference of the European Society for Biomaterials, Chester, England, March 3-5, 1986 (Elsevier).

Williams, D.F. (1999). The Williams dictionary of biomaterials (Liverpool University Press).

Williams, O.A. (2011). Nanocrystalline diamond. Diam. Relat. Mater. *20*, 621–640.

Xia, F., Mueller, T., Golizadeh-Mojarad, R., Freitag, M., Lin, Y., Tsang, J., Perebeinos, V., and Avouris, P. (2009). Photocurrent Imaging and Efficient Photon Detection in a Graphene Transistor. Nano Lett. *9*, 1039–1044.

Xie, J., MacEwan, M.R., Schwartz, A.G., and Xia, Y. (2010). Electrospun nanofibers for neural tissue engineering. Nanoscale *2*, 35–44.

Yan, K., Peng, H., Zhou, Y., Li, H., and Liu, Z. (2011). Formation of Bilayer Bernal Graphene: Layer-by-Layer Epitaxy via Chemical Vapor Deposition. Nano Lett. *11*, 1106–1110.

Yang, C.-Y., Huang, L.-Y., Shen, T.-L., and Yeh, J.A. (2010). Cell adhesion, morphology and biochemistry on nano-topographic oxidized silicon surfaces. Eur Cell Mater *20*, 415–430.

Yang, L., Sheldon, B.W., and Webster, T.J. (2009). Orthopedic nano diamond coatings: Control of surface properties and their impact on osteoblast adhesion and proliferation. J. Biomed. Mater. Res. A *91A*, 548–556.

Yang, L., Li, Y., Sheldon, B.W., and Webster, T.J. (2012a). Altering surface energy of nanocrystalline diamond to control osteoblast responses. J Mater Chem *22*, 205–214.

Yang, N., Chen, X., Ren, T., Zhang, P., and Yang, D. (2015). Carbon nanotube based biosensors. Sens. Actuators B Chem. *207*, 690–715.

Yang, S.-T., Luo, J., Zhou, Q., and Wang, H. (2012b). Pharmacokinetics, Metabolism and Toxicity of Carbon Nanotubes for Biomedical Purposes. Theranostics *2*, 271–282.

Yoshikawa, H., Shikata, S., Fujimori, N., Sato, N., and Ikehata, T. (2006). Smooth Surface Dry Etching of Diamond by Very High Frequency Inductively Coupled Plasma. New Diam. Front. Carbon Technol. *16*, 97–106.

Yuan, Y., Liu, C., Lu, J., Tang, W., Gan, Q., Zhou, H., Qian, J., and Lu, X. (2011). In vitro cytotoxicity and induction of apoptosis by silica nanoparticles in human HepG2 hepatoma cells. Int. J. Nanomedicine *6*, 1889–901.

Zaidel-Bar, R., Cohen, M., Addadi, L., and Geiger, B. (2004). Hierarchical assembly of cell-matrix adhesion complexes. Biochem. Soc. Trans. *32*, 416–420.

Zamir, E., and Geiger, B. (2001). Molecular complexity and dynamics of cell-matrix adhesions. J. Cell Sci. *114*, 3583–3590.

Zhang, J., Zhou, M., Wu, W., and Tang, Y. (2013). Fabrication of Diamond Microstructures by Using Dry and Wet Etching Methods. Plasma Sci. Technol. *15*, 552–554.

Zhang, Y.Z., Venugopal, J., Huang, Z.-M., Lim, C.T., and Ramakrishna, S. (2005). Characterization of the Surface Biocompatibility of the Electrospun PCL-Collagen Nanofibers Using Fibroblasts. Biomacromolecules *6*, 2583–2589.

Zhao, J.-H., Reiske, H., and Guan, J.-L. (1998). Regulation of the cell cycle by focal adhesion kinase. J. Cell Biol. *143*, 1997–2008.

Zheng, X., Baker, H., Hancock, W.S., Fawaz, F., McCaman, M., and Pungor, E. (2008). Proteomic Analysis for the Assessment of Different Lots of Fetal Bovine Serum as a Raw Material for Cell Culture. Part IV. Application of Proteomics to the Manufacture of Biological Drugs. Biotechnol. Prog. *22*, 1294–1300.